Proceeding Book of
First Conference for Engineering Sciences and Technology (CEST-2018)
(Part 5)

Engineering Systems and Sustainable Development
&
Engineering Management

25-27 September 2018

Garaboulli - Libya

Table of Contents

Exergy Analysis of a Brine Mixing Once- Through MSF-BM Distillation Plant

Usama Ahmed Ezzeghni[1], Mohamed Abduljawad[2]
[1]elzoghni@gmail.com,[2]Maakaa@hotmail.com
[1]Department of Desalination Researches, Nuclear Research Center, Libya
[2]Department of Scientific Publications Authority of Natural Sciences, Research and Technology, Libya

ABSTRACT

Exergy analysis is a tool that can be used to detect the sites and causes of thermodynamic inefficiencies in a thermal process,as well as to prospect the design performance of any industry plants. The practice of such an analysis in seawater desalination plants is of increasing importance to discover the sites of the biggest irreversible losses. In this papera full exergy analysis of a brine mixing once through multi stage flash MSF-BM desalination plant was carried out to identify the component that has the largest exergy destruction. The MSF-BM desalination plant is located at 30 km north-west of Tripoli the capital of Libya.

Exergy flow rates are estimated all over the plant and exergy flow diagram is prepared. The results of the exergy analysis show that the multi-stage flash unit, pumps and motors are the major sites of highest exergy destruction, where 61.48% of the entire input exergy took place in the MSF unit, and 19.8% happens in the pumps and motors. The second law of efficiency was estimated to be 6.24%, which seems to be low that mean some improvements should be made to improve the plant efficiency and reduce exergy destruction, the improvement can be made to the MSF unit by increasing the number of flashing stages and to the pumps and motors by installing modern pumps with high efficiency.

Keyword— seawater desalination; exergy; exergy flow rates, exergy analysis.

1. Introduction

The leading desalination approaches used are multi-stage flash distillation (MSF), which establishes 44% of installed world capacity, and reverse osmosis (RO) with constitutes 42% that also comprises a no filtration (NF). Consequently, these two approaches create about 86% of total world capacity. The outstanding 14% is made up of electro dialysis (EDR) (6%), vapor compression (VC) (4%), and multiple-effect distillation (ME) (4%) [1].Even if these techniques are well established, there is a necessity to push the state of the art forward to make the operation of these plants more effective. An evaluation of the idealized and actual desalination technologies displays that the actual energy cost of desalination is around 5–10 times the cost under ideal operation. This matches to a second law efficiency of under 20% and points out that there are good chances in the MSF plants for improvements. The initial step in any upgrading or development project is diagnostics, and the dominant diagnostics tool in thermodynamics is second law analysis. Such an analysis aids to discover

the locations of maximum entropy generation and, thus, exergy destruction then to recognize the components that are responsible for the highest losses in the system [2].

All studies approved that desalination technologies haveatotal exergy efficiency less than 30 %, multi-stage flashdesalination type is considered the lowest exergy efficiency amongst the desalination technologies, its energy efficiency fluctuates between 1.8% - 7.73 %. Papersavailable in exergy desalination field are not much due to the shortage of the data and complexity of exergy estimation of the seawater streams [3]. Osman A. Hamed et al.showed that second law simulation papersrevealed that exergy destruction of the MSF distillers varied between 16.7 to 23.6 kWh/m3 compared to the others of only 2 kWh/m3 of an ideal reversible process.So, it has been recommended that hard work researches are to be done to decrease the energy consumption of the MSF distiller.

The second law of thermodynamics (exergy analysis) becomesfurtherappreciated to measure the performance of the desalination systems. Exergy analysis interprets for the obtainable forms of energy in the system streams and energy supply with a reference environment and recognizes the major losses of energy/exergy destruction. This helps in evolvingan effective desalination processes by reducing the hidden losses [4].

The exergy analysis is principally derived from second law of thermodynamics and provides a perfectbasis of the inefficiencies of a MSF desalination plant. The aim of this paper is to make an exergy analysis,exergetic efficiency, and exergy destruction of MSF-BM desalination plant. The analysis is performed for the plant based on the available operating data.

2. Plant Description

The MSF desalination plant has been erected in Tajoura 30 km north-west of Tripoli the capital of Libya. The plant contains 12 stages and designed to produce 1200 m3/day of distillate water [2]. Figure 1 shows the schematic diagram of the plant. The feed seawater is pretreatedwith antiscalant, antifoam chemicals and sodium-bisulfite to remove residual chlorine, then, it passes through the tube bundle of the stage 12, to increase the feed seawater temperature further until it reaches the brineheater inlet temperature (98.6 °C), after passing through the brine heater, the feed water reaches the top brine temperature (108 °C) using outside heating steam supplied by an external boiler at a temperature of 115 °C. The heated feed seawater goes into the first distillingchamber and flashes to avapor pass through a wire mesh called a demister to trap the entrained droplets and the vapor condenses over the tube bundle and collected on trays as a distilled water, the same thing happens in each stage.The produced distillatesin each stage are collected in an external distillate pipe and then discharged out of the plant using a distillate pump. The outstanding concentrated feed seawater is discharged out of the plant through the blow down pump. Due to the summer/winter fluctuations of the seawater temperature (min 15 °C/max 28 °C), the plant is provided with an automatic remixing device, which saves the inlet temperature of the feed seawater at 28 °C [5].

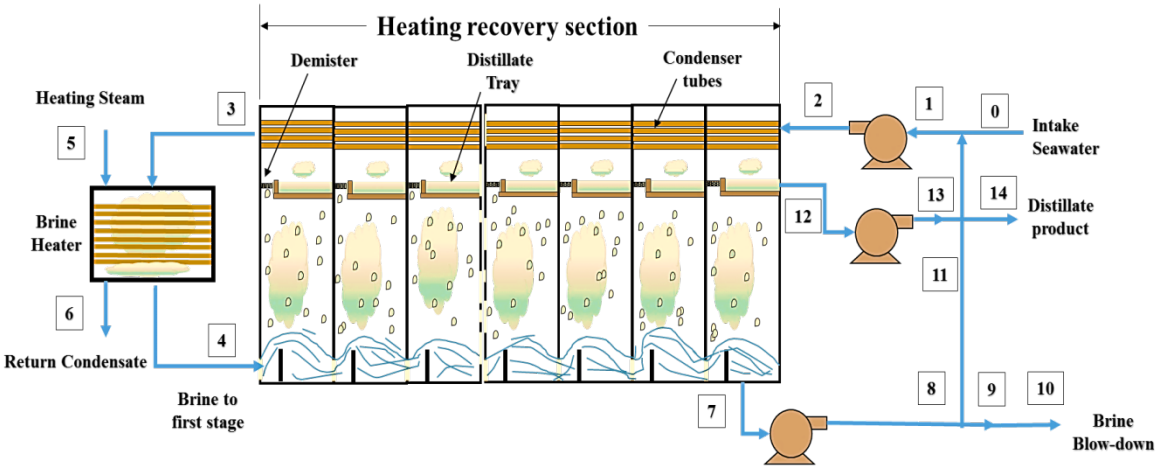

Figure 1: Schematic of the MSF-BM distillation plant.

3. Exergy Analysis

This once through MSF desalination plant wasanalysed under the following assumptions without losing accuracy, to simplify the model and make the distillation process shown in Figure 1 anidealized distillation process:

- All components of the system are assumed time-invariant (steady state) with negligible potential and kinetic energy effects.
- The reference state temperature and pressure are the temperature of the feedseawater and 1 atm, respectively.
- The salinity of the incoming raw water is constant.
- Distillate product is salt free.
- The saline water or themixture of salt and water is an ideal solution so the mixture properties are the average of component properties.
- Saline water, which consists of salt and water,is incompressible constituents.
- Thermodynamic properties of seawater are taken as that for sodium chloride solutions, since the latter is the primary constituent (80- 90%) in seawater.
- The impact of chemical exergy to total exergy is minor and insignificant.
- The flashing chambers and other system components are assumed to have negligible heat losses.

The properties of seawater depend on its pressure, temperature and salinity. The later can be defined as ppm (parts per million on a mass basis), percentage (sal), salt mass fraction (mfs) or a salt mole fraction (xs). mfs and xs are described as [4, 5]:

$$mf_s = \frac{m_s}{M_m} = \frac{N_s M_s}{N_m M_m} = x_s \frac{M_s}{M_m} and Mf_w = \frac{M_w}{M_m} = x_w \quad (1)$$

where m is mass, M is the molar mass, N is the number of moles, and x is the mole fraction. The letters s, w, and m stands for salt, water, and seawater, respectively [6].

The molar mass of the seawater is

$$M_m = \frac{m_m}{N_m} = \frac{N_s M_s + N_w M_w}{N_m} = x_s M_s + x_w M_w \quad (2)$$

The molar masses of NaCl and water are 58.5 kg/kmol and 18.0 kg/kmol, respectively [6].

Mass fractions are used for salinity calculations, where mole fraction used for the minimum work calculations. Combining equations 1 and 2 and noting that $x_s + x_w = 1$ gives the following relations:

$$x_s = \frac{M_w}{M_s\left(1/mf_s - 1\right) + M_w} and x_w = \frac{M_s}{M_w\left(1/mf_w - 1\right) + M_s} \quad (3)$$

Solutions that have a concentration less than 5 % are considered dilute solutions that behave as an ideal solution, so the effect of unlike molecules are neglected. Seawaters and saline underground waters are all ideal solutions since they have about a 4% salinity [4, 5].

The enthalpy and entropy of a mixture are determined from

$$H = \sum m_i h_i = m_s h_s + m_w h_w \text{ and } S = \sum m_i s_i = m_s s_s + m_w s_w \quad (4)$$

Dividing by the total mass of the mixture gives the quantities per unit mass of mixture

$$H = \sum m_i h_i = m_s h_s + mf_w h_w \text{ and } S = \sum mf_i s_i = mf_s s_s + mf_w s_w \quad (5)$$

During mixing, no heat is released or absorbed that means the enthalpy of mixing and the mixture of an ideal gas is zero (and thus the enthalpies of its single constituents). Consequently, the enthalpy of an ideal mixture at a defined temperature and pressure is the summation of the enthalpies of its single constituents at the same temperature and pressure [7], then, it follows that the enthalpy of a seawater which can be determined from the relation above by evaluating the enthalpies of individual components at the mixture temperature and pressure.

The feed seawater to the desalination plant is at about 15°C, 1 bar, and a salinityof 40,000 ppm, these condition can be taken as a conditions of theenvironment, then the properties at the dead state become T0 = 298.15°K, P0 = 1 bar = 101.325 kPa; salinity = 40,000 ppm = 4 %.

4. Enthalpy and Entropy of Pure Water and Salt

Properties of pure water are available in arrangedtables or computerprograms. Water properties expected by the built-in functions of the Engineering Equation Solver (EES) software at temperature and pressure were used [6]. Furthermore, the equations6 and 7can be used for calculating enthalpy and entropy, respectively for pure water properties and provide a very close values to that achieved by EES software [6].

$$h_w = 141.355 + 4202.07 * t - 0.535 * t^2 + 0.004 * t^3 \quad (6)$$

$s_w = 0.1543 + 15.383*t - 2.996*t^2 + 8.193*t^3 - 1.370*10^{-7}*t^4$ (7)

The reference state of salt is taken at 0°C, so the enthalpy and entropy of salt at temperature T can be estimated by following equation

$h_s = h_{so} + C_{ps}(T - T_o)$ and $h_s = h_{so} + C_{ps}\, ln(T/T_o)$ (8)

The specific heat of salt C_{ps}=0.8368 kJ/kg. °K. The enthalpy and entropy of salt at T_o = 15°C h_{so} = 12.552 kJ/kg and s_{so}= 0.04473 kJ/kg. °K, respectively (The enthalpy and entropy of incompressible constituents are independent of pressure) [4].

The entropy of each constituent in an ideal solution at a defined temperature T and pressure P is

$\bar{S}_i = S_{i,pure}(T, \bar{P}) - R_u \ln x_i$ (9)

Then the entropy of a saline solution (salt and water)is

$\bar{S} = x_s \bar{s}_s + x_w \bar{s}_w = x_s[\bar{S}_{s,pure}(T,P) - R_u \ln x_s] + x_w[\bar{S}_{w,pure}(T,P) - R_u \ln x_w] = x_x \bar{S}_{s,pure}(T,P) - R_u(x_s ln x_s + x_w ln x_w)$ (10)

The entropy of saline water per unit mass is estimated by dividing by the molar mass of saline water. So the equation 10 can be written as:

$S = mf_s s_{s,pure}(T, P) + mf_w s_{w,pure}(T, P) - R_m(x_s \ln x_s + x_w \ln x_w)$ (kJ/kg.°K) (11)

The specific exergy of each stream is given by

$\Psi = h - h_o + T_o(S - S_o)$ (12)

Then the exergy flow rate related becomes

$\dot{X} = \dot{m}\Psi = \dot{m}[h - h_o + T_o(S - S_o)]$ (13)

By means of the previous equations, the specific exergy and exergy flow rates at different locations shown in Figure1 are estimated.

The overall exergy balance for any system can be expressed as[8].

$X_{in} = X_{out} - X_{destroyed} = \Delta X_{system}$ (14)

If there is no work interaction (adiabatic steady sate system), the earlier equation can be simplified to

$X_{destroyed} = X_{in} - X_{out}$ (15)

The exergy efficiency of all constituents can be estimated by

$\eta_c = 1 - X_{destroyed}/X_{out}$ (16)

5. Results and Discussion

Tajoura desalination plant was analysed using the relations prescribed above, where the specific exergy, the exergy flow rates and the rate of exergy change at different locations are calculated, and the results are tabulated in Table 1. The locations of the states are illustrated in the diagram of Tajoura plant shown in Figure1. The feed seawater enters the plant and the final permeate and concentrate leaving the plant are at

the same dead state temperature and pressure, but at different salinities. Thus, the exergies of the concentrate line differ only due to the change in salinities, as it can be seen from Table 1 the raw feed seawater at state 0 has zero exergy since it is at the dead state. The brine at state 10 leaves the system at a high salinity of 58,700 ppm.

The results of the analysis are obtained using the EES software and are given in Table 1. Saline water is heated from(98.61^{o}C) 371.76^{o}K to (108 ^{o}C) 381.15°K at a rate of 3621 kg/s by super-heated steam at 179.91^{o}C in a heat exchanger. Steam leaves the heat exchanger at the same temperatureas saturated liquid. An energy balance on the heat exchanger gives the condensation rate of steam to be 2.06 kg/s, where the heat transfer rate to the saline water from steam is

$$\dot{Q}_{in,steam} = \dot{m}_{steam} h_{fg} = 4142.36\ kJ/s$$

Taking the dead state temperature to be To288.15^{o}K, the rate of exergy supply by the steam is

$$\dot{X}_{in,steam} = \dot{m}_{steam}(\Delta h - T_o \Delta s)\ or \dot{m}_{steam}\left(h_{fg} - T_o T s_{fg}\right)$$
$$\dot{X}_{in,steam} = 1508.36\ kJ/s$$

The total exergy rate is the sum of the exergy variations through the pumps and can be expressed as

$$\Delta\dot{X}_{pumps} = \Delta\dot{X}_{seawater\ pump} + \Delta\dot{X}_{distillate\ pump} + \Delta\dot{X}_{brine\ blow\ down\ pump}$$
$$= \left(\dot{X}_2 - \dot{X}_1\right) + \left(\dot{X}_8 - \dot{X}_7\right) + \left(\dot{X}_{13} - \dot{X}_{12}\right) = 9085.24\ kW$$

For a combined pump-motor efficiency of 79%, the exergy supplied in the form of electric power is

$$\dot{X}_{in,pumps} = \frac{\Delta\dot{X}_{pumps}}{\eta_{pump-motor}} = 11500.30\ kW$$

Where, a combined pump-motor efficiency can be expressed as the ratio of the mechanical energy transferred to the fluid over the electrical energy consumed [7].

$$\dot{X}_{in,\ total} = \dot{X}_{in,\ steam} + \dot{X}_{in,\ pumps} = 13008.67\ kW$$

Table 1: Properties and exergy flow rates at various locations all over the plant.

Location	Temperature, T, °K	Pressure P, kPa	Salinity, ppm	Mass flow rate, kg/s	Specific exergy ψ, kJ/kg	Exergy flow rate, Ẋ, kW
0	288.15	101.325	40,000	52.58	0.00	0.00
1	301.15	281.325	52,100	123.12	25.4365	3131.801
2	301.15	700	52,100	123.12	4.291	7915.647
3	371.73	700	52,100	123.12	102.929	12672.882
4	381.15	700	52,100	123.12	111.66	13747.794
5	453.06	1000	-	2.06	733.797	1508.360
6	453.06	1000	-	2.06	0.000	0.000
7	310.57	101.325	58,700	123.12	9.60737	1182.881
8	310.57	180	58,700	123.12	16.8889	2079.402
9	310.57	180	58,700	52.58	16.8889	888.076
10	288.15	101.325	58,700	52.58	9.56663	503.045
11	310.57	180	58,700	70.54	16.8889	1191.326
12	310.57	101.325	1	13.89	22.2146	308.537
13	310.57	300	1	13.89	41.8758	581.608

The minimum work requirement to extract product water with a mass flow rate of 51.25 kg/s from the incoming seawater with a salinity of 40,000 ppm at 15°C, 1 at min to 13.89 kg/s of fresh water with zero salinity and 29.67kg/s of concentrate water with a salinity of 58,700 ppm at the same temperature and pressure. The minimum work input for a steady flow adiabatic process is the work input required for a reversible adiabatic process and is equivalent to the variance between the leaving exergy streams and the entering exergy streams, plus the salinity exergy [8].Where, the inlet and exit streams are at the same temperature and pressure, and thus, this work is totally due to the composition of the entering and leaving streams. Therefore

$$\dot{W}_{min} = \dot{X}_{outgoing\ brine\ and\ product\ water} - \dot{X}_{incoming\ seawater} = \dot{X}_{14} + \dot{X}_{10} - \dot{X}_{0} = 811.58\ kW$$

The second-law efficiency is a degree of the process approximation to a reversible process, and it specifies the range accessible for potential improvements, noting that the second-law efficiency ranges from 0 for a totally irreversible process to 100 percent for a totally reversible process[9], the second law efficiency of the plant is the ratio of the minimum required inlet exergy to the total actual exergy, which can be expressed as:

$$\dot{X}_{II} = \frac{\dot{X}_{in,min}}{\dot{X}_{in,total}} = 6.36\ \%$$

This value indicates that this MSF plant at the specified rates could be accomplished using only 811.58kW of exergy (or work input) instead of13008.67kW. Then, the total exergy destruction becomes

$$\dot{X}_{destroyed,total} = \dot{X}_{in,total} - \dot{X}_{in,min} = \dot{X}_{in,total} - \dot{W}_{min} = 12197.08\ kW$$

The real value of second law analysis becomes more evident when the analysis is performed at the component level, and the sites of maximum exergy destruction upto the smallest exergy destruction are calculated according to following exergy balance equations:

$$\dot{X}_{destroyed,pumps} = \dot{X}_{in,pumps} - \Delta\dot{X}_{pumps} = 2415.06\ kW\ (19.8\ \%\ of\ total)$$

The exergy balance for any system undergoing any process is expressed as:

$$X_{in} - X_{out} - X_{destroyed} = \Delta X_{system}$$

For adiabatic steady state system, which has no energy transfer by work and no change in exergy, the relation above can be simplified to

$$\dot{X}_{destroyed} = X_{in,\ by\ mass} - \dot{X}_{out,\ by\ mass}$$

The exergy destruction fraction within a component is determined from

$$f_{Destroyed}\frac{\dot{X}_{destroyed,component}}{\dot{X}_{destroyed,\ total}} = \frac{\dot{X}_{destroyed,component}}{12197.08\ kW}$$

The amounts and fractions of exergy destroyed in the various components are determined to be as follows:
For the MSF unit:

$$\dot{X}_{destroyed,MSF} = (\dot{X}_2 + \dot{X}_4) - (\dot{X}_3 + \dot{X}_7 + \dot{X}_{12})$$
$$\dot{X}_{destroyed,MSF} = 7499.14\ kW\ (61.48\%)$$

For the steam-brine HX:

$$\dot{X}_{brine\ HX} = (\dot{X}_3 + \dot{X}_5) - (\dot{X}_4 + \dot{X}_6) = 433.45\ (3.56\%)$$

For the mixing point:

$$\dot{X}_{destroyed,\ mixer} = \dot{X}_0 + \dot{X}_{11} - \dot{X}_1 = -1940.47\ kW\ \ (15.9\ \%)$$

For the discharged brine:

$$\dot{X}_{destroyed,\ brine} = \dot{X}_9 - \dot{X}_{10} = 385.03\ kW\ (3.16\ \%)$$

For the product water:

$$\dot{X}_{destroyed,\ product} = \dot{X}_{13} - \dot{X}_{14} = 273.07\ kW\ (2.24\ \%)$$

The exergy analyses were conducted to obtain that the largest exergy destruction about 61.48 % of the total exergy input occurs within the MSF unit, followed by the next largest exergy destructions occur in the pumps

and their motors 19.8 %, and the heat exchanger 3.56 %. The remaining exergy destruction are 3.16% and 2.24% of total exergy happens at the brine and product streams, respectively. The locations of the above stated amounts and percentages are shown in Figure 2.

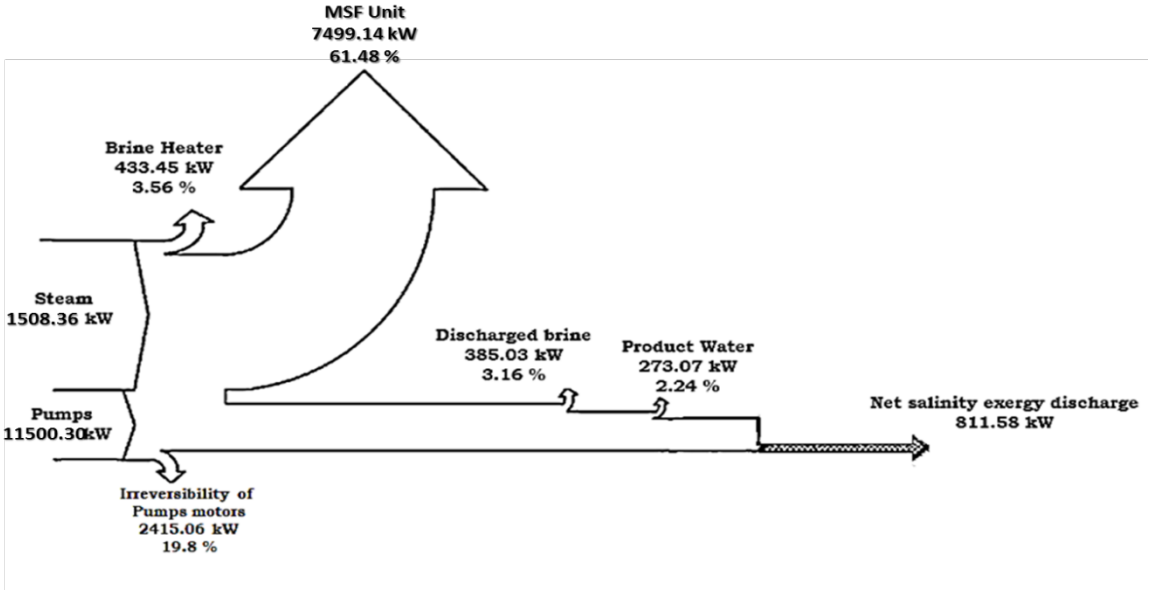

Figure 2: Exergy flow diagram with exergy destruction amount and percentages.

6. Conclusion

In conclusion, exergy analysis was found cooperative and significant tool for investigating the MSF-BM desalination plant from the vision of optimum usage of energy and must be taken into consideration at preliminary steps of design. Furthermore, it is shown that second-law efficiency (exergetic efficiency)is a valuable tool for a decision-maker to optimize the performance of different designs, where the second law efficiency was evaluated to be 6.24%, which is very low, in reality the second law efficiency of a modern power plant is over 50%. Therefore, it offers a potential for performance improvement. The exergy analysis shows that, the highest exergy destruction was 61.48% that occurs in MSF chambers followed by the pumping motor with 19.8% of the total input exergy that means some modifications for performance improvement can be considered according to the modern designs, as well as high efficient motors can be used to increase the second law efficiency. Moreover, an important exergy savings can be achieved by using hybrid designs. Additionally, the heat loss by the power plants can be used as heat source for generating the steam for the brine heater to enhance the performance of the desalination plants.

References

[1]. K. Wangnick, 1998 IDA Worldwide Desalination Plants Inventory, Wangnick Consulting, in cooperation with IDA, IDA Report No. 16, 2000.

[2]. O. Hamed, Thermal performance of multi stage flash distillation plants in Saudi Arabia, Al Jubail plant and others. Desalination 2000; 128:281–92.

[3]. M. Al-Weshahi, A. Anderson, G. Tian, Exergy Efficiency Enhancement of MSF Desalination by Heat Recovery from Hot Distillate Water Stages.

[4]. U. Ezzeghni, M. El-bourawi, Exergy analysis of a 10,000 m3/day Tajoura SWRO desalination plant, The 1st International Conference on Chemical, Petroleum, and Gas Engineering (ICCPGE 2016) 20th – 22th December 2016, Alkhoms-Libya.

[5]. G. Gude, N. Nirmalakhandan, S. Deng,A. Maganti, Desalination at low temperatures: An exergy analysis. Desalin. Water Treat. 2012, 40, 272–281.

[6]. M. Abduljawad, U. Ezzeghni, Optimization of Tajoura MSF desalination plant, Desalination 254 (2010) 23–28.

[7]. N. Kahraman and Y.A. Cengel, Exergy analysis of a MSF distillation plant, Energy Conv. Mgmt., 46 (2005) 2625–2636.

[8]. N. Kahraman, Y. Cengel, B. Wood and Y. Cerci, a combined RO, NF, and EDR desalination plant. Desalination, 171 (2004) 217–232.

[9]. Improving the thermodynamic and economic efficiencies of desalination plants: Minimum work required for desalination and case studies of four working plants. Desalination and water purification research and development program final report No. 78, U.S. Department of the interior, November 2003.

The Optimal Membrane Type for the Next Membrane Replacement of Tajoura SWRO Desalination Plant

Usama Ahmed Ezzeghni[1]
[1]elzoghni@gmail.com
[1]Department of Desalination Researches, Nuclear Research Center, Libya

ABSTRACT

Desalination of seawater in Libya has the capability to increase the accessible resources for producing drinkable water. Desalination of seawater with reverse osmosis membrane technology is one of the most significant techniques in the field of seawater desalination, for the latter technique the membrane manufacturers had created a new advanced membranes that deliver a high output fresh water and high salt refusal that cause a decline in operating cost through lower energy consumption compared to the other thermal desalination technologies .This paper aims to compare between several membrane products developed by different companies to improve the productivity of Tajoura Seawater Reverse Osmosis (SWRO) Desalination plant with high quality fresh water. The membrane type SW30HRLE-440i was selected for the next membrane replacement, which increases the plant productivity from 12,000 to 14,300 m^3/d with decreasing the number of membrane elements from 1080 to 900 membrane elements. In addition, the suggested membrane provides a high rejection, which results in an improved water quality with a salinity of less than 100ppmwhere it was almost 200 ppm, as well as it allows the plant to be designed and operated at a lower operating cost through a reduced specific energy consumption, which was8.492 to 5.48 kWh/m^3 and can be less than 2 kWh/m^3 if a modern energy recovery device (ERD) is used with a significant modification to the plant.

Keyword— reverse osmosis; advanced membranes; low energy; high rejection, high quality.

1. Introduction

Reverse osmosis (RO) desalination technology has been well-known for more than three decades. Progressive advances in membrane materials and high energy saving through energy recovery devices have made modern RO process more attractive and economically competitive than other desalination technologies [1].Due to increased consumption of fresh water in Libya and the noticed improvements of a reverse osmosis technology, it has led to increased demand of this technology locally and globally. Furthermore, identifying the future needs for desalination technology development, as well as a research and development activities that will result in cost-effective and more efficient desalination technologies that can meet the upcoming requirements [2]. In this paper Tajoura (SWRO) plant will be developed in parallel with the occurred developments of spiral wound membrane elements that permits desalination plants to be designed and

operated to either lower operating cost through reduced energy consumption, or to decrease membrane replacement cost by increasing plant productivity at lower operating flux.

2. Tajoura reverse osmosis plant

The seawater desalination plant illustrated in figure 1 located at Tajoura on the Mediterranean coastline about 30 km east of Tripoli. The plant was planned to yield about 10,000 m^3/day of fresh water with a total dissolved solid of less than 200 milligrams per liter (ppm). The main purpose of the plant is to provide Nuclear Research Center (NRC) with an industrial and drinking water and to substitute the deficiency of drinking water at Tajoura city. It is consisting of a two passes. The first pass uses polyamide membranes to desalt seawater and the second pass is used to desalt the product of the first pass.

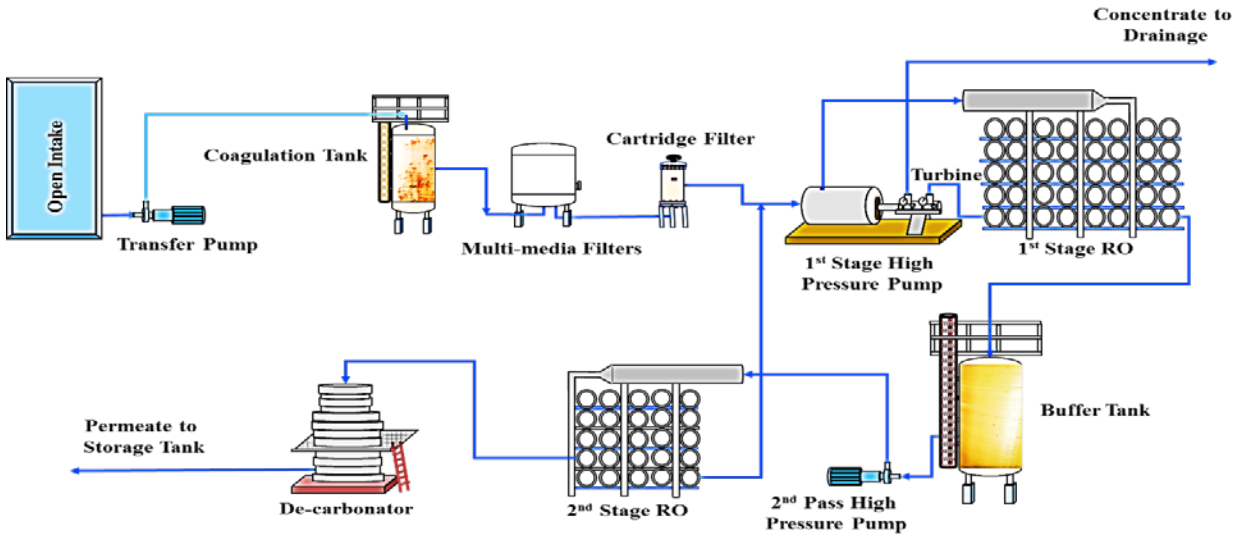

Figure 1: Schematic diagram of the SWRO desalination plant.

Tajoura SWRO desalination plant with design parameters shown in table 1[3], where seawater intake head is fitted at a distance of 1,300 m into the sea 7 m underneath the sea level and 6 m overhead the sea bottom. The feed water collected by gravity into a basin with a capacity of 5,580 m3through two 760 mm diameter plastic pipes at the seashore, then 750 m3/hr (1,500 m3/hr for 100% operation) are pumped to the pre-treatment side.

Table 1: The major design parameters of Tajoura desalination plant.

Item	First stage	Second pass*
Number of RO racks	4	2
Pressure vessels (PVs) configuration	1 stage	3 stages (24-12-6)
No. of PVs	180	84

No. of membranes	1080	504
No. of membranes per PV	6	6
Nominal diameter, inch	8	8
Membrane model	TFC 2822SS-360	TFC 8600 PA
Design pressure, bar	82.8	41
Working pressure, bar	54	31
pH	5–6	5–6
Maximum temperature, ^{o}C	45	45
Feed flow, m^3/d	34,285	552
Permeate flow, m^3/d	12,000	426
Concentrate flow, m^3/d	22,285	84
Design salt rejection, %	99.6	98
Recovery, %	35	85
Permeate salinity, mg/L	> 200	170

*The second pass of the plant was not included in this study because the drinking water specifications can be achieved by the first stage only.

The pre-treatment contains an online coagulation-flocculation tank, 8-media filters and 5 μm cartridge filters. Some chemicals are added before the feed water reaches the coagulation flocculation tanks. The chemicals are anti-scalants, which are injected to decrease scales accumulation, sulphuric acid used for pH adjustment, Copper sulphate as a disinfectant, sodium hydrogen sulphite for removing chlorine residue if added and ferric chloride sulphate for flocculation.
The pre-treated feed water then is fed to the RO assembly. The RO assembly consists of two passes. The first stage or pass contains four racks with a high-pressure pump for each. The pre-treated water exit from the cartridge filters is fed to first stage by means of four high pressure pumps coupled to a recovery turbine to recover about 30% of its energy requirement. The permeate of the first pass is collected in two inter-connected buffer tanks, and then it is fed to two racks of a second pass by mean of two other high-pressure pumps.

The product of the first stage is recovered by 85% using the second pass and collected in an intermediate tank for further post treatment. The brine stream from the second pass is recycled back and combined with the feed water of the first stage after the cartridge filter. The product will be sent through a degasifierfor removing carbon dioxide and the final product treated by sodium hydroxide for pH adjustment and chlorinated by calcium hypochlorite before reaching the final storage tank [4].

3. A comparison between suggested membrane elements

Several membrane types developed by different manufacturers were evaluated based on commercially available RO process design softwares to predict the performance of Tajoura SWRO plant, optimizing membrane selection and operating conditions. Additionally, an estimation of water production quantity and quality from a given input parameters. Such of these programs are FilmTec (ROSA), Hydranautics (IMSDesign) and Toray Industries (TorayDS).

Table 2: Comparison between suggested and installed membranes.

Company Name	Koch	Toray	Hydranautics	DOW Filmtec
Design software		TorayDS	IMS design	ROSA
Configuration	1 stage	1 stage	1 stage	1 stage
No. of PVs	180	150	150	150
No. of membranes	1,080	900	900	900
No. of membranes per PV	6	6	6	6
Nominal diameter, inch	8	8	8	8
Membrane model	TFC 2822SS-360	TM820V-440	SWC6 MAX	SW30HRLE-440i
Max. operating pressure, bar	82.8	83	83	83
Working pressure, bar	55	53	50.8	54.92
pH	8	8	8	8
Maximum temperature,oC	45	45	45	45
Feed flow, m^3/d	34,285	34,285.7	34,285.7	34,285.71
Permeate flow, m^3/d	12,000	12,000	12,000	12,000.12
Design salt rejection, %	99.6	99.8	99.6	99.7
Recovery, %	35	35	35	35
Permeate salinity, mg/L	> 200	164.6	276.1	98.92
Feed salinity, mg/L	36,204	37,978.26	37,980.65	37,993.95

A permeate salinity goal of less than 300 mg/L was achieved for all the suggested membranes. Table 2 shows a performance comparison of different membranes to validate high productivity, less salt passage, lower energy consumption that will contribute in reduction of the unit water cost of Tajoura SWRO plant. The membranes and the suppliers related to are listed below:

- DOW Filmtec (SW30HRLE-440i);
- Toray and (TM820V-440), and
- Hydranautics (SWC6 MAX).

4. Unit product cost

The unit product cost decreased continuously over the years due to developments occurred in membrane productivity with less energy consumption. An economic evaluation analysis was achieved based on the calculation done by Element Value Analysis (EVA) tool that has been added to ROSA 9.1 program. The attained results are shown in table 3, which show very close values of the capital estimation of membrane elements, energy expenses, membrane replacement expense, operating expense and the water cost net present value (NPV). The earlier expenses were calculated in parallel with optimization of Tajoura SWRO plant. The following parameters should be taken into considerations:

- Production capacity (m^3/h) = 500 (12,000 m3/d)
- Permeate recovery (%) = 35
- Interest rate (%) = 8
- Power cost (L.D. kWh)= 0.068

The plant lifetime expected to be 25 years according to the latest refurbishment done by a Canadian company Jadmedic in 1998 [3], an interest rate of 8 % and unit power costs of 0.068 L.D./kWh. All estimations based on common market prices in early 2016.

Table 3: Estimated water cost.

Projection Results			
Permeate production (m^3/h)	500	500	500
Feed pressure (bar)	53	50.8	54.92
Concentrate pressure (bar)	52	49.3	53.37
Recovery (%)	35.00	35.00	35.00
Capital Expense			
Membrane Model	TM820V-440	SWC6 MAX	SW30HRLE-440i
Company Name	Forever Pure Place	Forever Pure Place	Watersurplus
Total elements	900	900	900
Element cost ($/element)	975.00	846.40	754.00

Capital for elements ($)	877500.00	761760.00	678600.00
Capital ($/m³)	0.01	0.01	0.01
Operating Expense			
Pumping power (kW)	2703.20	2639.7	2741.6
Pump specific energy (kWh/m³)	5.47	5.28	5.48
Brine energy recovery (kWh/m³)	-122.41	-122.41	-122.41
Net energy consumption (KWh/m³)	127.88	127.69	127.89
Net energy cost ($/yr)	22851893.03	22816832.14	22851893.03
Energy expense NPV (Net Present Value) ($)	203288847.88	243564576.44	243938843.61
Energy expense ($/m³)	86.96	86.82	86.96
Membrane replacement cost			
Replacement rate (%/yr)	15	15	15
Replacement price ($/element)	975.00	846.40	754.00
Replacement cost for elements ($/yr)	131625.00	114264.00	101790.00
replacement membrane NPV ($)	1405067.42	1219742.63	1086585.47
Membrane replacement expense ($/m³)	0.32	0.28	0.25
Operating expense subtotal			
Operating expense NPV ($)	245343911.02	244784319.07	245025429.08
Operating expense per m³	87.28	87.10	87.20
Total			
Cost NPV ($)	877500.00	761760.00	678600.00
Life Cycle Cost ($/m³)	0.01	0.01	0.01
Total System			
Operating expense NPV ($)	245343911.02	244784319.07	245025429.08
Cost of water NPV ($/m³)	2.25	2.24	2.24

5. Results and discussion

DOW Filmtec (SW30HRLE-440i) was selected as a candidate membrane for the next membrane replacement because the permeate salinity is 98.92 ppm, which was the lowest permeate salinity achieved compared by the other membranes. Furthermore, the number of membrane elements of the first stage were decreased from 1080 to 900 elements, thus, decreasing the next membrane replacement cost and /the number of throwing away membranes. Consequently, the number of pressure vessels of the first stage can be decreased from 180 to 150 (30 PVs extra), as well as the first stage racks are decreased from four racks to three racks. The earlier results don't include the second pass of the plant. Therefore, the second pass can be used for any other purposes.

If the extra 30 pressure vessels are comprised, the product capacity can be increased from 12,000 m3/d to 14,300.15 m3/d with a salinity of 99.59 mg/L, which is still smaller than the salinity achieved by the first stage of the current installed membranes taken into consideration the feed pressure within 54-55 bar, see detailed design results in table4.Finally, the specific energy consumption decreased from 8.492 to 5.48, then to 5.47 kWh/m3, if the extra PVs are used, the earlier results are not including ERD and can be less than 2 kWh/m3 if modern ERDs are used.

Table 4: Detailed design results of using all the extra pressure vessels of the 1st stage

Company Name	Koch	DOW Filmtec	DOW Filmtec
Design software used		ROSA	ROSA
Configuration of PVs	1 stage	1 stage	1 stage
No. of PVs	180	150	180
No. of membranes	1,080	900	1,080
No. of membranes per PV	6	6	6
Nominal diameter, inch	8	8	8
Membrane model	TFC 2822SS-360	SW30HRLE-440i	SW30HRLE-440i
Max. operating pressure, bar	82.8	83	83
Working pressure, bar	55	54.92	54.77
Feed flow, m^3/d	34,285	34,285.71	40,857.14
Permeate flow, m^3/d	12,000	12,000.12	14,000.15
Concentrate flow, m^3/d	22,285	22,285.59	26,556.99
Design salt rejection, %	99.6	99.7	99.7
Recovery, %	35	35	35
Permeate salinity, mg/L	> 200	98.92	99.59
Feed salinity, mg/L	36,204	37,993.95	37,993.95
Specific energy consumption (kWh/m^3)	8.492	5.48	5.47

6. Conclusions

The productivity of the plant was increased with lower energy consumption and less number of membrane elements and pressure vessels (PVs)with insignificant modification to the piping system of the plant if needed. For reasonable comparison, the recovery of the plant was not increased to avoid massive modification to the plant. Additionally, the plant can be optimized to decrease the unit product cost to less than 2 kWh/m3 by replacing a conventional pretreatment and the energy recovery device with up-to-date

techniques. In conclusion, latest improvements in membrane technology have made SWRO desalination more attractive because they had demonstrated significant enhancements in the rejection performance and the productivity of seawater reverse osmosis at lower feed pressure and less number of elements and pressure vessels, which will contribute in reduction of desalted water price, consequently, resulting in great improvement of the plant performance.

References

[1]. H. Iskandar, M. Zhang, and J. Steven, "Simulation and Economic Optimization for a Brackish-Seawater Mixed Feed Reverse Osmosis Process Iskandar", Singapore.

[2]. U. Ezzeghni, and M. El-Bourawi, "Exergy analysis of a 10,000 m^3/day Tajoura SWRO desalination plant", The 1st International Conference on Chemical, Petroleum, and Gas Engineering (ICCPGE 2016) 20th – 22th December 2016, Alkhoms-Libya.

[3]. El-Azizi, and A. Omran, "Design criteria of 10,000 m^3/d SWRO desalination plant of Tajura, Libya", Desalination, vol. 153, pp. 273-270, 2002.

[4]. M. Aboabboud, S. Elmasallati, and Y. Albriki.,"Tajoura reverse osmosis seawater desalination plant operating and maintenance experience", Desalination, vol. 203, pp. 119-133, 2007.

[5]. M. Ashour, and S. Ghurbal, "Economics of seawater desalination in Libya", Desalination, vol 165, pp. 215–218, 2004.

Feasibility Study of Cardboard Waste Recycling

Mahdi Esmieo[1], Moad Shaklawon[2], Omar Shaneb[3]
[1]mahdi.esmieo@gmail.com, [2]moad_379@yahoo.com, [3]omar_shaneb@yahoo.com
[1, 2, 3]Department of Industrialengineering, College of Industrial Technology - misurata, Libya

ABSTRACT

Waste management and utilization strategies are major concerns in several countries. Cardboard recycling is a common technique for treating Paper waste, as production recipe contains waste mass by 80%, printed paper contains toxic substances that are used in the manufacture of inks and colors, and their disposal by incineration produces toxic fumes as well as carbon in the form of small grains attached to the air and attack the human respiratory system. In most developed countries where land is scarce and the environmental controls are strict, environmental policies tend to reduce landfill disposals as much as possible. In this paper a feasibility study of cardboard waste recycling in Misurata has been conducted. The paper explores the technical options available for a such recycling. Determine the factors that are considered important for the economic success of the project. In addition, a feasibility study has been conducted. Several economic indicators such as payback period, internal rate of return have been estimated. The results have shown that cardboard recycling is economically feasible. Furthermore, a sensitivity analysis for the important factors have been conducted in order to show their effect on the feasibility that system.

Keyword— Cardboard, economic, recycling, feasibility study, waste.

1. Introduction

Rapid expansion of industry, urbanization and increasing of population, especially in large cities like Misurata, has dramatically increased the amount of solid waste generated in Libya. However, issues related to sound municipal solid waste management – including waste reduction and disposal – have not been addressed adequately. In addition, the collection and the separation treatment of solid waste are still neglected. In the last few years, the Environmental General Authority in Libya has worked to create regulations and instructions for waste management, but up to now they are still under development [6]. This belongs to the fact that there is only little information available regarding recycling, handling and disposal of waste. Therefore, an appraisal of the current situation regarding solid waste management in Libya is required [1]. Cardboard recycling is a common practice of solid waste management in European countries, for it renders the economic success of the project. On the contrary, most of the solid waste in Libya is still dumped. Municipal solid waste contains valuable cardboard that could be recycled.

Solid waste management and cardboard waste recycling (CWR) have attracted significant attention and great deal of research in several countries such as Denmark [8], America [7], Australia [4], South Africa [5], and India [2]. Rare studies on solid waste have been conducted in Libya indicating that no proper management is

existing yet [3,6]. Thus, work is still required to establish a database, information and statistics on CWR, collection, transportation and treatment. In this paper, economic indicators was investigated and its factors that are considered important for the economic success of the project was determined.

2. Cardboard Recycling.

Cardboard is one of the most commonly used materials for packaging and comes in a variety of forms. Also referred to as corrugated cardboard. It is a recyclable material that could be recycled by cardboard factories to save money. It is a recyclable material that could be recycled by cardboard factories to save money Instead of being disposed as landfill or burn them. Cardboard recycling is the reprocessing and reuse of thick sheets or stiff multi-layered papers that have been used, discarded or regarded as waste. Products that are made from recycled cardboard include more cardboard boxes, egg cartons and even kitty litter.

3. Study area

Misurata is the third largest city in Libya. It serves a community of about 400,000 people. The study has been conducted in the city of Misurata, which situated in the western north part of Libya as a case study. In this paper, CWR feasibility study in the city of Misurata has been investigated through an extensive survey contained information on collection, internal transport and treatment.

3.1. Waste collection, transportation and final treatment

Solid wastes generated at all zones are collected by municipal companies, and then transported to the final dumping site. There are three trans-shipment points in the city. The municipality has the responsibility for offsite transportation of the waste to the final disposal site. From daily to three times a week[6], the municipality labor collect the solid wastes from the on-site storage containers and transport them along with general domestic waste to open dumping sites outside the city. Generally, simple trucks and in some cases uncovered tractors are used for waste transportation[6]. These open tractors are passing within residential areas which increases the potential risk to the public and the environment. All domestic waste dispose, are in open dumping sites outside of the city[6]. In these open dumping sites, the waste is buried and sometimes combusted. Figure 1 shows the quantity of CW in one of the zones.

Figure 1: Waste collection in Misurata

Figure 2 depicts the qualitative analysis of solid waste in Misurata identifies organics as the major component (56%), followed by plastics (26.5%). This high plastic rate is due to the widespread use of disposables rather than the reusable for different purposes (e.g. bottles, packing materials and food bags). Whereas paper had the third highest percentage (8%) [6].

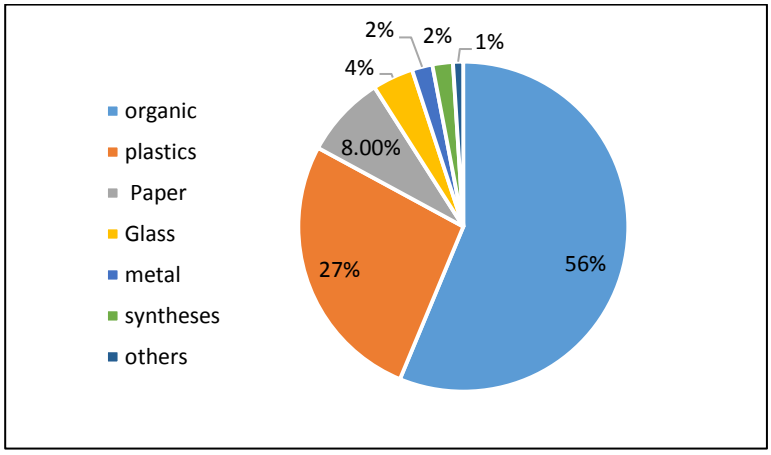

Figure 2: The qualitative analysis of solid waste in Misurata [6]

4. Feasibility Study

The present study was conducted through various field visits to several areas within the city of Misurata as well as cardboard factories in the city. This study is concerned with thefeasibility study of establishing a CR plant to produce egg dishes. The assumed plant capacity is 20 ton per month to produce 250,000 dishes(i.e. 1200 dishes per hour).

4.1. Raw materials

The raw material used in the recycling of cardboard depends heavily on the waste of paper and cardboard by up to 80%. To produce one ton of carton roll, the following quantities and materials shown in table 1 are required:

Table 1: Cardboard Waste in the city of Misurata

Material description	%
Corrugated Cardboard (Mixed Cardboard)	80 %
paper-making additives(pulp)	18 %
Chemicals& reagents	0.2 %
Abiatic acid	1.8 %

This industry needs a large amounts of water for the cleaning and forming process, and then the paper is re-dried until the percentage of water reaches only 6%, which is the percentage allowed in the carton. Thus, the weight of the egg dish is 80 g.

4.2. Cardboard Recycling Process

The cardboard recycling process involves a number of steps, including collection, transportation, sorting, processing into usable raw materials and finally using that raw material to produce new egg dishes products. At the reprocessing plant, cardboard and water are mixed together at high speed in a 'Turboflex Pulp Maker' to break up the cardboard into separate fibres. Contaminants such as staples, wires, plastics and strings are removed by passing the pulp through a cleaning and screening equipment. The pulp is then treated with chemicals and heated to loosen ink and glue so they can be washed out. The cleaned pulp is diluted with water and mixed with small amounts of paper-making additives. The paper is then turned into new Egg dishes products, using the same pressing and drying process used to make paper and cardboard from virgin materials.

In the refining stage, the pulp is beaten to make the paper fibers swell. In this process, egg dishesare obtained. When the goal is to produce white recycled paper, the pulp is bleached with oxygen or chlorine dioxide to make them brighter or whiteror coloring using other artificial colors.

4.3. Costs

4.3.1 Materials Cost

Table 2 shows the first year total materials cost. The total cost equals to the summation of materials feeaaccording to annual production capacity.

Table 2: Cost of materials

Material description	Quantity	Unit Cost, $	Contribution, $/20 ton
Mixed Cardboard	16 ton	70	1120
paper-making additives (pulp)	3.6 ton	272	979.2
Chemicals & reagents	40 kg	0.83	33.2
Abiatic acid	0.360 ton	363	130.68
Grand total per year			2263.08

4.3.2 Assumptions

- Recycling equipment's & installation cost= 99,000 $.
- Waste input to incinerator = 75% of the total waste.
- Depreciation rate = 5%.
- The yearly operational cost of the recycling plant includes utility costs water 28,500$ at a rate of 44 m^3 per month, electricity 12,000 Kw monthly, human resource costs shown in table 3, and other administrative costs, excluding equipment maintenance cost equal to 40,000 $.

Table 3: Cost of Employment

job description	Job Requirements	number	Salary$	Total salary $
Production Manager	project management	1	1500	1500
Production Supervisor	Supervision and control	1	1100	1100
Labor operation	Production & processing	5	800	4000
Grand total per				6600 /month

- The average population growth (for the last 30 years) equal to 2% [9].

5. Calculation and Results

The indices calculated are the yearly profit, net present value, and break-even point. Tables 4 and (5) explain the calculations for the first year. Table 2 illustrates the total quantity of waste collected each year.

Table 4: Waste generated

• **Possible waste per year**	
Cardboard waste per year	1500
Waste incinerated (75%)	1125
• **Ability**	
Time	8 hr/day
Capacity line	1200 pc /hr
Capacity	3,000,000 pc/year

Table 5 shows the first year total revenue. The total revenue equals to the summation of egg dishes selling revenue. The average price for dish equal to 0.30 $.

Table 5: shows the first year total revenue

Description	**Quantity**
costs	
Fixed Costs	36,000 $
• Variable Costs	
Operational Costs	427,800 $
Maintenance	40,000 $
Raw materials	27,156.9 $
Total Variable costs	494,956 $
Total costs	530,956 $
• **Revenue**	
Egg dishes(average price =0.30 $)	3,000,000*0.30
Total Revenue	900,000 $
Net Profit	306,190.1

Whereas: Contribution= unit price- unit variable cost.

Breakeven point= Fixed cost/contribution

Breakeven point=$\frac{36000}{0.30-0.20} = 360{,}000$

Figure (3) depicts the yearly profit of the plant. It is clear that the project loses only during the first 2 years under the given conditions.

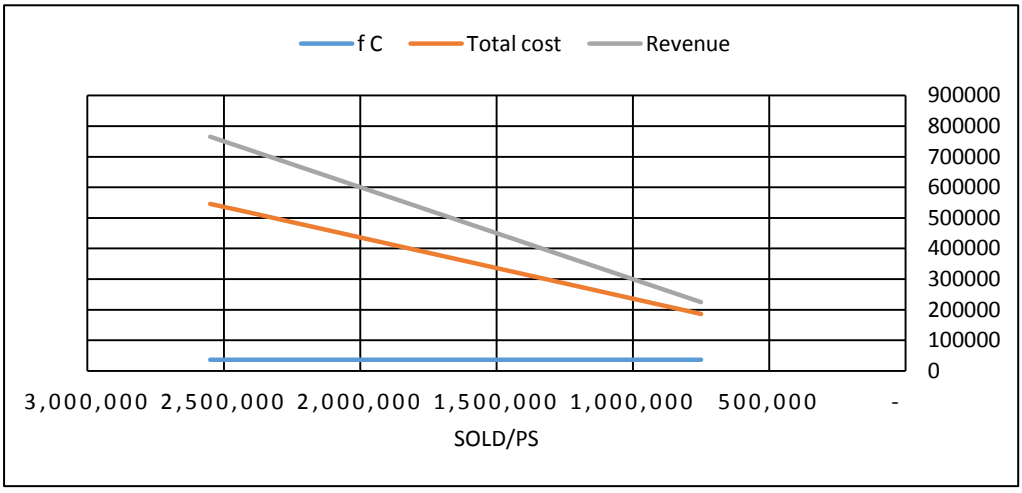

Figure 3: yearly profit

6. Conclusions

In light of the increasing importance for environmentally waste recycling while maintaining the proper stewardship of pollution and solid waste, CWR plants have the ability to become a vital part of the Libya industry. The result of the cost analysis indicates potential economic savings for the Recycling system in Misrata. It is suggested that a similar study should be undertaken focusing on other waste types so as to further underpin future waste management objectives in Libya.

References

[1]. Omran, A.Gebril, A. Pakir, Municipal Solid Waste Management in BENGHAZI (LIBYA): Current Practices and Challenges, *Environmental Engineering and Management Journal*, Vol.9, No. 9, 1289-1296, 2010.

[2]. Amitava Bandyopadhyay , "A regulatory approach for e-waste management: a cross-national review of current practice and policy with an assessment and policy recommendation for the Indian perspective", Int. J. of Environment and Waste Management , Vol. 2, No.1/2 pp. 139 - 186,2008.

[3]. Population in The city of Misurata 2014, Municipility of Misurata Report, 2014.

[4]. Joe Pickin, Paul Randell, "Australian National Waste Report 2016,"Department of the Environment and Energy, june, 2017.

[5]. Packaging Council of South Africa, "Design for Recycling for packaging and paper in South Africa," March, 2014.

[6]. Mohamed Sawalem, Ibrahim Badi, Suleman Aljamel, Evaluation of Solid Wastes for Utilisation in Biogas Plant in Libya – a Case Study, *IJESRT*, November, 2015.

[7]. Scott M. Kaufman, "ANALYSIS OF TECHNOLOGY AND INFRASTRUCTURE OF THE PAPER RECYCLING INDUSTRY IN NEW YORK CITY," Columbia University. May, 2004.

[8]. Hazel Fargher, Perry Franklin, Rachel Komara, "Increasing Paper and Cardboard Collection for Recycling in Denmark. May, 2015.

[9]. http://www.tradingeconomics.com/libya/population-growth-annual-percent-wb-data.html

Designing And Optimizing 10,000 m^3/day Conventional SWRO Desalination Plant

Usama Ahmed Ezzeghni[1]
[1]elzoghni@gmail.com
[1]Department of Desalination Researches, Nuclear Research Center, Libya

ABSTRACT

Desalination of seawater has been considered as one of the most promising techniques for supplying a fresh water in Libya. Reverse osmosis (RO) is one of the main technologies for big size desalination plants for the reason that it offers an ability of producing a high quality and quantity of fresh water from seawater with a minor specific energy consumption compared to the other thermal evaporation processes. This paper aims to collect and apply the most useful mathematical equations and software of designing a seawater RO desalination plant with a capacity of 10,000 m^3/day. Moreover, its pretreatment equipment such as sedimentation tank, high-pressure pump, multimedia and cartridge filters.

IMS design software developed by Nitto Hydranuatics Company used for designing and optimizing the membrane assembly of the suggested plant. Additionally, the energy recovery device (ERD) specification accomplished by the same earlier software. In addition, the recommended anti scalant dose predicted by PWT Pro Dose software.

The recovery of the plant increased to more than 40% with less number of membrane elements due to installing new advanced membranes (SWC6 MAX) developed by Nitto Hydranuatics Company. Moreover, pressure exchanger device recommended for the designed plant to decrease the specific pumping energy from 4.81 kWh/m^3 to 2.09 kWh/m^3, which saves more energy, thus, decreases the unit product cost of the plant.

Keyword— seawater desalination; reverse osmosis technique, plant design.

1. Introduction

The seawater desalination option is one of the most important strategic decisions for drinking water source in Libya, especially after growing the population and its gathering at the Libyan coast regions, which exceeds 1,900 kms. The option of using RO desalination technology is one of the most recommended technique, because of the efforts of the membrane's manufacturers in developing new membranes with high productivity and quality as well as, the efforts of ERDs manufacturers in reducing the specific energy consumption, by getting benefit of the wasted pressure of concentrated water. Additionally, advantages that make RO desalination as a competitor option compared to the other thermal desalination methods it can be operated and maintained easily with lower operating cost. Furthermore, design flexibility of the plant according to the available space. It should be noticed that the world's largest RO plant was built in Israel at a capacity of 333,000m^3/d [1].

From the vision of the developments in RO technology and its selection by many countries as a challenging option, this paper aims to design a reverse osmosis desalination plant with a production capacity of 10,000 m^3 / day based on seawater analysis sample of a Libyan coast (Tripoli city), the design includes selecting membrane type, calculation the number of membranes, pressure vessels and several pre-treatment equipment such as sedimentation tank, multi-media and cartridge filters, as well as, high pressure pump and energy recovery device.

2. Proposed Plant Description

The feed water is collected into a sedimentation tank for removing the largest particles and then pumped by transfer pumps through a multimedia filters containing three types of media layers (anthracite, sand and garnet)to reduce the Silt Density Index (SDI) and turbidity to less than 3% and one NTU, respectively. Then a filtered water to be passed through a cartridge filters containing filters with pore size not exceeding 5 microns. The filtered feed water is ready to be pumped through the membrane assembly by means of high-pressure pumps. The desalinated water is then delivered to the product storage tanks and the concentrated water is returned to seawater in some different discharge ways to avoid any environmental problems. Energy recovery devices will be installed in the concentrated stream to reduce the rate of specific energy consumption and thus, reduce the cost of fresh water production. Figure 1 shows the overall schematic diagram of the projected plant.

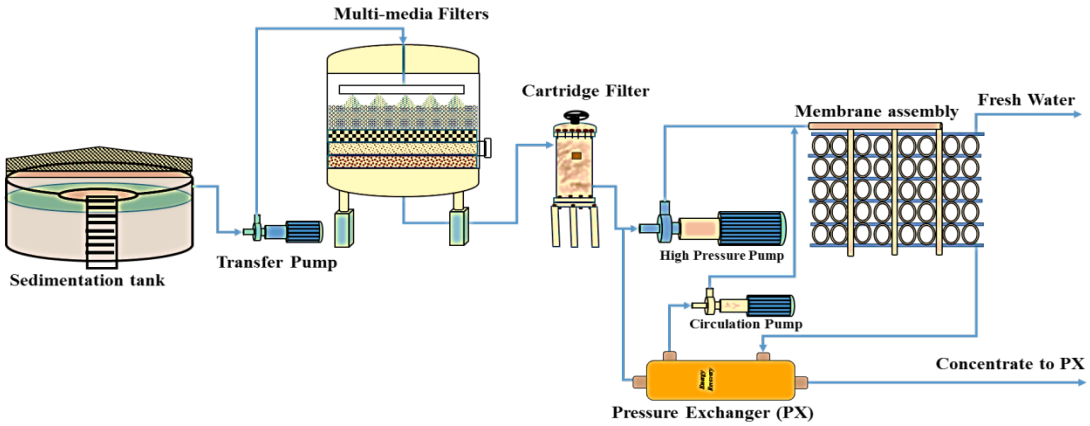

Figure 1: General schematic diagram of the proposed plant.

3. Design Calculations

In this section a detailed calculations for all the equipment shown in Figure 1 will be covered in the next subsections, it should be noticed that, the design calculations presented down here are based on seawater analysis of Libyan offshore. The most important required chemical components for plant design are shown on Table 4.

3.1. Clarification (Sedimentation) Tank

The clarification is the first step in feed water pre-treatment section, it is used to give the opportunity for removing the particles that may block the filtration system as well as, to add some chemicals such as disinfectants, coagulants and flocculants if needed.

Sedimentation chamber rise rate and slow mix chamber detention time are the most important factors utilized in sizing clarification tanks.

- Detention Time

Detention time is the theoretical average length of time the water is in the clarifier tank. Detention time depends on two following parameters:

- Volume of the clarifier, and
- Water flow rate.

The detention time can be attained as follows:

$$D_t = \frac{V_c}{F} \quad (1)$$

where

D_t= Detention time

V_c= Volume of clarifier

F= Flow rate

Where the typical detention time of most clarifiers varies between 20 to 30minutes[2], therefore, the volume of slow mix chamber can be calculated as follows:

$$V_{smc} = F \text{ x} D_t \quad (2)$$

where

V_{smc}= Volume of slow mix chamber

V_{smc} = 535.465 m^3 (Based on 30 minutes detention time).

$$A_{smc} = \frac{\mathrm{V_{smc}}}{\mathrm{h_{smc}}} \quad (3)$$

where

A_{smc} = Slow Mix Chamber Area

h_{smc} = Slow Mix Chamber Height

Where typical height recommended by different companies are between 3 and 6 m.

A_{smc} =146.39 m^2

$$(d_{smc})^2 = \frac{(4)*(A_{smc})}{3.14} \quad (4)$$

where

d_{smc} =Slow Mix Chamber Diameter

$(d_{smc})^2$ =186.48 m^2

d_{smc} =13.66 ~ 14 m

- Rise rate

Rise rate is a mainparameter in defining the clarifier efficiency. It is also well-known as the surface loading rate, surface settling rate, or overflow rate. Rise rate is defined as the flow per unit surface area of the clarifier, and it varies between 25 to 75 m^3/d per m^2 [2].

$$A_{TWS} = \frac{F_C}{R_R} \quad (5)$$

where

A_{TWS} = Treated Water Surface Area.

F_C = Clarifier Flow rate

R_R = Rise rate

A_{TWS} =438 m^2

Therefore, the area of the total clarifier can be calculated as follows:

$$A_{TC} = A_{TWS} + A_{smc} \quad (6)$$

where

A_{TC} =Total Clarifier Area

A_{TC} =584.41m^2

$$(d_c)^2 = \frac{(4)*(A_{TC})}{3.14} \quad (7)$$

where

d_c = Clarifier diameter

$(d_c)^2$ =744.47 m^2

d_c ~ 27 m

3.2 Transfer Pumps

Transfer pumps are used to pump the clarified seawater to the pressure required by multimedia filters, which can be calculated as follows:

Outlet pressure = Required pressure at the top outlet (4.5 bar)

Gross feed flow to filtration plant = 1070.93 m^3/hr

Four pumps are recommended to pump the raw water to filtration system, three in operation and one standby, to avoid plant shutdown during maintenance duties.

Feed flow per pump = 356.97 ~ 360 m^3/hr

Where the pressure and feed flow to filtration plant are known, the transfer pumps can be chosen using a coverage chart, which makes it possible to make a preliminary selection through a group of pump sizes based on a specific impeller speed.

3.3 Multi-Media Filters

The dimensions of the multi-media vessels are calculated as follows:

- Filter Dimensions and Media Quantities
- Diameter

The vessel diameter is based on the normal service flow rate, the service water requirement and the relationship between area and diameter.

$$F_f = \frac{F_{fp}}{N_f} \quad (8)$$

where

F_f = Feed flow per filter

F_{fp} =Feed flow to filtration plant

N_f =Number of filter units

F_f =133.87$\frac{m^3}{hr}$

$$A_f = \frac{F_f}{F_{sd}} \quad (9)$$

where

A_f = Required cross sectional filtration area per filter

F_f =Feed flow per filter

F_{sd} = Service down-flow rate

A_f =7.44 m^2

$$ID \left(\frac{Af*4}{\pi}\right)^{\frac{1}{2}} \quad (10)$$

where

ID = Required internal diameter

= 3.08 m

- Media Quantities

Table 1 shows the filtering material layers for each media for the designed plant. A typical multi-media filter has the following top to bottom layer configuration (media bed depths shown are the minimum allowed).

- (0.45 - 0.60 m) of anthracite;
- (0.2 – 0.3 m) of sand, and
- (0.10 – 0.15 m) of garnet [3].

Table 1: Filtering material

Filtering material layer	Grain size, mm	Layer depth, m (in)	Media quantity(m^3)
Anthracite	0.85–0.95	0.6 (23.6)	4.5
Sand	0.45–0.55	0.3 (11.8)	2.2
Supporting layer (Garnet)	0.3	0.15 (5.9)	1.1

$Q_M =$

$$L_T * \frac{(ID)^2 * \pi}{4} \quad (11)$$

where

$Q_M =$ Media Quantity

$L_T =$ Layer Thickness

Straight Shell Height

A multi-media filter requires 50% minimum freeboard to allow bed expansion during the backwash cycle.

$\text{Straight}_{\text{Shell Height}} = (\text{Depth}_{\text{Anthracite}} + \text{Depth}_{\text{Sand}} + \text{Depth}_{\text{Garnet}}) \text{x} (1 + 50\% \text{ Freeboard}) \text{Straight}_{\text{Shell Height}} =$ 1.58 m

- Service and Backwash Performance per Filter
- Service Flow Rate

The allowable flow rate through a multi-media filter is 290 - 530 $m^3.d^{-1}/m^2$. Normal service flow is 290 - 350 $m^3.d^{-1}/m^2$. Flow rates of 470 - 530 $m^3.d^{-1}/m^2$should only be used for short periods of time, when one filter is being cleaned and the other filters must temporarily process the higher flow rate. Flow rates above 530 $m^3.d^{-1}/m^2$must not be used, as impurities will be driven through the media bed.

Gross water throughput per filter unit per cycle = Feed flow per filter $*$ Backwash frequency (13)

Gross water throughput per filter unit per cycle= 3212.79 m^3

- Backwash Flow Rate

The backwash flow rate is an essential parameter to expand the filter media depth via 30%,it depends on temperature, because the pressure pushing up the filter media is a function of the water viscosity, which decreases with increasing temperature.

Backwash flow rate (without air)=Required cross-sectional filtration area per filter x Water up flow during backwash (without air)(14)

Backwash water flow rate(without air)=$260.4 \frac{m^3}{hr}$

Backwash time (without air) = 10 min

$$\text{Backwash water volume (without air)} = \frac{\text{Backwash water flow (without air) x Backwash time without air}}{60} \quad (15)$$

Backwash water volume(without air)= $43.38 m^3$

$$\text{Raw water volume used to rinse} = \frac{\text{Feed flow per filter} \times \text{Rinse time (at service flow)}}{60} \quad (16)$$

Rinse time (at service flow) = 5 min

Raw water volume used to rinse = 11.16 m^3

Water up-flow during backwash - together with air= Air up-flow during backwash + Water up-flow during backwash - without air (17)

Water up-flow during backwash - together with air= 85 m/h

Backwash water flow rate (with air) = required cross sectional filtration area per filter ∗ Water up-flow during backwash - together with air (18)

Backwash water flow rate (with air) = 632.4 m^3/hr

$$\text{Backwash water volume (with air)} = \frac{\text{Backwash water flow (with air)} * \text{Backwash time with air}}{60 \text{ min}} \quad (19)$$

Backwash time with air = 5 min

Backwash water volume (with air) = 52.68 m^3

Total filtered water volume required for backwash=Backwash water volume (without air) + Backwash water volume (with air) (20)

Total filtered water volume required for backwash= 96.06 m^3

Total filtered and raw water required for backwash= Raw water volume used to rinse + Total filtered water volume required for backwash (21)

Total filtered and raw water required for backwash = 107.22 m^3

- Rinse Flow Rate

To adequately rinse the media bed, the flow rate must be at least 350 $m^3.d^{-1}/m^2$for 1 bed volume.

Rinse Flow = Rinse Flow Rate ∗ $(\text{Diameter})^2 * \pi/4$ (22)

Rinse Flow = 2607.71 m^3/d

- Air Scour Flow

For an effective air scour, the air flow rate of the recommended design blower must be at least 50 $m^3.hr^{-1}/m^2$(3 SCFM/ft^2) at 0.5 bar.

Air flow-rate requirement = Required cross-sectional filtration area per filter ∗Air up-flow during backwash (23)

Air flow-rate requirement = 371.85 m^3/hr

- Net Production per Filter

Net production of filtered water = Gross water throughput per filter unit per cycle- Total filtered water volume required for backwash (24)

Net production of filtered water = 3116.73 m^3

Time of production of net volume filtered water = Backwash frequency-(Backwash time with air+ Backwash time without air+ Rinse time (at service flow))/60(25)

Time of production of net volume filtered water = 23.67 hr

Net production rate of filtered water = Net production of filtered water/ Time of production of net volume filtered water (26)

Net production rate of filtered water =131.69 m^3/hr

Net production rate = Net production rate of filtered water ∗ Number of filter units (27)

Net production rate = 1053.54 m^3/hr

3.4 Cartridge Filters

The filter elements of a cartridge filter are selected based on two measures, the nominal micron rating and the service water flow rate. The standard diameter of the filter elements is 2.5 inches. The standard length of the filter elements can be either 30 or 40 inches. The choice of 30-inch or 40-inch cartridges often depends on the availability of standard filter housings. In general, there is not much cost difference between housings for 30-inch or 40-inch cartridges, so if there are no other constraints a 40-inch cartridge system generally is the most economical.

- Filter Element Quantity and Height

The number of 10" lengths of cartridge required for a system can be calculated as follows:

Quantity = Service water requirement / Flow per 10-inch length (28)

(10-inch lengths) (at available pressure drop)= 1170.6~1171element

Using a filter element that can support 0.9 m^3/h per psid per 10-inch length, the quantity of filter elements for the entire system can be calculated as follows:

$$\text{Quantity (40-inch lengths)} = \frac{\text{Quantity (10-inch lengths)}}{\text{Quantity (10-inch elements per element)}} \quad (29)$$

= 292.75 ~ 293 element

No. of cartridge vessels = Quantity (40-inch lengths) / Quantity per vessel (30)

= 5.86 ~ 6 cartridge vessels

Feed flow per filter = Service water requirement / No. of cartridge vessels (31)

Feed flow per filter = 175.59$\frac{m^3}{hr}$

3.5 High Pressure Feed Pump

Selection of the high pressure pump (HPP) depends on the minimum and maximum flow rates, discharge pressure required, suction pressure available and the maximum temperature, where these parameters can be obtained from IMSDesign detailed report. Table 2 shows design parameters of the high pressure feed pumps.

- Variable Speed Pumps

Variable speed motors are used to control motor operating speed. This allows a pump to operate at different speeds and thus reduce pump size and/or number of stages and eliminate the need for a speed-increasing

gearbox in some applications. High-speed pumps are especially useful for high head, low-flow applications and the ability to alter pump speed allows operation over a wide range of conditions. Variable speed drives also provide a pump system with a built-in soft start and stop to prevent shocks to the system and water hammering to the membranes.

Table 2: High pressure pump design parameters

Power Calculation (without ERD)	
Pump pressure (bar)	52.9
Product flow m^3/d	10000
Pump flow m^3/d	25000
Pump efficiency %	83
Motor efficiency %	93
VFD efficiency %	97
Power/stage/pass Kw	2004.4
Brake horse power BHP	2686.8
Total pumping power kW	2004.4
Pumping specific energy kwh/m^3	4.81

3.6 Reverse Osmosis Membrane System

The following steps were used to design the membrane assembly of the SWRO desalination plant.

- Selection of Membrane Element Type

Elements are selected according to feed water salinity, feed water fouling tendency, required productivity and salt rejection, as well as energy requirements, where the membrane selected for the designed plant is SWC6 and IMS Design software were used to give the information required for the designed system. This software is available on the Website of Hydranautics Company. Table 3 lists all the specifications of SWC6 MAX membranes.

Table 3: Membrane specifications(SWC6 MAX)

Performance	
Permeate Flow	50 m^3/d
Salt Rejection	99.8% (99.7% min)
Applied Pressure	55 bar
Type	
Configuration	Spiral Wound
Membrane Polymer	Composite Polyamide
Membrane Active Area	40.8m^2

Application Data	
Maximum Applied Pressure	83 bar
Maximum Chlorine Concentration	< 0.1 ppm
Maximum Operating Temperature	45 °C
pH Range, Continuous (Cleaning)	2-11
Maximum Feed water Turbidity	1.0 NTU
Maximum Feed water SDI (15 mints)	5
Maximum Feed Flow	17.0 m^3/h
Minimum Ratio of Concentrate to Permeate Flow for any Element	5:1
Maximum Pressure Drop for Each Element	15 psi

- Selection of Average Membrane Flux

The flux design selection depends on an experimental data, experience where the typical membrane design fluxes based on the feed supply. The recommended design flux for this plant is 13.5 l/m^2-h.

- Number of Elements Needed

The number of elements N_E can be calculated using equation (32) by dividing the design permeate flow rate Q_P by the design flux f and by the membrane active area of the chosen element S_E (ft^2 or m^2).

$$N_E = \frac{Q_P}{f.S_E} \quad (32)$$

where

N_E = Total number of elements.

Q_P =required permeate flow.

S_E = Membrane active area, and

f = Average flux.

N_E = 756 membrane elements

- Number of Pressure Vessels Needed

For this plant, 6-element vessels will be used, so, the number of pressure vessels will be:

$$N_V = \frac{N_E}{N_{EpV}} \quad (33)$$

where

N_V =Total number of pressure vessels.

N_E = Total number of elements; and

N_{EpV} = No. membrane element per PV.

N_{EpV} = 756 / 6 = 126 PVs

- Number of stages selection

The stage number of the RO plant a describes the number of pressure vessels in series, where the inlet feed water will goes through till it leaves the desalination plant as brine. Typically, the number of serial element positions is linked with the system recovery and the number of stages, for the designed SWRO plant the recovery is 40% and one stage plant will be selected to avoid the expected scaling problems and the uncaring in operation and monitoring of the plant. The RO stage consist of two parallel RO racks with 126 pressure vessels. Each pressure vessel contains six spiral wound RO membranes.

Table 4: Seawater analysis (Libyan offshore sample)

PH	8	CO_3	12.653	mg/l
Cations	mg/l		Anions	mg/l
Ca	455		HCO_3	163
Mg	1427		SO_4	2915
Na	11600		Cl	20987
K	419		F	0
NH_4	0		NO_3	0
Ba	0		PO_4	0
Sr	0		SiO_2	2
Cal. TDS	37981		B	0

- Membrane Systems Report

Integrated Membrane Solutions Design (IMS Design) software was used to design, optimize and analyze the performance of the designed plant and testing the configuration according to seawater analysis shown in Table 4. The design parameters of the designed desalination plant are presented in Table 5.

Table 5: Design parameters of the plant

Company Name	Hydranautics
Design software used	IMS design
Pressure vessels (PVs) configuration	1 stage
Permeate recovery %	40
Average flux, lmh	13.5
No. of pressure vessels (PVs)	126
No. of membranes	756
No. of membranes per (PV)	6
Nominal diameter, inch	8
Membrane model	SWC6 MAX
Max. operating pressure, bar	83
Working pressure, bar	52.9
Ph	8
Maximum temperature, ^oC	45
Feed flow, m^3/d	25000
Permeate flow, m^3/d	10000
Concentrate flow, m^3/d	15000
Design salt rejection, %	99.6

Concentrate salinity, mg/l	63119.2
Permeate salinity, mg/l	295.51
Feed salinity, mg/l	37981

3.7 Energy Recovery Devices (ERD)

In SWRO desalination plants, about 55 to 60% of the feed pressure leaves the plant with approximately 870 psi (60 bar) through the brine stream. This energy can be recovered to decrease the specific energy consumption of the plant using turbocharger, pelton wheel and pressure exchanger.

Table 6: Pressure exchanger parameters

Parameter	Power Calculation (without PX)	Power Calculation (with PX)	
	Pass 1	Pass 1	ERD boost
Pump pressure (bar)	52.9	54.1	1.7
Product flow m^3/d	10000	10000	-
Pump flow m^3/d	25000	10153.9	14846.1
Pump efficiency %	83	83	83
Motor efficiency %	93	93	93
VFD efficiency %	97	97	97
Power/stage/pass Kw	2004.4	832.6	37.2
Brake horse power BHP	2668.8	1116	49.9
Total pumping power kW	2004.4	869.8	
Pumping specific energy kwh/m^3	4.81	2.09	

The high-pressure concentrate is fed into the energy recovery device, where a pressure exchanger (PX) will be suggested for this plant. This PX supplies about 94 % of the high-pressure pump's energy requirement. Table 6 shows power calculation of the designed plant with and without pressure exchanger, which is achieved by IMSDesign software.

3.8 Chemical Requirements

Most of SWRO desalination plants need some chemicals to be added to the feed water before passing through the membrane assembly. The chemicals are dosed based on the feed water analysis, there are several chemicals added to the feed water such as disinfectant, coagulant and flocculants, sodium meta-bisulfide if chlorine is injected to the feed water. In this design the feed water needs to be treated with antiscalant to prevent the scales accumulation on the membranes surface. A detailed information will be described in the following subsection.

- Antiscalant

For dosage rate calculation of antiscalants, the manufacturers should be contacted. Overdosing should be avoided. Attention must be taken that no significant amounts of cationic polymers are existing once dosing

an anionic scale inhibitor, because precipitation reactions may happen, similarly may occur, by dosing a negatively charged antiscalant and cationic poly electrolytes or multivalent cations (e.g., aluminum or iron). In SWRO plants working with total dissolved solids of more than 35,000 mg/L, scaling is not that problematic as in brackish water desalination plants BWRO since the permeate recovery of the SWRO plants is limited to 30-45%, but still, an antiscalant is recommended if operating the SWRO plants with a permeate recovery of 35% or more[4].

A computer model developed by Professional Water Technologies, Inc. was used to determine the performance of an antiscalant (TITAN ASD 200 SC LIQUID SUPER CONC) supplied by the same antiscalant manufacturer. Table 7 shows the results ofthe computer model indicate that an antiscalant dose of 0.2 mg/l at the feed side and 0.3 mg/l at the concentrate side would effectively control membrane scaling based on the input feed water chemistry and a design recovery of40 percent.

Table 7: The suggested antisclant dosage rate

Product Selection	
TITAN ASD 200 SC LIQUID SUPER CONC	
Recommended Dose Rates	
Feed (mg/l)	Concentrate (mg/l)
0.2	0.3
Est. Product usage (100%)	
kgs/day	mt/yr

4. Results and Discussion

The plant designed with advanced SWC6 MAX membranes increases the productivity of the plant with less number of membrane elements and pressure vessels, this design was compared with an existing SWRO plant in Tajoura, with the same capacity, it is found that the number of elements, as well as the number of pressure vessels were decreased from 1080 element to 756, which will decrease the cost of the next membrane replacement as well[5].Furthermore, the pumping specific energy of the HPPs were decreased due to installation of PX with a hydraulic efficiency in the rangeof94-96%, in addition to that the overall recovery were increased from 35% to 40% and it can be increased to more than 50%, but the researchers suggested 40% recovery to avoid scaling, fouling problems and decreasing chemicals consumptions. As far as the pressure exchanger was selected as ERD for designed SWRO plant, the pressure exchanger conversion efficiency of more than 94%, and therefore, the unit designed saves more than 60% of the destroyed power, which will decrease the unit product cost.

5. Conclusion

In conclusion, the SWRO desalination plant were designed and optimized using IMSDesign software. Furthermore, some mathematical equations were collected and applied for designing several pretreatment equipment. Therefore, the design was prepared and ready for development by other researchers or students; whatever other ideas of SWRO plant design are becomes recognizable.

The optimal design of SWRO process has been addressed in this work using an advanced membrane (SWC6 MAX) developed by Hydranautics Company. The design of plant with a new SWRO element had improved permeability and quality; these features provide system designers with new options to reduce the capital cost of the system as well as, the operating cost. Although the new low energy membranes run at lower pressure.

The greatest sensible and applied way to rise efficiency or decrease the power input of the designed plant meaningfully seems to be replacing the throttling valve and old turbine or reverse running pumps on the brine stream by modern pressure exchanger, the use of a pressure exchanger as energy recovery system enables decreasing the total pumping power of the reverse osmosis desalination plants.

References

[1]. N. Voutchkov, Desalination engineering: planning and design. New York: McGraw-Hill, 2013.

[2]. FSC Architects &Engineers, Class II Water Treatment Plant Operator Program Manual, (2003).

[3]. N. Voutchkov, Considerations for selection of seawater filtration pretreatment system, Desalination 261 (2010) 354–364.

[4]. Technical Manual, Dow Water & Process Solutions, FILMTEC Reverse Osmosis Membranes, June, (2004).

[5]. I.M. El-Azizi and A.A. Mohamed Omran, Design criteria of 10,000 m3/d SWRO desalination plant of Tajura, Libya. Desalination, 153 (2003) 273–279.

Wind Energy Reliability Analysis based on Monte Carlo Simulation Method

Khaled Abdusamad
kmatok70@gmail.com
Mechanical Engineering Department, Garaboulli Engineering Faculty, Elmergib University, Libya

ABSTRACT

Reliability is defined as the probability that an item will continue to achieve its intended function without failure for a specified period of time under operation conditions. The challenges of addressing energy supply and climate change are expected to drive the growth of renewable-based electrical generation such as from wind. Consequently, worldwide growth in wind energy is expected to increase as more wind turbines are installed to meet clean electricity demand and decrease the usage of fossil fuel. However, wind has risks and uncertainties that need to be addressed, perhaps the most significant challenge wind speed variability, which emphasizes that it cannot be considered as a reliable means of meeting the electrical loads. This paper suggests a Monte Carlo summation method, which can be utilized to apply reliability analysis in order to obtain the most-likely resistance-load relationship and the system probability of failure. A case study, which is based upon collected data from actual measurements, is presented in order to study the performance of a group of wind-turbines that deliver electricity to satisfy the demand of a certain load in a suggested area.

Keyword— Reliability, Wind energy, Probability of failure, Monte Carlo summation, Weibull distribution

1. Introduction

Due to the increase in the demand of electric power and great trend to integrate the wind energy with different renewable sources, the concept of reliability has become a very important factor in the overall wind energy systems. In the recent years, the production of electric power based on wind energy is developing remarkably, which results great development in the performance of wind turbines in general. The main factor in making wind energy industry more efficient is improvement the reliability of wind turbine performance. This has led to many wind turbine reliability models being developed. Therefore, it is very significant to continue developing new and accurate reliability models. Researchers have recognized the advantages of integrating both reliability and performance in a consolidated mathematical model. For instance, a reliability evaluation of a laboratory-based Micro Grid system consisting of wind, is proposed using a Monte Carlo Simulation method for the system well-being analysis [1]. The study showed the system well-being computation index provided a bridge between the deterministic and probabilistic methods and defined indices that can be useful in a practical Micro Grid reliability evaluation. In another study conducted by Sameer Vittal et. al, the system performance and reliability analysis of wind turbines using Monte Carlo

methods based on system transport theory was utilized to develop a per formability model of extreme-weather wind turbines [2]. An enhanced model for calculation of reliability indices for different wind power plants configuration concepts was studied[3]. The autoregressive moving average model was used combined with the sequential Monte Carlo simulation in order to predict the expected energy not served more accurately during the failure. K. Hagkwen, and C. Singh suggested a reliability simulation in wind farm with different wind turbines at different heights, and it was found that as the height of some wind turbines is higher, energy loss by wake effect drops due to shear effect [4].A new Monte Carlo simulation procedure and nearby regional weather station data are used to predict wind speed and turbine energy. The results indicated that the replacement of on-site wind data can replace provide accurate predictions of proposed nearby wind turbine[5].Another computational model using one year of wind speed data of a weather station located downwind of the wind turbine site resulted in the greatest match of simulation results to the measured values. A forecasting method that applies Resistance–Load technique to estimate the reliability of a wind-energy system is studied in. The method is a combination of a prediction and risk-based approach, whereas the prediction technique models the power generation and demand scenarios, while the Resistance–Load technique, estimates reliability of the system [6].

The current work presents an application of Monte Carlo summation method, which can be utilized to estimate the reliability of the wind energy system. In this study, probability of failure is a significant parameter to determine the proposed target through obtaining the most-likely resistance-load and performance relationship. The following sections of the current paper is arranged as follows: Section 2 presents background about Monte Carlo simulation method procedure. Section 3 explains the methodology of the proposed model and the utilization of Resistance–Load technique to estimate the system performance based on its requirements. In order to demonstrate the use of the proposed method and its capability, case study is provided in Section 4. The obtained results and discussion regarding the proposed model are showed in Section 5. Finally, conclusions and suggestions for further research are presented in Section 6.

2. Monte Carlo Simulation

Monte Carlo simulation is a powerful statistical analysis tool, which widely used in engineering fields to evaluate the probability of failure of the energy systems. This simulation performs random sampling and conducts a large number of experiments on computer, which displays the statistical characteristics of the model outputs to their distributions. The outline of Monte Carlo simulation consists of three steps, which is illustrated in Figure 1. In step 1, the*cumulative distribution functions*(CDF) of the random variable is equated to the generated random number u_i, that is, $F_X(x_i) = u_i$, and the equation is solved for x_i as follows [7,8]:

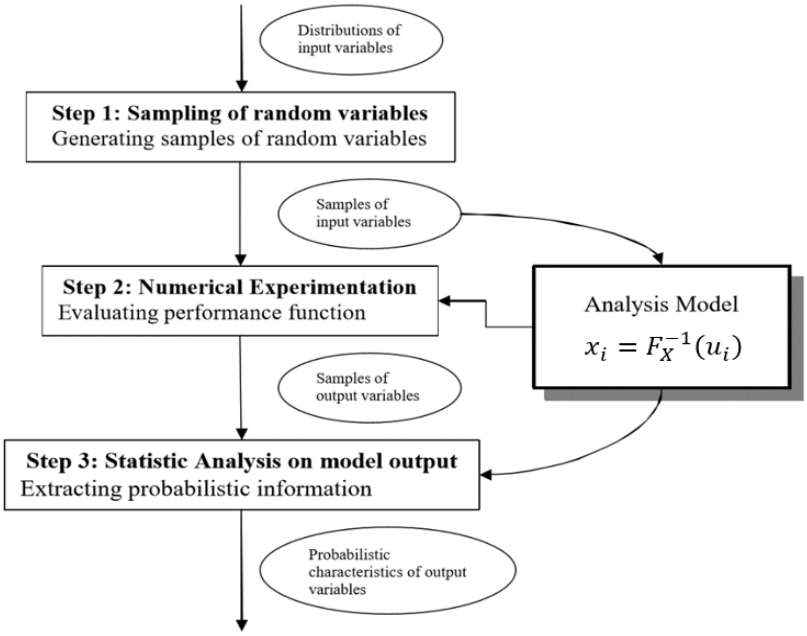

Figure 1: Monte Carlo Simulation Technique [7-10]

$$x_i = F_X^{-1}(u_i) \quad (1)$$

Evaluating the performance function represented in step 2. If the random variable X with parameters λ_X and $\zeta_X$is lognormally distributed , the ith random number x_i according to the lognormal distribution can be generated.

$$\ln(x_i) = \lambda_X + \zeta_X \phi^{-1}(u_i) \quad (2)$$

$$u_i = \phi\left(\frac{\ln(x_i) - \lambda_X}{\zeta_X}\right) \quad (3)$$

$$x_i = \exp\left(\lambda_X + \zeta_X \phi^{-1}(u_i)\right) \quad (4)$$

where u_i is random number ($0\ and\ 1$), and where λ_X and ζ_X are the two parameters of the lognormal distribution.A computer program can be written to generate random numbers according to any distribution. In fact, many available computer programs can generate random numbers for commonly used distributions. If the computer cannot generate a specific distribution, Eq. (1) can be used to obtain it. In step 3, statistical

analysis on the proposed model are applied in order to extracting probabilistic information through multiple tries [9-11]. Resistance–Load is an application of Monte Carlo technique, which widely used for the reliability assessment of systems having a certain "resistance", R, against an applied "load", L. The technique is utilized for an energy system considers the random nature of electrical generation and load simultaneously. The basic concept of Resistance–Load technique is that energy systems are considered reliable when power generation i.e. R, exceeds L value. Consequently, the probability of R >L can be determined by employing this method, which submits an expectation about the energy reliability of the selected wind farm. Forecasting reliability using R–L technique consists of several steps, which are summarized in the next section [6].

3. Methodology

In order to define the reliability of an existing wind energy system based on R–L technique, several steps must be considered. First, identifying of the random and deterministic variables of the proposed model should be taken into consideration to analyse the probability distribution of both variables. Then, determine the respective probability distribution parameters is required before modelling the R–L values. Finally, Monte Carlo simulation is applied to estimate the probability of failure of the entire system [6].

3.1. Identifying the Random and Deterministic Variables of the System

Forecasting reliability usingMonte Carlo simulationbased Resistance–Load technique requires identifying the random and deterministic variables of the proposed model. In this work, R represents the total energy output generated by the selected wind farm over several years; modeling its value requires simulated wind speeds (v) and system losses (loss). The generated power by a single wind turbine rotor is determined according to the following relation [12-14] :

$$P_W = \frac{1}{2} A \rho_a C_P v^3 \qquad (5)$$

where, P_w represents the generated or produced power by the rotor of a wind turbine, ρ_a is the air density, v is the wind speed, A is the rotor swept area of a wind turbine, and Cp is the performance coefficient of a wind turbine. System losses for a known probability distribution are simulated using distribution parameters, such as, mean and variance through Monte-Carlo simulation technique.The model of the system is described as follows:

$$Performance = (\frac{1}{2}\ A\ \rho_a C_P v^3 - losses) - Load \qquad (6)$$

The random variables of the proposed model are:

1-The air density ρ_a $(\frac{m^3}{kg})$ 2-The wind speed v (m/s) 3-The demeaned load L (Watt)

The deterministic variables of the system are:

1- The swept area of the wind turbine rotor A (m^2) refers to the area of the circle created by the blades as they sweep through the air.
2- Wind turbine power coefficientC_p, which is defined as the proration of the produced power by the wind turbine's generator to the power in the wind. The system losses is determined according to listed in Table 1:

Table 1: Summary Losses value is the wind turbines[6]

Type of Loss	Value (%)
WTG Unavailability ($loss_1$)	3
Collection and Substation Unavailability ($loss_2$)	0.5
Electrical and Transmission Loss ($loss_3$)	2
Utility/Grid Unavailability ($loss_4$)	0.5
King and Blade Degradation ($loss_5$)	3
Wake Induced Turbulence Loss ($loss_6$)	5

The total system losses can be calculated from the next formula:

$$P_{loss} = (loss_1 + loss_1 \dots\dots + loss_1)/100 * N_T * P_{out} \quad (7)$$

where N_T is the number of wind turbines in a wind farm.

3.2. Probability Distribution Analysis

In order to analyse the probability distributions for the wind speed, losses and load, graphical techniques, such as histogram and probability plot are required. Furthermore, modelling R and L values is based on distribution parameters and simulation techniques. By using Easy Fit software, the best wind speed distribution can be obtained. The software allows using different types of distributions and compare then in terms of some tests such as K-S test, Chi square test, and Anderson darling test.To obtain simulated wind speeds, probability distribution identification is required based on historical wind speed data. In line with pervious work, the current study's wind speed distribution can be described using Weibull distribution when Chi square test considered [9,10] The Weibull distributionis represented by two-parameter; Weibull shape parameter (K), and Weibull scale parameter C, which are determined based on the mean ($\bar{v}$) and standard deviation (σ_v)of wind data [15-17].

$$K = \left(\frac{\sigma_v}{\bar{v}.}\right)^{-1.086} \quad (8)$$

$$\frac{C}{\bar{v}} = \left(0.568 + \frac{0.433}{K}\right)^{-1/K} \quad (9)$$

Weibull shape parameter, k, generally ranges from 1.5 to 4 for most wind conditions. In addition, Weibull distribution whose cumulative distribution function (CDF) is given as follows [15-17]:

$$F(v) = P[V \leq v) = \int_0^v f(v)dv = 1 - exp\left\{-\left(\frac{v}{C}\right)^K\right\} \quad (10)$$

where $P(\leq v)$ is the probability of the measured wind speed is less than or equal v. Figure 2 illustrates the effect of the shape parameter on the cumulative distribution function. Equation 11 presents the definition of the Weibull probability density function. Figure 3 displays the effect of the shape parameter on the probability density function [15-17].

$$f(v) = (v) = \left(\frac{k}{c}\right)\left(\frac{v}{c}\right)^{k-1} \exp[-\left(\frac{v}{c}\right)^k] \quad (11)$$

When the shape parameter K is equal to 2, the P.D.F. is given its own name, the Rayleigh probability density function, which is defined as follows [15-17]:

$$f(v) = \frac{2V}{c^2} * \exp\left[-\left(\frac{v}{c}\right)^2\right] \quad (12)$$

The equation of the cumulative Rayleigh function isdefined as follows [15-17]:

$$F(v) = 1 - \exp\left[-\frac{\pi}{4} * \left(\frac{v_i}{\bar{v}}\right)^2\right] \quad (13)$$

3.3. Modelling the Resistance (R) and Load (L) Values.

An energy system's load is considered independent of wind speed, and the resistance represents the total electrical output generated by the wind turbines over several years. Modelling R-L values requires first simulated wind speeds (v), air density (ρ_a), and system losses (loss).

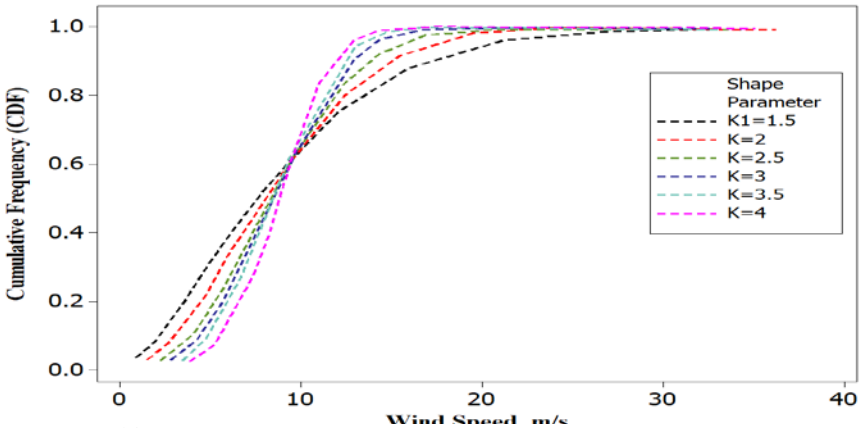

Figure 2: The Effect of the Shape Parameter on the Cumulative Distribution Function

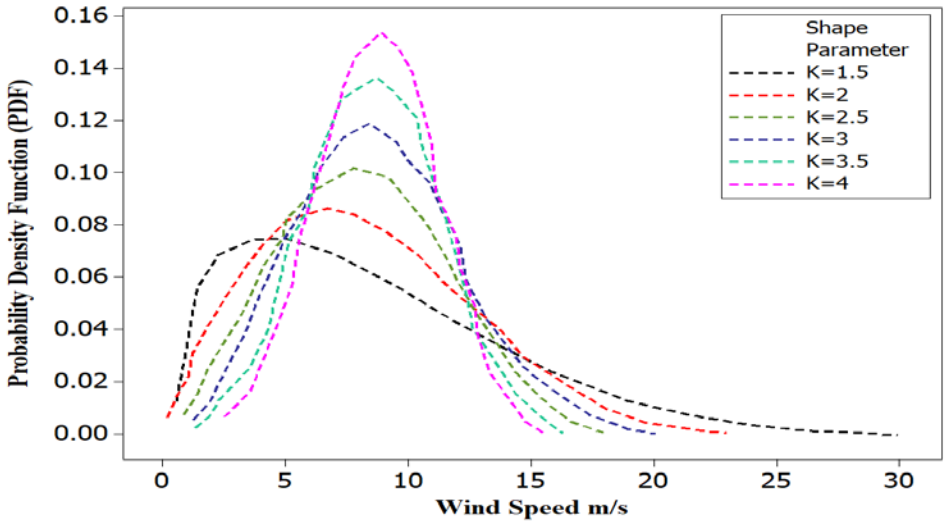

Figure 3: The Effect of the Shape Parameter on the Probability Density Function

Using the simulated losses and wind speeds, the net generated P_{NET} from each wind turbine is calculated from the following equation:

$$P_{NET} = P_w - P_{LOSS} \quad (14)$$

The reliability of the proposed system is carried out to study the probability of failure to satisfy the load power demand and calculate P(R<L). The total net power (resistance) is determined as follows:

$$The total net power\ (R) = N_T * P_{NET} \quad (15)$$

3.4. Determine the Probability of Failure

The probability of failure represents the probability of failure, which requires a knowledge about the wind turbine specification. In this issue, the power curve of each single wind turbine displays the required specification to apply Monte Carlo simulation.

4. Case Study

In order to utilize the proposed model to determine the reliability of the wind energy systems, collected data, which are related to an area in Tripoli -Libya is selected [18]. The specifications of the wind turbines that are selected to be set up in the area are illustrated in Table 2 [19].In addition, Fig, 4, which shows the dependence between wind speed and produced electrical power of the selected wind turbine. It can be realized that there are three stages should be explained. Stage 1 occurs when the wind speed between (3m/s) to the rated speed (11m/s). Then, stage 2 occurs when the wind speed between the rated speed(11m/s) to the cut off speed (20m/s). Finally, stage 3 occurs when the wind speed more than or equal the cut off speed at

(20m/s).Therefore, there is a need to find the produced power at each stage for each turbine in the proposed wind farm, which can be determined as follows:

- Stage 1: $P_{produced} = \frac{1}{2} A \rho_a C_P v^3 - Losses$ - Stage 2: $P_{poduced} = 1057\ KW - losses$

-Stage 3: $P_{out} = 0\ W$

Table 2: 1057kW Wind Turbine General Specification [19]

Category	Specification
Rated Power	1057 1057
Number of Blades	3 blades
Rotor Diameter	60 m
Cut-In Wind Speed	3 m/s
Rated Wind Speed	11/m/s
Hub Height	66 m
Cut-Out Wind Speed	20 m/s
Coefficient of Power	40%

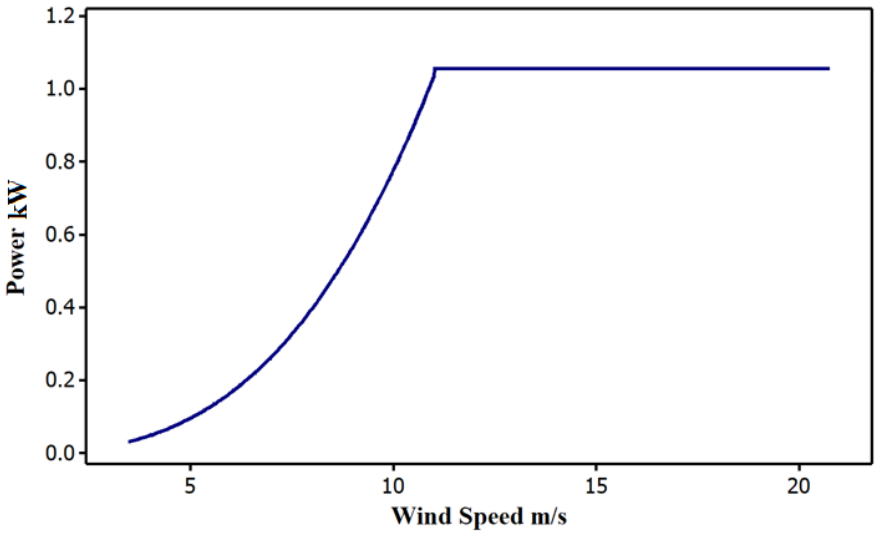

Figure 4:1057kW Wind Turbine power curve

The obtained data is representing in the average of wind speeds, air pressures, and temperatures for every day in the year during the study period of the selected area. Figure 5 displays the fluctuations of the average wind speed throughout the study for the same location [18]. Since, the obtained wind speed data are measured at 10 m,an adjustment must be made to obtain wind speeds at the turbine hub height. Several common

functions that describe the change in mean wind speed with height are utilized. With the aid of Eq. 15, the average wind speed at the turbine hub height is determined.

$$v_z = \quad v_R * \left(\frac{Z}{Z_R}\right)^{\alpha} \tag{16}$$

where α is the friction coefficient for various terrain characteristics, which is determined from Table 3. Finally, the suggested wind farm consists of twenty-wind turbine to cover the load in the selected area. Section 5 presents the results that obtained from applying the proposed model.

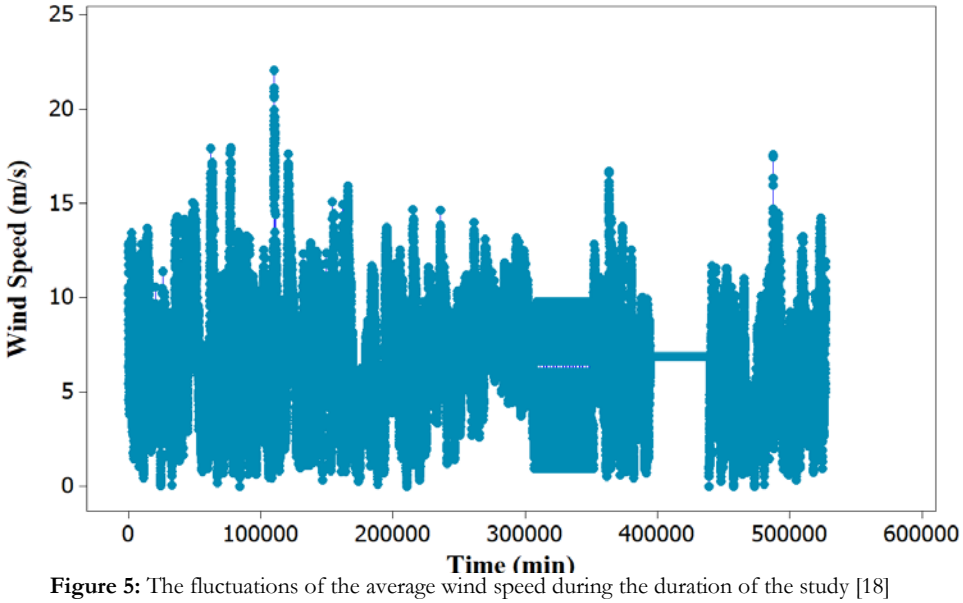

Figure 5: The fluctuations of the average wind speed during the duration of the study [18]

Table 3: The friction coefficient for various terrain characteristics [12,13]

Type of terrain	Roughness class	β
Water areas	0	0.01
Open country, few surface Features	1	0.12
Farm land with building and hedges	2	0.16
Farm land with many trees, Forests, villages	3	0.28

5. Results and Discussion

The obtained results indicate that there is dramatic changesin the wind speed when it reaches 9m/s. The performance before this value is negative, which means the demand power of the selected area is greater than the produced power by the proposed wind farm. Figure 6 displays wind speed time series with respect to its frequency. The diagram shows that most available wind speeds range from 9 m/s to 10 m/s. Figure 7 shows the Weibull probability density function and cumulative distribution function of the wind speed. Weibull

probability density function curve displays the wind speed probability distribution of the obtained wind speed data. Furthermore, Weibull cumulative distribution curve describes the probability that every single value of the obtained wind speed data takes a value less than or equal to the wind speed variable. The curve shows that the likelihood of the selected wind turbines operating at the rated speed is approximately 25%. The behaviour of the performance of the proposed system with respect to the wind speeds is illustrated in Fig 8. It is obvious that the performance reaches 129 MWat 20 m/s butthe frequency of this value is low. However, when wind speed is between (3-8) m/s, the system performance is negative, which submits an indication that the probability of failure of the proposed system in this range is significant value. Table 4 presents details regarding the system generated power against the load of the selected area. The Monte Carlo simulation results are illustrated in Table 5 with several trails. It is noted that as the number of simulations is increase the probability of failure converges, computation error decreases and run time increases significantly.

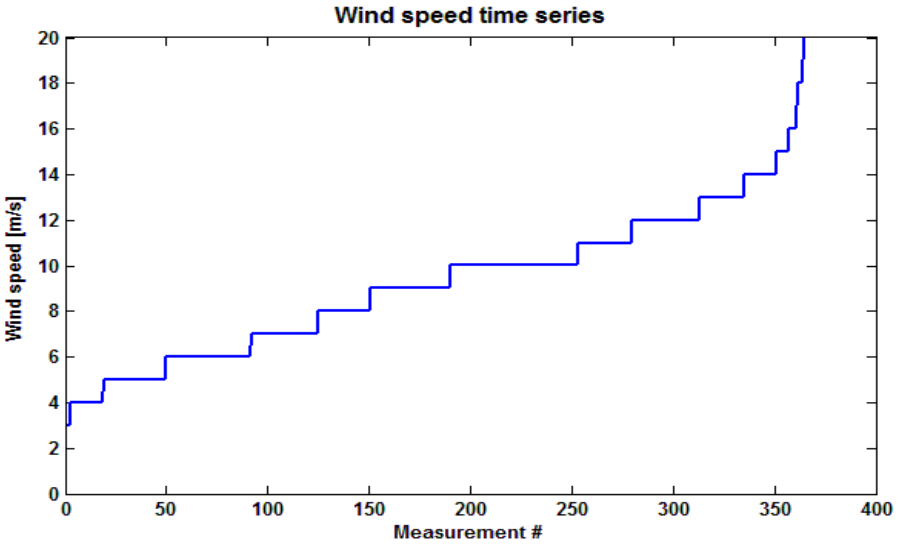

Figure 6: Wind speed time series

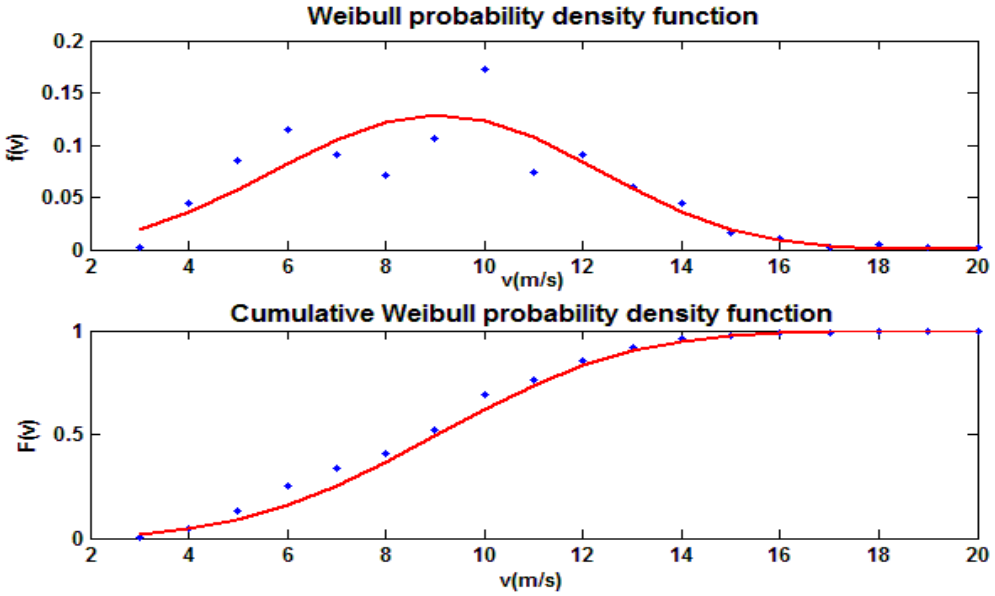

Figure 7: Weibull probability density function and cumulative distribution function

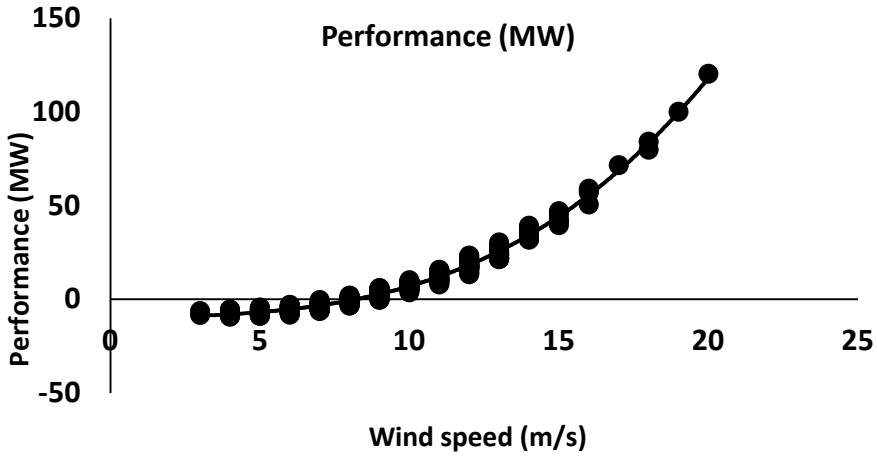

Figure 8: The trend of the system performance with respect to the wind speed

Table 4: The system simulation results

Wind speed m/s	Resistance MW	Load MW	Performance MW	Wind speed m/s	Resistance MW	Load MW	Performance MW
3	0.7	7.9	7.3-	12	27.1	9.0	18.0
4	1.1	8.2	7.1-	13	33.8	9.2	24.6
5	2.1	9.1	7.0-	14	43.3	8.4	34.9
6	3.4	9.3	5.9-	15	52.1	9.1	43.0

7	5.2	8.8	3.6-	16	65.0	8.9	56.2
8	7.7	8.4	0.7-	17	76.9	8.0	68.9
9	11.3	8.5	2.7	18	88.8	7.2	81.7
10	15.5	7.6	7.9	19	114.1	8.6	105.5
11	20.6	8.4	12.2	20	139.3	10.0	129.3

Table 5: System probability of failure and error with several trails numbers

Number of trails	Number of failures	Pf (%)	Error (%)	Simulation time(sec)
10000	2530	25.3	8.6946	2.1359
100000	25174	25.17	2.7449	19.979
1000000	252880	25.29	0.86933	2522.8

6. Conclusions

In this study, an effective method based on Monte Carlo simulation is performed to determine the reliability of wind energy systems. The proposed technique is represented to obtain the most-likely generated power-power demand and performance relationship to estimate the system probability of failure in the selected area.It is found that as the number of simulations is increase the probability of failure slightly decreases; computation error reduces significantly and run time increases remarkably. Further, it can be summarized that the wind speed has the most influence on the performance of the wind energy systems, then the demanded power. To obtain simulated wind speeds, it was found that wind speed distribution can be described using Weibull distribution when Chi square test considered. This model may be considered as platform and can be used for other locations in Libya. Future work should be focused on different types of wind turbines and several areas in Libya in order to estimate the most proper locations that represent high the reliability of wind energy systems.

References

[1] Youli, Su, and Ken Nagasaka, "Monte Carlo simulation method used in reliability evaluation of a laboratory-based micro grid," *Proceedings of the international multi conference of engineers and computer scientists*, Vol 2. 2010..https://pdfs.semanticscholar.org/f26e/969fffc5f035281927cb9670eb25abf8e3f3.pdf

[2] Vittal, Sameer, and Michel Teboul, "Performance and reliability analysis of wind turbines using Monte Carlo methods based on system transport theory," *46th AIAA/ASME/ASCE/AHS/ASC Structures, Structural Dynamics and Materials Conference*, p. 2218. 2014. https://arc.aiaa.org/doi/abs/10.2514/6.2005-2218

[3] Topić, Danijel, DamirŠljivAc, and Marinko S Tojkov, "Reliability model of different wind power plant configuration using sequential Monte Carlo simulation," *Eksploatacjai Niezawodnosc-Maintenance and Reliability*, p. 237. Jan, 2016. http://bib.irb.hr/datoteka/632590.EiN_2016-2_article_11.pdf

[4] Kim, Hagkwen, and Chanan Singh, "Reliability Simulation in Wind Farm with Different Wind Turbines," *Proceedings of National Power Systems Conference*, 2012. http://www.iitk.ac.in/npsc/Papers/NPSC2012/papers/12170.pdf

[5] Gallagher, Ron, and Andrew Curtis Elmore, "Monte Carlo simulations of wind speed data," *Wind Engineering 33(6)*, p. 661-673. Dec, 2009. http://journals.sagepub.com/doi/abs/10.1260/0309-524x.33.6.661

[6] Chaudhry, Nikhil, and Larry Hughes, "Forecasting the reliability of wind-energy systems: A new approach using the RL technique," *Applied energy 96*, p. 422-430. Aug, 2012. https://www.sciencedirect.com/science/article/pii/S0306261912001778

[7] Mooney, Christopher Z, "*Monte carlo simulation*," Vol. 116. Sage Publications, Apr, 1997.

[8] Christopher, W, "Wind Turbine Reliability: Understanding and Minimizing Wind Turbine Operation and Maintenance Costs," Department of Energy. 2006.

[9] Rao, Singiresu S., Singiresu S. Rao, and S. S. Rao, "*Reliability-based design*," 1992. https://prkwrhnfx07.storage.googleapis.com/MDA3MDUxMTkyNg==07.pdf

[10] Haldar, Achintya, and Sankaran Mahadevan, "*Probability, reliability, and statistical methods in engineering design*," New York: Wiley. Vol. 1.2000. https://prkwrhnfx07.storage.googleapis.com/MDQ3MTMzMTE5OA==07.pdf

[11] Hall, P. L., and J. E. Strutt, "Probabilistic physics-of-failure models for component reliabilities using Monte Carlo simulation and Weibull analysis: a Parametric Study a parametric study," *Reliability Engineering & System Safety*. V0l 3. p. 233-242. Jun, 2003. https://www.sciencedirect.com/science/article/pii/S0951832003000322

[12] Manwell, James F., Jon G. McGowan, and Anthony L. Rogers, "*Wind energy explained: theory, design and application*," John Wiley & Sons. Sep, 2010.

[13] Jain, Pramod, "*Wind energy engineering*," McGraw-Hill Education. Jan, 2016.

[14] Gipe, Paul, "*Wind energy basics: A guide to small and micro wind system*," White River Junction, VT: Chelsea Green publishing company. Mar, 1999.

[15] Murthy, DN Prabhakar, Michael Bulmer, and John A, "Weibull model selection for reliability modelling," *Reliability Engineering & System Safety 86*. V0l 3. p. 257-267. Dec, 2004. https://www.sciencedirect.com/science/article/pii/S0951832004000237

[16] Xie, M., and Lai, C.D, "Reliability Analysis Using an Additive Weibull Model with Bathtub-shaped Failure Rate Function," *Reliability Engineering & System Safety 52*. V0l 1. p. 87-93. Apr, 1996. https://www.sciencedirect.com/science/article/pii/0951832095001492

[17] Lai, C. D., Min Xie, and D. N. P. Murthy, "A modified Weibull distribution," *IEEE Transactions on reliability* 52. V0l 1. p. 33-37. Mar, 2003. https://ieeexplore.ieee.org/abstract/document/1179794/

[18] Data. Provided by Center of Solar Energy Research and Studies, 2015

[19] Data of a Variable Speed Wind Turbine, 1057 KW rated power, three phase permanent magnetic type 440/660 V 60 Hz. Provided by Dr. Kathryn Johnson, Colorado School of Mines, 2013

Zero Energy and Low Water Schools: Case Study- Building of Garaboulli Engineering Faculty-Libya

Salhin M. Alaud [1],Khalid M. H. Jaballa[2], Abdulghani M. Ramadan[3]
[1]s.alaud@elmergib.edu.ly, [2]kmh_man@yahoo.com, [3]amramadan@elmergib.edu.ly
[1]Civil Department, Garaboulli Engineering Faculty, Elmergib University, Libya
[2, 3] Mechanical Department, Garaboulli Engineering Faculty, Elmergib University, Libya

ABSTRACT

The current paper presents the design methodology for reducing the water consumption to reach a zero energy building. The building of the Garaboulli Engineering Faculty (GEF), Libya was chosen as a case study. The required energy will be supplied by renewable energy. In order to meet the required loads, solar energy is used in the design to generate heating, cooling, and electric power by using different techniques such as solar thermal collectors and photovoltaic panels. Moreover, rain water is used as a source of water supply for the building. To reach the low water and Zero Energy aims, different techniques such as recycling of grey water and solar cooling were adopted. Finally, the proposed system will be feasible for a long term of operation.

Keyword— Zero energy, Low water, Renewable energy, Rain water.

1. Introduction

The daily required of energy used increases continuously with a growing population. New buildings are constructed faster than old ones and thus increase the consumption of energy. On the other hand, the load on government supply of electricity or water increases over time. In the educational buildings, the increasing of consumption is depends on increase of student number.

Recently, water and power outages have increased as a result of increased demand of energy and water, and poor production capacity. From this perspective, alternatives ways are needed to find water and energy and ensure constant supply without interruption. Introducing of zero energy principle with rationing the water and energy uses into school buildings are particularly necessary when the supply of energy and water are intermittent. The zero energy is defined by the annual of the total energy amount used by the building that renewable energy sources. In general, a net zero energy is a building with highly reduced energy needs through efficiency gains such that the renewable technologies can supply the energy needs. In this paper, Garaboulli Engineering faculty building has designed to be low water consumption and zero energy building. Solar panels can generate the required amount of electricity that consumed by the faculty building every year. The large area of the building's roof allows collecting an ample amount of rainwater. Reuse of grey water for some purposes throughout the building will also save extra water.

2. Description and Aims of the Project

The building of Garaboulli Engineering Faculty is located at the north of the Garaboulli city on total area 17000 m². The surface area of the main and attachment buildings is about 2100 m². The green area is more than 2000 m². The main building has four toilets with four sinks in each of six parts in two stories with total of 24 toilets and 24 sinks. A small kitchen is also including in the building. There are another toilet and kitchen in the gate building. The construction has 15 class rooms, 1 theatre, 2 electronic labs and 16 offices. Figure 1 illustrates the plan of the building and surrounded garden area. The project aims to benefit of the large surface area to generate the energy (electric, heating and cooling) from the solar and to collect the rain water to reduce the dependency on the general city network.

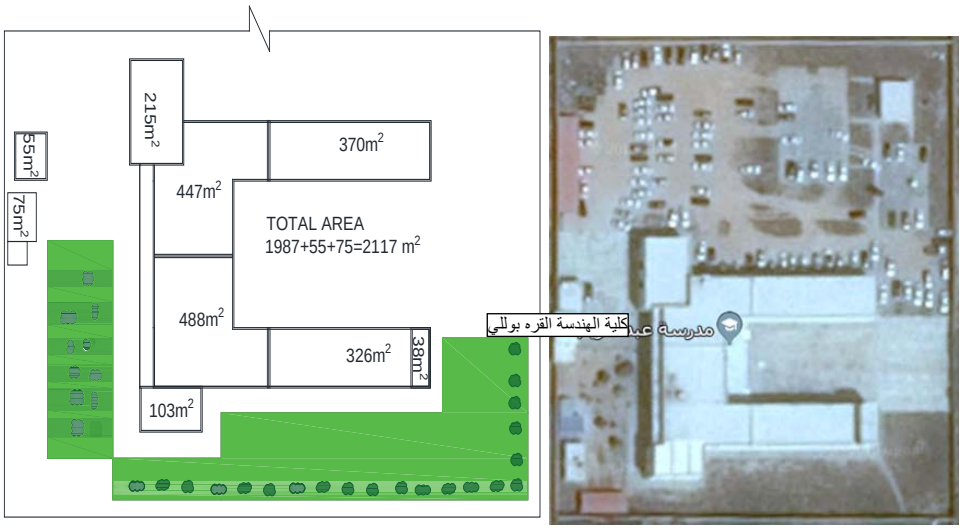

Figure 1: Garaboulli Engineering Building, Plan (left) and air photo (right)

3. Design Methodology

The current research attempts to find a suitable design to minimize the usage of water consumption from the city network by collecting the rain water and recycle the grey water or dispense on the network electricity by designing solar panels and heaters to generate the energy.

3.1. Low Water

Rainwater exploitation may not be sufficient to cover the total consumption of water, as this requires a very large area of water storage. Annual rainfall in some areas is also insufficient. The best ways are: rainwater exploitation to relieve the consumption from the public network, rationalize the consumption of water and recycling the grey water.

3.1.1 Rain Water Collection

In general, Libya has a dry climate with intense rain storms and short in duration. Along the north of Libya, the rainfall months are from September to May, with most severe from October to January. The annual rainfall for Garaboulli city is taken a similar of the average of annual rainfall of the two nearest cities, Tajura and Tripoli, which have recorded data. The average of annual rainfall of these cities were similar in two different studies, 288 mm/year, where the results of Tajura was based on 40 years(Board, 2008) and in Tripoli was based on 30 years of data (M.RAMADAN, 1999). The catchment area of the main building of the college (2000 m^2) has considered. For the runoff, it is estimated that 15% of the rain water volume is released during the time required to fill the detention facility(Board, 2008). This is due to unavoidable any leakages or a possible overflow in the gutter downpipe system, or in the case of the downpour is too light to produce sufficient runoff. However, the total volume of detention facility is designed on 85 % of the total rainwater collected as in Equation 1.

$$q = 0.85 \times 288 \times 2000 = 489.6 \times 10^3 l/year = 489.6\, m^3/year \quad (1)$$

3.1.2 Water Consumption

There are many studies and standards determine the varying mount of consumption in the universities and schools, such as 4.86 -6.3 litters / student / day for secondary schools(Shuraideh, 2015) and 125 - 180 *l/capita/day* for Universities (Zhang, 2010). The large amount of the consumption at universities is due to use of larger this amount in laboratories, gardens and other facilities, while in the school case, the consumption only for drinking, washing and toilet flushing.The water consumption can be divided into:

1. Toilet flushing which make up about 30% of overall water consumption which produce the black water.
2. Wash basins, and floor cleaning that produces grey water as well as bidet faucets which mix with toilet sludge.
3. Water used to irrigate the garden.
4. Laboratory consumption such as concrete labs

Gray water can be recycled to use in the toilet flushing and irrigate the garden after a filtration and treatment process. Figure 2 illustrates the cycle of rain and city network water.

There are no reliable data for the water consumption in the targetFaculty.Since the water consumption in the Faculty is limited to: *i.* washing; *ii.* toilet flushing; and *iii.* a small Garden, the consumption in our study for i and ii is estimated to be *6l/capita/day*. If we consider that the consumption rate is limited to school days only and the number of annual school days is 280, the quantity required for annual consumption of water is 280 x 6 = 1680*l*/capita/year.

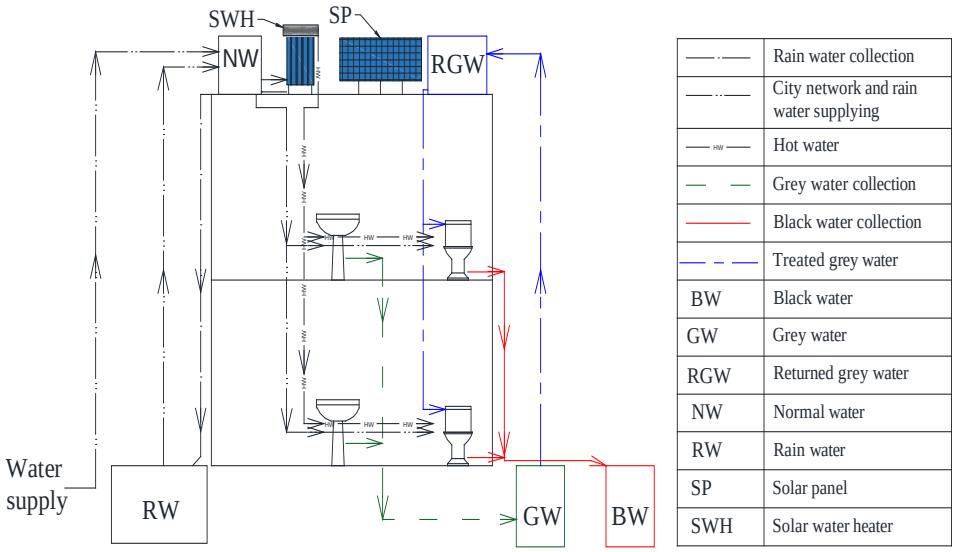

Figure 2: General section of water cycle

Assuming that the total daily number that can be presence in the college is a maximum of 700 people, thus, the annual consumption required is 700 x 1680 = 1176x10³*l/capita/year* or98$m^3/month$. The use of grey water in the flushing will save about 30%of the consumption amount, thus, the needed consumption will be68.6 $m^3/month$. The garden consumption (iii) is estimated to be 30$m^3/month$, therefore, the monthly amount of water consumption is 98.6 $m^3/month$ or say 100 $m^3/month$. Figure 3 illustrates the monthly average collected from rainwater(M.RAMADAN, 1999) compared to the total monthly consumption as a percentage. The total rain water collected is 489 $m^3/year$ and the total consumption requirement 1200 $m^3/year$, thus, the needed water from the city network is 711 $m^3/year$ with save more than 40% of the consumption.

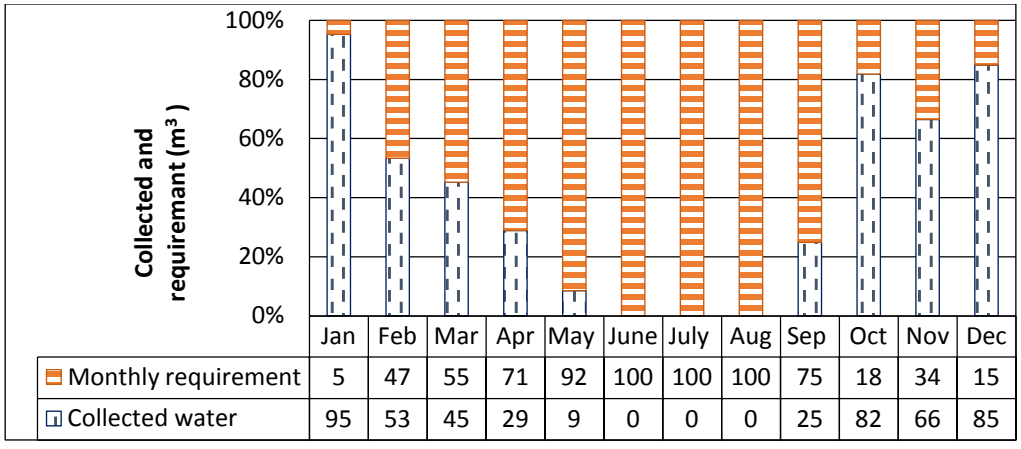

	Jan	Feb	Mar	Apr	May	June	July	Aug	Sep	Oct	Nov	Dec
Monthly requirement	5	47	55	71	92	100	100	100	75	18	34	15
Collected water	95	53	45	29	9	0	0	0	25	82	66	85

Figure 3: Collected water and monthly requirement

3.2. Cooling, Space Heating and SHW Loads

In order to a achieve Net Zero Energy (NZE), Combi-system is the highest prospective technology which can offer that. A solar Combi-system is providing space heating, Service Hot Water (SHW) and cooling stock by solar collectors and an absorption cooling cycle. In this paper, for the purpose of designing a solar heating system, f-chart method and ϕ-utilizability method are integrated together to merge the advantages and merits of the two methods to get more accurate and precise results[5],[6]. In order to start design process, relevant weather data required are shown in RetScreen software including local weather data, air temperature, latitude, tilt angle, daily solar radiation on horizontal surface...etc[8]. Moreover, Table 1 shows the input and design data for faculty of engineering at Garaboulli, includes the number of occupants, average daily service hot water consumption per capita in addition to other related data. In addition, Table 2 shows the proposed solar collector specifications. The first step in the design of solar thermal system is to determine the energy demand of the building by using RetScreen software, and assumption a faculty operation whole the year. Table 3 summarizes the different energy demands for the space heating, cooling, service hot water, and electric devises (Baseline energy) such as computers, lighting, surface pumps that calculated according to annual consumption of the faculty building. It should be noted that the total heating load requirement which covered by solar thermal system is calculated as following in Equation 2;

$$Total\ heating\ load\ =\ heating\ for\ cooling\ +space\ heating\ load\ +SHW\ load \quad (2)$$

Total heating load $=3.65 \times 10^{12}$ (J)

Table 1: Input and design data for the faculty building

S. No.	Item	Value	unit
1	Latitude	32	^{o}N
2	Tilt Angle	42	degree
3	Number of Students	700	
4	Average Service Hot Water Consumption	2.3	L/day/student
5	Water Service Temperature	60	^{o}C
6	Water Density	1000	kg/m^3

Table2: The proposed Solar Collector Specifications

S. No.	Item	Value	unit
1	Type of Collector	Tubular	
2	Gross Area of collector	4.619	m^2
3	(F_RU_L)	-1.26	W m^{-2o} C^{-1}
4	$F_R(\tau\alpha)_n$	0.51	
5	Collector Flow Rate	0.566	L/s
6	Collector Fluid Specific Heat	3600	J kg^{-1o}C^{-1}
7	Collector Fluid Density	1034	kg m^{-3}
8	Heat Exchanger Effectiveness	0.8	
9	Storage Tank Capacity	1610	Litre

Table3: Energy demands for the faculty building

Month	Cooling load demand (J)	Heating load for cooling demand(J)	Heating load (J)	SHW (J)	Total heating load(J)	Electric devices load (kWh)
Jan	0.00	0.00	2.15 x10^{11}	8.95 x10^{09}	2.23 x10^{11}	10,477.3
Feb	2.69 x10^{09}	4.21 x10^{09}	1.91 x10^{11}	8.37 x10^{09}	2.04 x10^{11}	9,463.4
Mar	3.32 x10^{10}	5.19 x10^{10}	1.85 x10^{11}	9.22 x10^{09}	2.47 x10^{11}	10,477.3
Apr	4.67 x10^{10}	7.30 x10^{10}	1.67 x10^{11}	8.53 x10^{09}	2.49 x10^{11}	9,225.6
May	1.57 x10^{11}	2.46 x10^{11}	9.00 x10^{10}	8.18 x10^{09}	3.44 x10^{11}	9,533.1
Jun	2.22 x10^{11}	3.47 x10^{11}	3.39 x10^{10}	7.21 x10^{09}	3.88 x10^{11}	9,225.6
Jul	2.48 x10^{11}	3.87 x10^{11}	2.08 x10^{10}	6.86 x10^{09}	4.15 x10^{11}	6,308.8
Aug	2.49 x10^{11}	3.89 x10^{11}	2.08 x10^{11}	6.53 x10^{09}	4.16 x10^{11}	6,308.8
Sep	2.26 x10^{11}	3.54 x10^{11}	3.11 x10^{11}	6.37 x10^{09}	3.91 x10^{11}	6,105.3
Oct	1.27 x10^{11}	1.98 x10^{11}	9.62 x10^{10}	6.98 x10^{09}	3.01 x10^{11}	9,185.6
Nov	4.04 x10^{10}	6.32 x10^{10}	1.75 x10^{11}	7.39 x10^{09}	2.46 x10^{11}	8,889.3
Dec	0.00	0.00	2.15 x10^{11}	8.35 x10^{09}	2.23 x10^{11}	9,185.6
Annual demand		2.11 x1012	1.44 x10^{11}	9.29 x10^{10}	3.65 x10^{12}	104,386.40

Heating for cooling is defined as the heating energy which is required for absorption cooling system. It can be calculated as follows;

Heating for cooling = cooling load demand x COP

In this study, the absorption cooling system COP is equal to 0.64.

Next step, by using ϕ-chart method, the number of collectors and the solar monthly energy collected by collectors can be estimated with following Equation 3;

$$Q = F_R(\overline{\tau\alpha})\overline{H_T}\overline{\emptyset} \quad (3)$$

Where is:

Q, the monthly energy collected by collectors (J/m^2).

$F_R(\tau\alpha)_n$, is readily determined from collector specifications.

H_T, is the monthly average daily radiation on tilted surface on the collector.

ϕ, is the monthly average daily utilizability.

In order to calculate the required collectors' area in square meters and the available total annual solar energy (J/m^2) in site. First, the solar radiation on tilted surface on collector in (Kwh/m^2) should be calculated. Table 4 summarizes the estimated average monthly solar radiation on tilted surface on collectors. Furthermore, the monthly and annual solar thermal energy collected by collectors is also shown in Table 5.In view of the data shown in Tables 4 and 5, total annual solar thermal energy available $=3.49 \times 10^{09}\ (J/m^2)$, and total annual thermal energy demand $=3.65 \times 10^{12}\ (J)$, taken from Table 4.Then, total collector area required is determined by Equation 4;

$$Total\ Collector\ Area\ Required = \frac{Total\ Annual\ thermal\ energy\ demand}{total\ annual\ solar\ thermal\ energy\ available} \quad (4)$$

Table4: The average monthly solar radiation on tilted surface on collectors

Month	$\overline{H_o}$	$\overline{H}$	K_T	H_d	H_b	R_b	ϱ_g	$\overline{H_T}$	$\overline{H_T}$
	J/m²) x10⁷	(kWh/m²)	(-)	(J/m²) x10⁶	(J/m²) x10⁷	(-)	(-)	(kWh/m²)	(J/m²) x10⁷
Jan	1.99	2.9	0.53	3.83	0.661	1.90	0.2	4.50	1.62
Feb	2.42	4	0.60	4.39	1.00	1.60	0.2	5.61	2.02
Mar	3.06	5	0.59	6.28	1.17	1.24	0.2	5.67	2.04
Apr	3.63	6	0.60	7.40	1.42	0.96	0.2	5.72	2.06
May	4.00	6.5	0.58	8.23	1.52	0.78	0.2	5.43	1.96
Jun	4.14	7	0.61	8.32	1.69	0.70	0.2	5.49	1.98
Jul	4.07	7.1	0.63	8.02	1.75	0.73	0.2	5.69	2.05
Aug	3.79	6.5	0.62	7.54	1.59	0.86	0.2	5.80	2.09
Sep	3.30	5.5	0.60	6.69	1.31	1.10	0.2	5.76	2.07
Oct	2.66	4	0.54	5.62	0.878	1.44	0.2	4.96	1.79
Nov	2.12	3.1	0.53	4.08	0.708	1.79	0.2	4.59	1.65
Dec	1.85	2.3	0.45	3.69	0.459	2.01	0.2	3.52	1.27

Table 5: The monthly and annual solar thermal energy collected by collectors

Month	H_T(kWh/m²)	R	a	B	$r_{t,n}$	$r_{d,n}$	R_n	a	b	c	Ø	Q (J/m²) x10⁸
Jan	4.50	1.55	0.55	0.53	0.16	0.15	1.58	-0.82	-0.69	0.48	1	2.5
Feb	5.61	1.40	0.59	0.49	0.16	0.14	1.42	-1.15	-0.35	0.69	1	2.8
Mar	5.67	1.13	0.65	0.44	0.14	0.13	1.14	-1.11	-0.38	0.67	1	3.2
Apr	5.72	0.95	0.70	0.38	0.13	0.12	0.96	-1.15	-0.35	0.69	1	3.14
May	5.43	0.84	0.75	0.34	0.13	0.12	0.83	-1.10	-0.40	0.65	1	3.08
Jun	5.49	0.78	0.77	0.32	0.12	0.11	0.78	-1.21	-0.29	0.73	1	3.01
Jul	5.69	0.80	0.76	0.33	0.13	0.12	0.80	-1.29	-0.21	0.80	1	3.23
Aug	5.80	0.89	0.72	0.36	0.13	0.12	0.89	-1.25	-0.25	0.76	1	3.29
Sep	5.76	1.05	0.67	0.41	0.14	0.13	1.05	-1.17	-0.33	0.70	1	3.16
Oct	4.96	1.24	0.61	0.47	0.15	0.14	1.26	-0.89	-0.61	0.52	1	2.81
Nov	4.59	1.48	0.56	0.52	0.16	0.15	1.50	-0.82	-0.68	0.48	1	2.52
Dec	3.52	1.53	0.53	0.54	0.17	0.16	1.56	-0.40	-1.11	0.28	1	1.99
Total Annual solar thermal energy available												34.9

Total Collector Area Required = $3.65 \times 10^{12}\,(J) / 3.49 \times 10^{09}\,(J/m^2)$= 1046 ($m^2$)

The number of collectors required is calculated by Equation 5;

$$Number\ of\ collectors\ needed = \frac{Total\ Collector\ Area\ required}{Area\ of\ single\ collector} \quad (5)$$

Number of collectors needed = (1046/4.619) = 226.4 collectors approx. **227** collectors.

After that, the estimated solar fraction which is defined as the percentage of the energy requirements that can be met by a solar energy system. It is calculated by f-Chart method. Table 6 shows the energy met by the solar system and solar fraction. The solar collector combi-system proposed is collector type Tubular – with model SEIDO5-16 AS/AB and tilt angle of 42° with horizontal surface. The working fluid used in this collector is anti-freezing with water solution. For cooling, the absorption cycle is used to cover the cooling load with COP 0.64.All the process of working fluid inside the system between the hot region and cold region are controlled by sophisticated computerized system [7].

Table6: Energy met by the solar collector and the value of solar fraction

Month	Total Heating Energy demand (J/month) x10^{11}	second per month	$\frac{(\tau\alpha)}{(\tau\alpha)_n}$	X (-)	Y (-)	f (-)	f actual (-)	Energy met by collector (J) x10^{11}
Jan.	2.23	2678400	0.96	-3.686	1.145	1.154	1.00	2.23
Feb.	2.03	2419200	0.96	-3.618	1.418	1.286	1.00	2.03
Mar.	2.46	2678400	0.96	-3.200	1.310	1.202	1.00	2.46
Apr.	2.48	2592000	0.9	-2.941	1.187	1.119	1.00	2.48
May	3.43	2678400	0.9	-2.087	0.844	0.850	0.85	2.92
Jun.	3.87	2592000	0.9	-1.709	0.732	0.747	0.75	2.89
Jul.	4.14	2678400	0.9	-1.614	0.732	0.740	0.74	3.07
Aug.	4.16	2678400	0.9	-1.597	0.745	0.748	0.75	3.11
Sep.	3.91	2592000	0.9	-1.687	0.760	0.765	0.76	2.99
Oct.	3.01	2678400	0.96	-2.380	0.939	0.933	0.93	2.80
Nov.	2.45	2592000	0.96	-3.029	1.029	1.036	1.00	2.45
Dec.	2.22	2678400	0.96	-3.642	0.898	1.003	1.00	2.22
Total	36.5	Annual solar fraction					0.87	31.7

3.3. Photovoltaic System Design

The Photovoltaic system is used to cover the electrical power demand for the faculty building. Two cases are considered; On-Grid design and off-Grid design. Table 7 shows the specification of module used to produce the electric power (kWh) [8].

By using PV watts program, the monthly power production output (kWh/month) can be estimated as shown in Table 8.It gives the monthly power production under the conditions; tilt angle 42°, the module face on

south direction, and assuming 15% losses due to shadow, wiring and dust. It should be noted that the net total electric energy needed and sent to Grid is zero. In this sense, the electric design is net zero energy class.

Table7: Energy met by the PV system with specifications of PV module used

Design PV System		
Efficiency of the inverter	0.9	AC to DC
Voltage DC system	49	volte
Peak Amp for module	7.86	
Peak sun hours	4	hr/day
Design module system	Mono-silicon module	
Type of Module	Grape Solar	Gs-S-385-TS
Power of module (W)	385	Watt
Area of a module m^2	2.56	m^2
Nominal voltage for module	49	Volte

Table 8: Electric energy demand and PV power production On –Grid output data

Month	Heating demand still not covered kWh	Electric device demand kWh	electric demand from PV system kWh	PV system Production kWh	Need from grid kWh	Send to grid kWh
Jan.	0.0	10,477.38	10,477.38	9,335	-1142.38	0
Feb.	0.0	9,463.44	9,463.44	9,385	-78.44	0
Mar.	0.0	10,477.38	10,477.38	11,716	0	1238.62
Apr.	0.0	9,225.6	9,225.6	11,985	0	2759.4
May	4,434.8	9,533.12	13,967.87	11,872	-2095.87	0
Jun.	5,415.7	9,225.6	14,641.29	11,894	-2747.29	0
Jul.	5,950.1	6,308.88	12,258.97	12,878	0	619.02
Aug.	5,789.0	6,308.88	12,097.87	13,284	0	1186.12
Sep.	5,071.5	6,105.37	11,176.84	11,968	0	791.15
Oct.	1,112.5	9,185.68	10,298.22	10,698	0	399.77
Nov.	0.0	8,889.37	8,889.37	8,922	0	32.628
Dec.	0.0	9,185.68	9,185.68	8,223	-962.68	0
Total			132,159.95	132,160.00	-7027	7027

In order to calculate the number of modules and total area meter square needed to cover the electric load, PVwatts program is used. The size of capacity for PV modules is (87.5 kW).Then, total number of PV modules can be calculated from Equations 6 and 7;

$$Size\ DC\ (KW) = Module\ Capacity \times No.of\ Modules \quad (6)$$

Thus, $No.of\ Modules = \frac{87.5\times1000}{385} = 227.27 = approx\ 228\ module$

$$The\ total\ area\ for\ PV\ modules\ =\ No.of\ modules\ x\ Area\ of\ module \quad (7)$$

$$= 228\ x\ 2.56 = 583.68\ m^2$$

Another method for design PV system called stand-alone system (off-grid system) in which the system is working without any auxiliary source or supply for electricity such as grid [9].

Stand–alone system use batteries to store a power replacing the grid, Table 9 show the specification of batteries. It should be noted that the total number of batteries used for the PV system in this study is 715 batteries with number of modules 426 covered 1091. $61m^2$.

Table 9: Specifications of the batteries for the stand-alone PV system

PV system for Stand-alone system		Unit
Discharge limit	0.75	
Battery current Amp. hours	300	Ah/day
Battery Voltage	12	Volt
Efficiency of battery	0.8	
Anatomy days	3	Days

4. Conclusions

In this paper, the low and zero energy building design principles are applied to the faculty of engineering building at Garaboulli-Libya. Collected rain water and recycled grey water quantities are designed to be used for drinking, washing and toilet flushing or irrigation. The cooling, space heating and service hot water demand is determined. In addition, the total number and the area of the solar collectors are also evaluated. The electric demand for the building is also determined. Two design scenarios for covering electrical demands are adopted; Off-Grid and On-Grid. Total number of PV modules and total area are also calculated. Results show that the net zero energy design could be applicable for space heating, cooling and electricity demand. However, low energy design principle could be the case of rain water and grey water demand since the quantities are not sufficient to meet the required water demand. Finally, the issue of insulation, walls material, shading and other architectural measures are not taken into considerations in this study.

References

[1]. Housing and Infrastructure Board, "Guidance Document," Program Management Department, Tajura, Libya, 2008.

[2]. A. M. Ramadan, "Design Methodology and Maintenance Strategy of a Solar Gradient Solar Pond Coupled with an Evaporation Pond," M.Sc thesis, Tripoli University, Tripoli, Libya,1999.

[3]. A. M. Shuraideh, "Water consumption Practices in Schools of Nablus directorate of Education, "M.Sc theses, Nablus: An-najah National University, 2015.

[4]. J. Zhang, "University of California Berkeley Water Usage and Conservation," Study Report, Chancellor's Advisory Committee on Sustainability, California, 2010.

[5]. F-Chart Active and Passive Solar Systems Analysis, online in 2008 at https:// www.fchart.com/fchart/fchart.shtm

[6]. I. F. Okafor and G. Akubue, "F-Chart Method for Designing Solar Thermal Water Heating Systems," International Journal of Scientific & Engineering Research, Volume 3, Issue 9, September 2012 , ISSN 2229-5518

[7]. C. Webera, M. Bergerb, F. Mehlinga, A. Heinricha, T. Núñeza1, "Solar Cooling with Water–ammonia Absorption Chillers and Concentrating Solar Collector – Operational Experience," International Journal of Refrigeration ,Volume 39, Pages 57-76, March 2014

[8]. RET Screen International webpage, online in 2018 athttp://www.retscreen.net

[9]. Jin-Hee Kim , Ha-Ryeon Kim , and Jun-Tae Kim , "Analysis of Photovoltaic Applications in Zero Energy Building Cases of IEA SHC/EBC Task 40/Annex 52," Sustainability 2015, 7, 8782-8800; doi:10.3390/su7078782, 2015

Synthesis and Characterization of Magnetic $CoFe_{1.9}Cr_{0.1}O_4$ Nanoparticles by Sol-gel Method and Their Applications as an Adsorbent for Water Treatment

Ibrahim A. Amar[1],Abubaker Sharif[2], Najat A. Omer[3], Naght E. Akale[4], Fatima Altohami[5], Mabroukah A. AbdulQadir[6]
[1]ibr.amar@sebhau.edu.ly, [2]abu.sharif@sebhau.edu.ly, [3]njat.abdalhfed@fsc.sebhau.edu.ly, [4]naja.algali@fsc.sebhau.edu.ly, [5]fat.altohami@sebhau.edu.ly, [6]mabr.alsalheen@fsc.sebhau.edu.ly
[1-6]Department of Chemistry, Faculty of Sciences, Sebha University, Sebha/Libya

ABSTRACT

Water contamination by synthetic dyes is considered as a serious environmental issue, globally. In this study, the adsorptive removal of a very toxic cationic dye, methylene blue (MB), from aqueous solution was investigated using spinel ferrite, $CoFe_{1.9}Cr_{0.1}O_4$ (CFC), magnetic nanoparticles as an adsorbent. $CoFe_{1.9}Cr_{0.1}O_4$ powder was successfully synthesized via a sol-gel process and characterized by X-ray powder diffraction (XRD), Fourier transform infrared spectroscopy (FTIR) and scanning electron microscope (SEM) techniques. The effect of various experimental parameters on MB removal including; contact time, initial dye concentration, adsorbent dosage, solution pH and temperature were investigated. The results revealed that about 94 % of MB was removed under the optimal operational conditions. The adsorption kinetics showed that adsorption data were better described by pseudo-second-order model (PSO). In addition, the adsorption isotherms follow Langmuir isotherm model and the maximum monolayer adsorption capacity was found to be 11.41 mg/g. The calculated thermodynamic parameters (i.e., ΔG^o, ΔH^o, ΔS^o) indicate that the proposed adsorption process of methylene blue onto $CoFe_{1.9}Cr_{0.1}O_4$ nanoparticles is exothermic and spontaneous in nature. The results suggest that the synthesized magnetic nanoparticles (CFC) can be employed for the removal of toxic cationic synthetic dyes from wastewater.

Keyword— Spinel ferrites, adsorption, magnetic nanomaterials, methylene blue removal, nanotechnology, water purification.

1. Introduction

Water contamination by synthetic dyes has become a serious worldwide environmental issue owing to their adverse effect to human beings and aquatic life [1]. Dyes are important class of materials that have been widely used as coloring agents in many industries (e.g., paper, textile, cosmetics, etc.) [2]. Most of organic dyes which are discharged into the environment are toxic, mutagenic and carcinogenic in nature [3, 4]. Methylene blue (MB), a cationic dye, has found widespread use in textile industry [2]. The exposure to MB can cause a various type of health problems including; vomiting, nausea, profuse sweating, increased heart rate, mental confusion, quadriplegia, jaundice and cyanosis, etc. [2, 5].Thus removal of this very toxic dye before getting discharged into water body is of crucial importance.

Adsorption is among different techniques (e.g., coagulation-flocculation, oxidation, membrane filtration, ion-exchange, photocatalytic degradation and biological treatment) that have been developed with the aim of treating dye-contaminated water. Adsorption is preferred due to its remarkable advantages such as; availability of various adsorbent types, ease of operation, low cost, simplicity of design, high removal efficiency and insensitivity to toxic pollutants, etc. [5-8].

Recently, magnetic nanoparticles (MNPs) have attracted considerable attention as adsorbent materials for the devolvement of next generation water treatment technology [9, 10]. Nanotechnology offers a great potential not only in advancing the current water treatment technologies, but also in providing a secure and sustainable water supply approach [11]. Among MNPs adsorbents, spinel ferrites (MFe_2O_4, M = Co, Mg, Mn, Zn, etc.) are considered as promising adsorbent materials owing to their large specific surface area, fast kinetics, ease of function alization, moderate saturation magnetization, ease of separation from water in the presence of external magnetic field, and thermal, chemical and mechanical stabilities, etc. [9, 10, 12]. Therefore, various spinel ferrites and their composites including; $MnFe_2O_4$[13], $NiFe_2O_4$[14], $Mn_{0.2}Zn_{0.8}Fe_2O_4$[15], XFe_2O_4/GO (X = Co, Mn, Ni) [16] and AC/$Mn_{0.6}Zn_{0.4}Fe_2O_4$[8] have been used as nano-adsorbents for MB removal from aqueous solutions. Recently, Reddy et al. [9] and Kefeni et al. [4] have reviewed the recent advances in the application of spinel ferrites nanoparticles (SFNPs) in the field of water purification. To the best of our knowledge, there is no report on using $CoFe_{1.9}Cr_{0.1}O_4$ (CFC) nanoparticles as adsorbent for the adsorptive removal of MB. Thus, the aim of the present work is to synthesise CFC nanoparticle and investigating its adsorption properties for MB removal from aqueous solutions.

2. Materials and Methods

2.1. Materials

Methylene blue dye (319.85 g/mol) was purchased from ScP (Surechem products). Cobalt nitrate ($Co(NO_3)_2{\cdot}6H_2O$) was purchased from Analyticals, Iron nitrate nonahydrate ($Fe(NO_3)_3{\cdot}9H_2O$) was purchased from Berck and Scientific Supplies. Chromium nitrate ($Cr(NO_2)_3.9H_2O$) was purchased from Farmitalia Carloerba-SPA. Citric acid ($C_6H_8O_7$) was purchased from Labkem. Ethylenediaminetetraacetic acid, EDTA, ($C_{10}H_{18}N_2O_8$) was purchased from Serva. Hydrochloric acid (HCl) was purchased from BDH Chemicals. Sodium hydroxide (NaCl) was purchased from Fluka. Amonia was purchased from Scharlau. All chemical were used as received without further purification.

2.2. Synthesis of $CoFe_{1.9}Cr_{0.1}O_4$Nanoparticles

$CoFe_{1.9}Cr_{0.1}O_4$ (CFC) magnetic nanoparticles were synthesized using sol-gel method [17]. Briefly, $Co(NO_3)_2{\cdot}6H_2O$, $Fe(NO_3)_3{\cdot}9H_2O$ and $Cr(NO_2)_3.9H_2O$ were used as starting materials. Calculated amounts of these materials were dissolved in deionized water. Then, citric acid and EDTA were added to the mixed solution before adjusting its pH value to around 6 using ammonia solution. The mixed solution was

evaporated to dryness and the resulted solid product was calcined in air at 600 °C for 3 h to obtain CFC powder.

2.3. Characterization of $CoFe_{1.9}Mo_{0.1}O_4$ Nanoparticles

XRD analysis was carried out using a Philips – PW 1800 diffractometer with CuKαradiation (λ=1.54186 Å). The sample was scanned over 2*θ*ranging from 1.4 to 79.4º, with a step size of 0.02º. Equations (1) and (2) were used to estimate the average particle size (*D*) and lattice parameters (*a*) of CFC nanoparticles [18].

$$D = \frac{0.9\,\lambda}{(\beta\cos\theta)} \quad (1)$$

$$d_{hkl} = \frac{\lambda}{2sin\theta} \quad ; \quad a = d_{hkl}\sqrt{h^2 + k^2 + l^2} \quad (2)$$

Where $\lambda$is the wavelength of the X-ray, θ is the Bragg angle,β is the full width at half maximum (FWHM) of the peak in radiance, *d* is the interplanar distance and $hkl$are the Miller indices.

Fourier transform infrared spectrum (FTIR) was collected in the region of 400 to 4000 cm^{-1}, in KBr pellets, using a Bruker Tensor 27 spectrophotometer. The surface morphology of CFC nanoparticles was investigated by scanning electron microscopy (SEM) using a LEO 1430PV instrument. Typical "drift method" was used to determine the pH of CFC nanoparticles at the point of zero charge (pH_{PZC}) using NaCl solution (0.1 mol/L) [19]. Then, 25 mL of NaCl was transferred to a series flasks and the initial pH value (pH_i) was adjusted to 3, 5, 7, 9 and 11 by adding either a 0.1 mol/L solution of HCl or NaOH. To each flask, 0.1 g of CFC nanoparticles was added and the flasks were closed tightly. After a shaking of 24 h, the final pH value (pH_f)was measured. The pH_{PZC} was obtained from the plot of ΔpH (pH_i-pH_f) against the pH_i[20]. All experiments were carried out at room temperature (~ 25 °C), otherwise stated.

2.4. Adsorption Experiments

A stock solution of MB (500 mg/L) was prepared by dissolving the accurate amount of MB into deionized water. The desired concentration of MB was obtained by diluting the stock solution. The adsorption experiments were performed in batch mode by shaking the adsorbent (CFC) and 20 mL of MB solution in a closed 25 mL Erlenmeyer flask for a certain agitation time at speed of 320 rpm using an orbital shaker (IKA-Werke). The MB adsorption into CFC surface was investigated under different experimental conditions including; contact time (0-120 min), initial dye concentration (25-55 mg/L), adsorbent dosage (0.01-0.20 g/20mL), initial pH (3-11), and solution temperature (25-55 ºC). A diluted solution of either HCl or NaOH at a concentration of 0.1 mol/L was used to adjust the pH of dye solution using a pH meter (Jenway model 3505). A single beam UV-vis spectrophotometer (Jenway model 6305)was used to determine the MB concentration before and after adsorption experiments at λ_{ma} of 662 nm[2]. The percentage of MB removal

(%*R*), the amount of MB adsorbed at any time t (q_t, mg/g) and the amount of MB adsorbed at equilibrium (q_e, mg/g), are calculated using the following equations [3, 21]:

$$\%R = \frac{C_o - C_t}{C_o} \times 100 \quad (3)$$

$$q_t = \frac{V(C_o - C_t)}{m} \quad (4)$$

$$q_e = \frac{V(C_o - C_e)}{m} \quad (5)$$

whereC_o is the initial dye concentrations (mg/L), $C_t$and $C_e$are the final dye concentration (mg/L) at any time t and at equilibrium, respectively.m is the adsorbent dosage (g) and V is the volume of dye solution (L). To minimize the experimental errors, the adsorption experiments were performed in triplicate and the data were reported as the mean ± SD.

3. Theory and Calculation

3.1. Adsorption Kinetics

In this study, two common kinetic models including; pseudo-first-order (PFO) [22]and pseudo-second-order (PSO) [23] were applied for better understanding the adsorption process kinetics. For this purpose, the experimental data were fitted to the linear forms of PFO (Equation (6)) and PSO (Equation (7)), as expressed below [24];

$$\ln(q_e - q_t) = \ln q_e - k_1 t \quad (6)$$

$$\frac{t}{q_t} = \frac{1}{k_2 q_e^2} + \frac{1}{q_e} t \quad (7)$$

where q_e and $q_t$are as stated above, $k_1$is PFO constant (min^{-1}) and $k_2$is PSO (g/mg min). The values of q_e and k_1 were calculated from the intercept and slope of the plot of $\ln(q_e - q_t)$versus t, respectively. The values of$k_2$andq_e and were calculated from the intercept and the slop of plot of t/q_tversus t.

3.2. Adsorption Isotherms

To describe the nature of adsorbate-adsorbent interaction, the two most widely used isotherm models namely Langmuir [25] and Freundlich [26] were employed. Therefore, the experimental data at varying initial dye concentrations (25-55 mg/L) were fitted using these isotherm models. Langmuir and Freundlich isotherm models are suitable for describing the adsorption on homogenous and heterogeneous surfaces, respectively.

The linearized forms of Langmuir and Freundlich isotherms can be expressed using Equations (8) and (9), respectively, as described below [24];

$$\frac{C_e}{q_e} = \frac{1}{q_{\max} K_L} + \frac{1}{q_{\max}} \quad (8)$$

$$\ln q_e = \ln K_F + \frac{1}{n} \ln C_e \quad (9)$$

where $q_{\max}$ is the maximum amount of MB adsorbed (mg/g), K_L and K_F are Langmuir (L/mg) and Freundlich((mg/g)/(mg/L)^n) constants, respectively. n is Freundlich intensity parameter (dimensionless), which indicates the surface heterogeneity or the adsorption driving force. The adsorption isotherm is favourable $(n < 1)$, unfavourable $(n > 1)$, irreversible $(n = 0)$and linear $(n = 1)$. The values of $q_{\max}$ and K_L, respectively, were calculated from the slope $(1/q_{\max})$ and the intercept $(1/q_{\max} K_L)$ of the linear plot of C_e against $C_e/q_{\max}$. The values of n and K_F, respectively, were calculated from the slope $(1/n)$and the intercept $(\ln K_F)$of the linear plot of $\ln C_e$ against $\ln q_e$. The feasibility of adsorption process can be evaluated using a dimensionless constant related to Langmuir isotherm called separation factor (R_L). The R_L value can be determined using the following equation [24].

$$R_L = \frac{1}{1 + K_L C_e} \quad (10)$$

The value of $R_L$suggests the type of the isotherm as follows; unfavourable $(R_L > 1)$, favourable $(0 < R_L < 1)$, irreversible$(R_L = 0)$ and linear $(R_L = 1)$.

3.3. Adsorption Thermodynamics

The thermodynamic parameters including Gibb's free energy change (ΔG^o), enthalpy change (ΔH^o) and entropy change (ΔS^o) were calculated using the following equations [24, 27];

$$\Delta G^o = \Delta H^o - T\Delta S^o \quad (11)$$

$$\ln K_c = \frac{-\Delta H^o}{R}\frac{1}{T} + \frac{\Delta S^o}{R} \quad (12)$$

$$K_c = \frac{C_s}{C_e} \quad (13)$$

where K_c is the distribution coefficient which calculated using Equation (13), C_s is thedye concentration on the adsorbent surface (mg/L), R is the gas constant(8.314 J/mol/K) and T is absolute temperature (K). The

values of ΔH^o (kJ/mol) and ΔS^o (kJ/mol) were determined from the slope and the intercept of the plot of $\ln K_c$ versus $(1/T)$, respectively.

4. Results and Discussion

4.1. Characterization of $CoFe_{1.9}Cr_{0.1}O_4$ Adsorbent

Figure 1 shows the characteristic of $CoFe_{1.9}Cr_{0.1}O_4$ (CFC)magnetic nanoparticles. The XRD patterns of CFC calcined in air at 600 °C for 3 h are shown in Figure 1(a). The result indicates that a single phase of spinel ferrite (CFC) was obtained and all the diffraction peaks in XRD pattern are well indexed to the cubic structure of magnetite (JCPDS card No. 19-0629). The average crystallite size (*D*), lattice parameters (*a*) and the unit cell volume (a^3) of CFC adsorbent were found to be 38.63 nm, 8.3160 ± 0.0996 Å and 575.29 $(Å)^3$, respectively. The FTIR spectrum of CFC nanoparticles is presented in Figure 1(b). As shown, the typical characteristic peak for all spinel oxides which corresponds to metal-oxygen vibration (Fe-O) was observed at 586cm^{-1}. The absorption peaks within the range of 874 to 1129 cm^{-1} are assigned to NO_3^- group that trapped during the synthesis of CFC nanoparticles. The observed peaks at approximately 1626 and 3402 cm^{-1} were attributed to O-H bending vibrations and O-H stretching vibrations, respectively [21, 28, 29]. Figure 1 (c) represents the SEM image of CFC magnetic nanoparticles which shows a heterogeneous structure with many pores. These pores are expected to enhance the adsorption properties of CFC nanoparticles. Figure 1(d) shows the pH at the point of zero charge (pH_{PZC}) of CFC nanoparticles. As can be seen, the pH_{PZC} value of CFC nanoparticles was equal to 6.33.

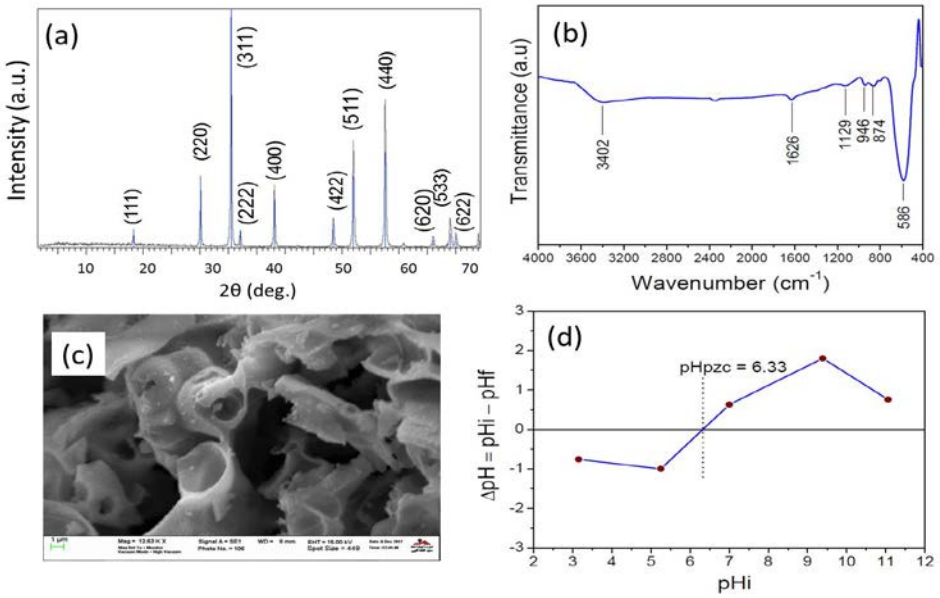

Figure 1:(a) XRD pattern, (b) FTIR spectrum, (C) SEM and (d) the point of zero charge of CFC magnetic nanoparticle

4.2. Adsorption Study

4.2.1 Effect of Contact Time

Figure 2 shows the effect of the contact time on the removal percentage (%R) of MB. In this experiment, 25 mg/L, 60 min and 0.01 g/20 mL were used as the initial MB concentration, contact time and adsorbent dosage, respectively. As can be seen, the %R increased significantly with increasing the contact time. In addition, a value of about 69.79% was attained when the contact time reached a 60 min after which no significant change in the %R was observed. This could be due to the saturation of the available active sites onto the adsorbent [30]. Thus, 60 min seems to be the optimum contact time.

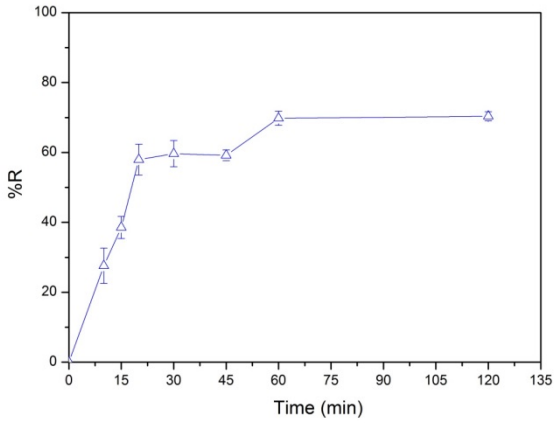

Figure 2: Effect of the contact time on the percent removal of MB

4.2.2 Effect of the initial dye concentration

The effect of MB dye concentration on the %R was investigated by varying the initial MB concentration from 25 to 55 mg/L and keeping the other operational condition at constant values (contact time of 60 min, adsorbent dosage of 0.01g/20 mL and room temperature. As shown from Figure 3, there is significant decrease in the %R value from 69.79% to 22.85% with increasing the MB concentration from 25 to 55 mg/L. This decrease in the percentage removal of MB could be due to the saturation the active adsorption sites of the adsorbent nanoparticles (CFC) after adsorbing a certain amount of MB dye molecules [31]. Therefore 25 mg/L was chosen as an optimum concentration for further studies.

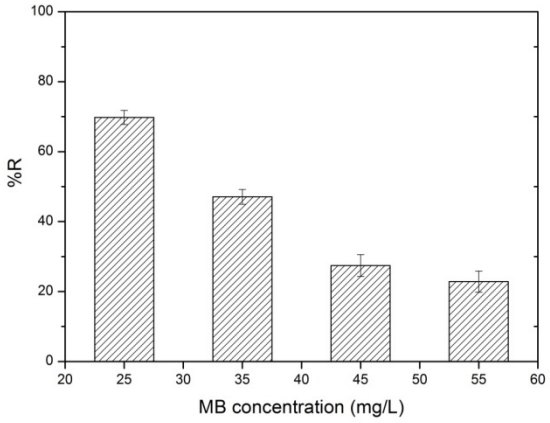

Figure 3: Effect of the initial dye concentration on the MB removal percentage

4.2.3 Effect of Adsorbent Dosage

The adsorption of MB (25 mg/L) using different adsorbent dosages (0.01-0.20 g/20 mL) is shown in Figure 4. The results reveal that the %R of MB increased from 45.92 to 69.97% by increasing the adsorbent dosage from 0.01 to 0.02 g/20 mL. This could be due to the increase in the number of active sites on the adsorbent surface [3]. However, no significant change in the %R was observed by future increasing the adsorbent dosage from 0.02 to 0.2 g/20 mL. Thus, 0.02 g/20 mL was chosen as the optimum adsorbent dosage. Figure 4 also shows that the amount of MB adsorbed at the equilibrium (q_e, mg/g) decreased significantly as the adsorbent dosage was increased 0.01 to 0.2 g/20 mL (22.96 to 1.83 mg/g). This may be due to the decrease in adsorbent total surface area as a result of aggregation or overlapping of the available active sites [2].

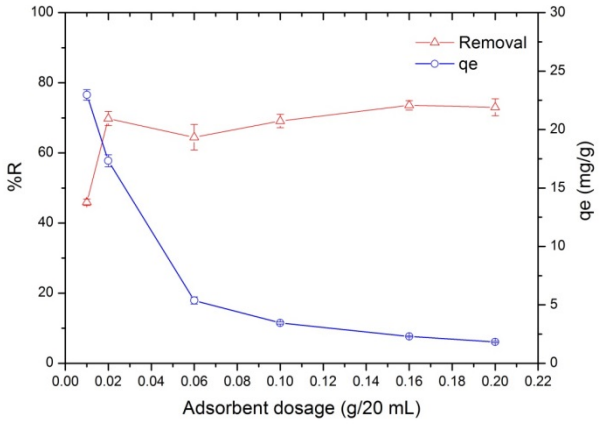

Figure 4: Effect of the adsorbent dosage on the MB removal percentage and the amount of MB adsorbed at the equilibrium

4.2.4 Effect of Solution pH

Figure 5 shows the effect of initial solution pH on the %R MB onto CFC nanoparticles. This effect was investigated by varying the initial pH of MB solution from 3 to 11 and keeping the other experimental condition at the optimized values. As shown, there is an increase in the %R value by increasing the solution pH from 3 to 5 (81.84 to 93.54%). However, the %R value decreased as the solution pH was further increased. Therefore, a pH value of 5 was chosen as the optimum value. As mention above, the pH_{PZC} of CFC was found tobe 6.33, suggesting that its surface will be positively charged below the pH_{PZC} and negatively charged above the pH_{PZC}[9]. MB is a cationic dye and gives positively charged ions in the aqueous solutions [32]. This means that the %R value should be high above 6.33 as the surface of CFC is negatively charged. In addition, MB molecules that contain Cl^- and NaOH that used for adjusting the pH values will undergo to replacement reaction and resulting in NaCl formation. Hence, the decreased %R values at high pH values (> 5) might be due to in the increase in the solution ionic strength that resulted from NaCl formation [33].

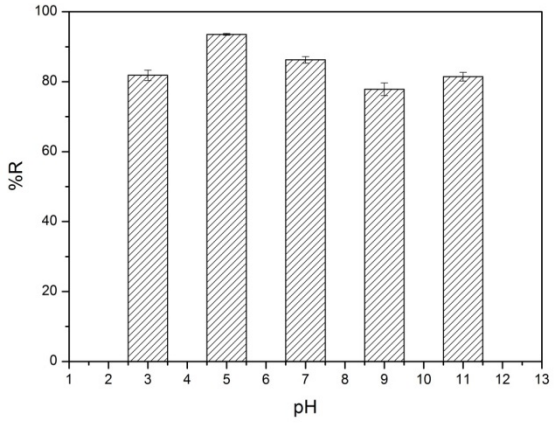

Figure 5: Effect of initial pH on the MB removal percentage

4.2.5 Effect of Solution Temperature

To investigate the effect of solution temperature on the %R of MB onto CFC nanoparticles, the experiment was carried out at different temperatures (25 to 55 °C) under the optimum operational conditions (contact time of 60 min, initial MB concentration of 25 mg/L and adsorbent dosage of 0.02 g/20 mL and pH value of 5). The results revealed that the %R decreased from 91.06 to 59.11% with increasing the solution temperature from 25 to 55 °C, as presented in Figure 6. This indicates that the proposed adsorption process is exothermic in nature. This decrease in the %R of MB with increasing solution temperature can be

attributed the increase in the mobility of dye molecule. Consequently, less MB molecules were adsorbed onto CFC nanoparticles at high temperature [6].

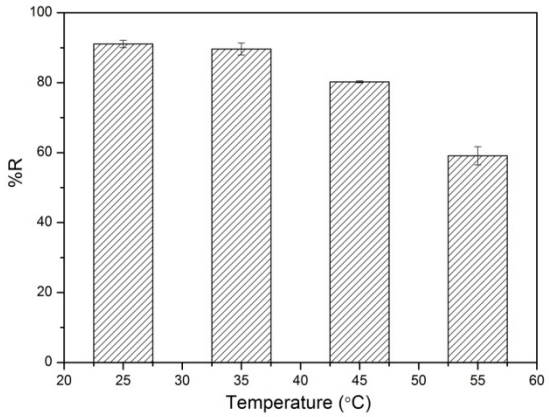

Figure 6: Effect of solution temperature on the MB removal percentage

4.3. Adsorption Kinetics

In the present study, pseudo-first-order (PFO) and pseudo-second-order (PSO) kinetic models were employed to evaluate the adsorption data using linear regression method. Table 1 lists the fitting parameters of these two models. As listed in the table, the calculated $q_{e,cal}$ value that obtained from PSO is close to the experimental $q_{e,exp}$ value, in contrast to the value obtained from PFO. In addition, the correlation coefficient (R^2)value of PSO was found to be 0.9759 which is higher than that of PFO (0.8208). This indicates that the pseudo-second-order model is more applicable for describing the adsorption kinetics of MB onto CFC nanoparticle.

Table 1: Kinetic parameters for the adsorption of MB onto CFC nanoparticles

$q_{e,exp}$(mg/g)	**Pseudo-first-order**		
	$q_{e,cal}$ (mg/g)	**k_1 (min^{-1})**	**R^2**
17.73	20.63	7.01×10^{-2}	0.8208
	Pseudo-second-order		
	$q_{e,cal}$ (mg/g)	**k_2 (g/mg.min)**	**R^2**
	19.25	6.69×10^{-3}	0.9759

4.4. Adsorption Isotherms

Langmuir and Freundlichisotherm parameters such as q_{max}, K_L, K_F, n and R^2 are listed in Table 2. According to the tabulated values, Langmuir isotherm model exhibits the highest correlation coefficient value ($R^2 = 0.9859$). This means that the proposed adsorption process is better described by Langmuir isotherm. Furthermore, the maximum adsorbed amount of MB (q_{max}) is found to be 11.41 mg/g. This value is higher than the value (3.31 mg/g) that reported by Patil et al. [34] for MB adsorption using an adsorbent composed of polyaniline-spinel ferrite (PANI-$NiFe_2O_4$) and lower than the value (40.97 mg/g) obtained using $Mn_{0.2}Zn_{0.8}Fe_2O_4$ as an adsorbent as reported by Hou et al. [15]. In addition, the calculated R_L values within the initial concentration range of 25-55 mg/L were less than unity (0.59-0.39), indicating the favourability of the adsorption of MB onto CFC nanoparticles [24].

Table 2: Adsorption isotherm parameters for adsorption of MB onto CFC nanoparticles

Langmuir isotherm		
q_{max} (mg/g)	**K_L (L/mg)**	**R^2**
11.41	0.109	0.9859
Freundlish isotherm		
K_F (mg/g)/(mg/L)^n	**n**	**R^2**
27.8	4.69	0.7455

4.5. Adsorption Thermodynamics

Table 3 summarizes the calculated thermodynamic parameters of MB adsorption on CFC nanoparticles. The negative values of ΔG^o at different solution temperatures (298-328 K) indicate the proposed adsorption process is feasible and spontaneous in nature. In addition, as the solution temperature increased, the negative ΔG^ovalues decreased, indicating that low temperature is favourable for MB adsorption. The negative ΔH^o value implies that MB adsorption is exothermic process in nature. Furthermore, the value of ΔS^o was negative, indicating the decreased randomness at the solid/liquid interface during the proposed process.

Table 3: Thermodynamic parameters for adsorption of MB onto CFC nanoparticles

		ΔG^o(kJ/mol)			
(kJ/mol)	**(J/mol.K)**	**298 K**	**308 K**	**318 K**	**328 K**
- 53.26	- 157.38	-6.36	-4.79	-3.21	-1.64

5. Conclusions

In summary, spinel ferrite, $CoFe_{1.9}Cr_{0.1}O_4$ (CFC), magnetic nanoparticles were successfully synthesized and employed as adsorbent for the removal of MB from aqueous solutions. The adsorption process was highly dependent on the operational conditions. More than 90% of MB was removed at the optimum conditions (i.e., contact time of 60 min, initial dye concentration of 25 mg/L, adsorbent dosage of 0.02 g/20 mL, initial solution pH of 5 and solution temperature of 25 °C. The kinetic study indicated the applicability of pseudo-second-order for describing the adsorption data. The isotherm study revealed that Langmuir isotherm better described the adsorption of MB onto CFC nanoparticles. The maximum adsorbed amount of MB was found to be 11.41 mg/g. The calculated thermodynamic parameters demonstrated that the proposed adsorption process was feasible, spontaneous and exothermic in nature. The results revealed that the prepared magnetic adsorbent (CFC) is a promising and can be employed for the removal of very toxic organic materials from wastewater.

Acknowledgment

The authors are thankful to the Department of Chemistry, Sebha University, Sebha, Libya for the financial support of this work. The authors also thank the Central Laboratory at Sebha University, Sebha Libya for providing the furnace for material calcination. The authors thank the Libyan Petroleum Institute, Tripoli, Libya for performing XRD and SEM analysis. The authors also thank Mr. Fathi Elsharif and Mr. Khaled Azzabi from the Nuclear Research Centre, Tajoura, Libya for performing FTIR analysis.

References

[1]. C. Santhosh, V. Velmurugan, G. Jacob, S. K. Jeong, A. N. Grace and A. Bhatnagar "Role of nanomaterials in water treatment applications: A review," Chemical Engineering Journal, vol. 306, pp. 1116-1137, 2016.

[2]. H. Singh, G. Chauhan, A. K. Jain and S. K. Sharma,"Adsorptive potential of agricultural wastes for removal of dyes from aqueous solutions," Journal of Environmental Chemical Engineering, vol. 5, pp. 122-135, 2017.

[3]. F. Moeinpour, A. Alimoradi, and M. Kazemi, "Efficient removal of Eriochrome black-T from aqueous solution using NiFe2O4 magnetic nanoparticles," Journal of Environmental Health Science and Engineering, vol. 12, pp. 112, 2014.

[4]. K. K. Kefeni, B. B. Mamba, and T. A. M. Msagati, "Application of spinel ferrite nanoparticles in water and wastewater treatment: A review," Separation and Purification Technology, vol. 188, pp. 399-422, 2017.

[5]. M. Rafatullah, O. Sulaiman, R. Hashim and A. Ahmad, "Adsorption of methylene blue on low-cost adsorbents: A review," Journal of Hazardous Materials, vol. 177, no. 1-3, pp. 70-80, 2010.

[6]. T. K. Mahto, A. R. Chowdhuri, and S. K. Sahu, "Polyaniline-functionalized magnetic nanoparticles for the removal of toxic dye from wastewater," Journal of Applied Polymer Science, vol. 131, pp. 40840, 2014.

[7]. Ahmed, S. H. Mohd-Setapar, C. S. Chuon, A. Khatoon, W. A. Wani, R. Kumar and M. Rafatullah, "Recent advances in new generation dye removal technologies: noval search for approaches to repocess wastewater," RSC Advances, vol. 5, pp. 30801-30818, 2015.

[8]. R. Wang, J. Yu, and Q. Hao, "Activated carbon/Mn0.6Zn0.4Fe2O4 composites: Facile synthesis, magnetic performance and their potential application for the removal of methylene blue from water," Chemical Engineering Research and Design, vol. 132, pp. 215-225, 2018.

[9]. D. H. K. Reddy, and Y. S. Yun, "Spinel ferrite magnetic adsorbents: alternative future materials for water purification?," Coordination Chemistry Reviews, vol. 315, pp. 90-111, 2016.

[10]. D. Mehta, S. Mazumdar, and S. K. Singh, "Magnetic adsorbents for the treatment of water/wastewater-A review," Journal of Water Process Engineering, vol. 7, pp. 244-265, 2015.

[11]. Y. Zhang, B. Wu, H. Xu, H. Liu, Hui, M. Wang, Y. He and B. Pan, "Nanomaterials-enabled water and wastewater treatment," NanoImpact, vol. 3–4, pp. 22-39, 2016.

[12]. J. Gomez-Pastora, E. Bringas, and I. Ortiz, "Recent progress and future challenges of high performance magnetic nano-adsorbent in environmental applications," Chemical Engineering Journal, vol. 256, pp. 187-204, 2014.

[13]. X. Hou, J. Feng, Y. Ren, Z. Fan and M. Zhang, "Synthesis and adsorption properties of spongelike porous MnFe2O4," Colloids and Surfaces A: Physicochemical and Engineering Aspects, vol. 363, pp. 1-7, 2010.

[14]. X. Hou, J. Feng, X. Liu, Y. Ren, Z. Fan, T. Wei, J. Meng and M. Zhang,"Synthesis of 3D porous ferromagnetic NiFe2O4 and using as novel adsorbent to treat wastewater," Journal of colloid and interface science, vol. 362, pp. 477-485, 2011.

[15]. X. Hou, J. Feng, X. Liu, Y. Ren,Z. Fan and M. Zhang,"Magnetic and high rate adsorption properties of porous Mn1-xZnxFe2O4 ($0 \leqslant x \leqslant 0.8$) adsorbents," Journal of colloid and interface science, vol. 353, pp. 524-529, 2011.

[16]. L. G. Bach, T. V. Tran, T. D. Nguyen, T. V. Pham and S. T. Do, "Enhanced adsorption of methylene blue onto graphene oxide-doped XFe2O4 (X = Co, Mn, Ni) nanocomposites: kinetic, isothermal, thermodynamic and recyclability studies," Research on Chemical Intermediates, vol. 44, pp. 1661-1687, 2018.

[17]. Y. Ling, J. Yu, B. Lin, X. Zhang, L. Zhao and X. Liu, "A cobalt-free Sm0.5Sr0.5Fe0.8Cu0.2O3-δ-Ce0.8Sm0.2O2-δ composite cathode for proton-conducting solid oxide fuel cells," Journal of Power Sources, vol. 196, pp. 2631-2634, 2011.

[18]. Y. P. Fu, S. H. Chen, and J. J. Huang, "Preparation and characterization of Ce0.8M0.2O2-δ (M = Y, Gd, Sm, Nd, La) solid electrolyte materials for solid oxide fuel cells," International Journal of Hydrogen Energy, vol. 35, pp. 745-752, 2010.

[19]. M. Kosmulski, Surface charging and points of zero charge: CRC press, 2009.

[20]. H. N. Tran, Y. F. Wang, S. J. You and H. P. Chao, "Insights into the mechanism of cationic dye adsorption on activated charcoal: The importance of π–π interactions," Process Safety and Environmental Protection, vol. 107, pp. 168-180, 2017/04/01/, 2017.

[21]. W. Konicki, D. Sibera, E. Mijowska, Z. Lendzion-Bieluń and U. Narkiewicz,"Equilibrium and kinetic studies on acid dye Acid Red 88 adsorption by magnetic ZnFe2O4 spinel ferrite nanoparticles," Journal of colloid and interface science, vol. 398, pp. 152-160, 2013.

[22]. S. Lagergren, "About the Theory of so-called Adsorption of Soluble Substances," Kungliga Sevenska Vetenskapasakademiens Handlingar, vol. 24, pp. 1-39, 1898.

[23]. Y. S. Ho, and G. McKay, "Pseudo-second order model for sorption processes," Process Biochemistry, vol. 34, pp. 451-465, 1999.

[24]. H. N. Tran, S. J. You, A. Hosseini-Bandegharaei and H. P. Chao, "Mistakes and inconsistencies regarding adsorption of contaminants from aqueous solutions: A critical review," Water Research, vol. 120, pp. 88-116, 2017.

[25]. Langmuir, "The constitution and fundamental properties of solids and liquids. Part I. Solids. ," The Journal of the American Chemical Society, vol. 38, pp. 2221-2295, 1916.

[26]. H. M. F. Freundlich, "Over the adsorption in solution," The Journal of Physical Chemistry, vol. 57, pp. 385-470, 1906.

[27]. L. R. Bonetto, F. Ferrarini, C. D. Marco, J.S. Crespo, R. Guégan and M. Giovanela, "Removal of methyl violet 2B dye from aqueous solution using a magnetic composite as an adsorbent," Journal of Water Process Engineering, vol. 6, pp. 11-20, 2015.

[28]. M. Stoia, and C. Muntean, "Preparation, Characterization and Adsorption Properties of MFe2O4 (M = Ni, Co, Cu) Nanopowders," Environmental Engineering and Managment Journal, vol. 14, pp. 1247-1259, 2015.

[29]. W. Wang, Z. Ding, M. Cai, H. Jian,Z. Zeng, F. Li and J. P. Liu,"Synthesis and high-efficiency methylene blue adsorption of magnetic PAA/MnFe2O4 nanocomposites," Applied Surface Science, vol. 346, pp. 348-353, 2015.

[30]. K. Erol, K. Köse, D. A. Köse, U. Sızır, S. İ. Tosun and L. Uzun,"Adsorption of Victoria Blue R (VBR) dye on magnetic microparticles containing Fe (II)–Co (II) double salt," Desalination and Water Treatment, vol. 57, pp. 9307-9317, 2016.

[31]. S. Chawla, H. Uppal, M. Yadav, N. Bahadur and N. Singh, "Zinc peroxide nanomaterial as an adsorbent for removal of Congo red dye from waste water," Ecotoxicology and Environmental Safety, vol. 135, pp. 68-74, 2017.

[32]. M. F. Zayed, W. H. Eisa, and B. Anis, "Removal of methylene blue using Phoenix dactylifera/PVA composite; an eco-friendly adsorbent," Desalination and Water Treatment, vol. 57, pp. 18861-18867, 2016.

[33]. Z. A. Al-Anber, M. A. Al-Anber, M. Matouq, O. Al-Ayed and N. M. Omari,"Defatted Jojoba for the removal of methylene blue from aqueous solution: Thermodynamic and kinetic studies," Desalination, vol. 276, pp. 169-174, 2011.

[34]. M. R. Patil, and V. Shrivastava, "Adsorptive removal of methylene blue from aqueous solution by polyaniline-nickel ferrite nanocomposite: a kinetic approach," Desalination and Water Treatment, vol. 57, pp. 5879-5887, 2016.

To What Extent Do Preschool Classrooms Match With The Architectural Design Considerations? Al-Khums City Centre, Libya As Case Study

Mustafa Zarigan [1], Lutfi Senan [2] , Muftah Omeman [3]
[1] mazarigan@elmergib.edu.ly, [2] lutfi.libyan@gmail.com, [3] Muftah_69@yahoo.com
[1, 2, 3] Department of Architecture and Planning Engineering, College of Engineering, Elmergib University, Libya

ABSTRACT

In the recent few years, there has been a continued increase in the number of preschools in Libya in general and in AL-Khums city in particular. The classrooms are crucially important in terms of child development during preschool education. There is a lack of prior local studies that deal with the architectural design standards of preschools. Indeed, most preschools in Al-Khums city were not standard and appropriately designed for children as preschools. They are originally residential buildings with switched usage. The main aim of this research is to investigate to what extent the classrooms match with the principles and design standards that specific to the Libyan context in the field of preschools design. These principles and criteria for the design of preschools in Al-Khums city will help decision-makers, architects, educational institutions, teachers, supervisors to ensure quality education that provided to children in a perfect indoor environment. To achieve the aim of this research, three preschools in the city centre has been selected. The results let to the conclusion that all of the classrooms are not enough for indoor children's activities. Hence, it is obvious from this small-scale study that the preschools in Libya do not respond to the needs of preschoolers. Thereby, the successful architectural design of preschools is the process that meets all the functional and educational requirements. This is done by taking into account the architectural design principles for the classrooms during the design process.

Keyword— Preschools, Classrooms, Spaces, Architectural Design Principles and Considerations.

1. Introduction

In the recent years, the outcomes of the early education and its role in improving a child's future academic performance have been understood. However, the quality of classrooms spaces was ignored. We have a long understanding that, more than any other building type, early childhood educational facilities have a profound impact on their occupants[1]. The children are greatly influenced by the spaces and facilities of the preschools [1]. Hence, the design of these facilities, cannot be understated as children in this country spend more than 1000 hours in preschool in two years.

Several developed countries including Canada, USA, UK, France, Belgium and Australia had detailed guidelines for architectural design principles and considerations in terms of preschool design. Nevertheless, Libya has few architectural design considerations that are insufficient to be a guide for architects. The main

scope of this research is to study indoor spaces in general and their status in classrooms in particular which appears to be more complex and raises some interesting architectural questions of significance to this research. Outdoor spaces, activities and environmental aspects are beyond this study.
There are no official statistics showing the number of children aged five and six years, but some academic sources suggest that the number of children under the age of six is up to 7 per cent (470,000).
This research demonstrates how the design of the tangible indoor environment should evolve to respond to the developmental needs of preschool in terms of classrooms. Both literature and analysis on preschool environments have been used to inform architects of particular design implications used to create a physical space successful in fostering and enhancing positive child development and effective learning.

2. Definitions

Terminology varies from country to country. A preschool, also known as nursery school, pre-primary school and kindergarten. It is an early childhood program in which children combine learning with the play before they begin compulsory education at primary school [2]. The term preschool which used in this paper is to address the educational settings visited, which are preparatory classes starting two years before primary schools. In addition, class size in this paper mentions the number of children learning in one space at one time, and how many square meters get every child.

3. Development of Preschools in Libya

In Libya, the first preschool - in its current form – was existed in 1910 and followed the method of Madame *Montessori* because the children had Italian nationality. In 1921, there were 3 preschools in Tripoli with 386 children of both sexes as well as one preschool in Benghazi and another one in Derna city. Later, in 1939, the number of preschools reached 8. After independence (1953), despite poverty and illiteracy, the Ministry of Social Security has incorporated the preschool phase into the learning system. In 1963, for the first time was referred to preschool (age 4-6 years). The following table shows the expansion of public preschools and the increase in the number of their children from 1960 to 1970[3].

Table 1: Development of preschools in Libya[3]

No	Academic Year	Number of Preschools	Number of Children
1.	1960-1961	18	1830
2.	1961-1962	17	1717
3.	1962-1963	14	1414
4.	1963-1964	21	1404
5.	1964-1965	18	1697
6.	1965-1966	21	1760

7.	1966-1967	21	1623
8.	1967-1968	24	1623
9.	1968-1969	18	1418
10.	1969-1970	19	1261
11.	1980-1981	40	-
12.	1981-1982	45	-
13.	1982-1983	56	-
14.	2006-2007	341	22731
15.	2008-2009	320	49929

After the revolution (2011), the preschool stage became part of the educational system of the Libyan Ministry of Education. In view of the continuous encouragement and interest of the Ministry, the number of preschools increased significantly in various cities including Al-Khums city. As a result, in 2015 the number of children in preschools increased by 50%. For this reason, the ministry established a special management for preschools and its functions are to prepare plans, programs, organise the laws and regulations as well as develop standards, conditions, specifications for buildings and equipment for preschools, including:

1. Adherence to international standards in selecting the site in proportion to the child at this stage.
2. Adhering to international standards in the design of kindergartens buildings in conformity with international quality standards.
3. Compliance with international safety and security standards in kindergartens.
4. The beautiful and exciting entrance to the child and the beloved he has who loves him in the kindergarten.
5. Floors, columns and stairs are equipped so as to reduce the injury of the child in case of falling.
6. The existence of emergency exits in sufficient numbers and to be in children's sites, and easy to reach.
7. The presence of fire extinguishers.

Today, preschool education is lasting two years and is for children aged four and five in order to prepare them for primary school at age of six. At the age of 4 children called the first year of foundation and 5 years of age called the second year of foundation before they go into primary school. This stage is optional. It can be publicly which funded by the education ministry or privately operated. Although, pre-schools do not have specific curricula or educational programs, the present curriculum is similar to the first year of primary school. Early years education in Libya is provided half-time for children which lasts three hours from 8:00 am to 11 am in public preschools. Meanwhile, the private is diversity[3].

4. Study Area

Al Khums (Khoms - Homs) is a city in north-western Libya. It is located on the Mediterranean coast about 120 Km east of Tripoli, the capital of the country. It has a population of around 220,000 people. Figure 1 shows the selected preschools in the study area.

$$f(x) = a_0 + \sum_{n=1}^{\infty} \left(a_n \cos \frac{n\pi x}{L} + b_n \sin \frac{n\pi x}{L} \right)$$

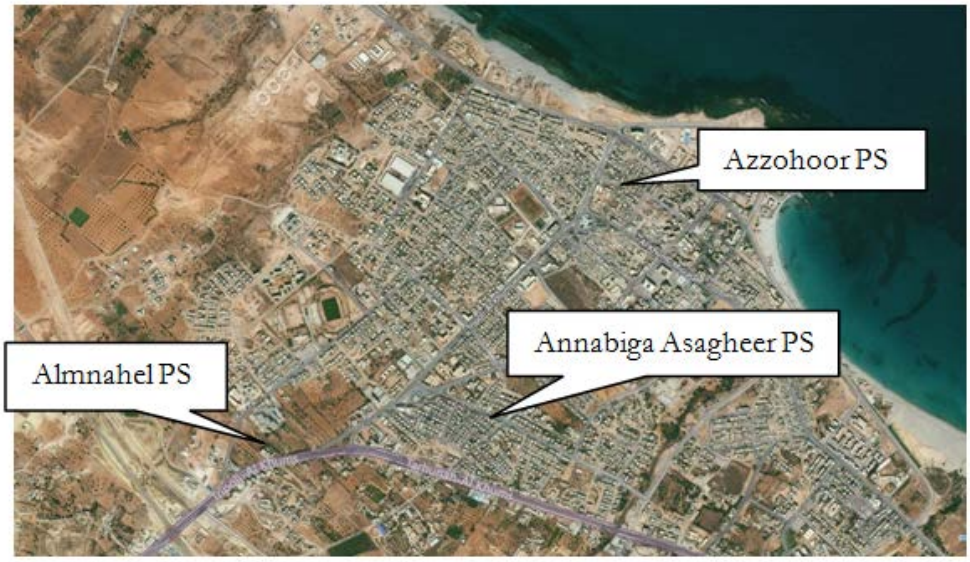

Figure 1: Alkums City- Study area

5. Results and Discussion

In preschool, classroom spaces are an important aspect of the learning environment for young children. The findings emphasize that not only the classrooms spaces but also the shape, furnishings and natural and artificial light and others.

5.1. Classrooms Spaces

Classrooms can vary in size and serve different functions, with children moving from one to another for different purposes. Instead of being single-purpose spaces, they can allow for a number of different activities, such as reading, research, group work and art. Olds (2001) stated that each child needs a space to place his/her own belongings which, in turn, give him a sense of ownership[4]. The classroom should well-equipped, with sufficient materials and toys. Planning considerations and design principles of preschools have been categorized and defined by the Libyan Urban Planning Department[5] as follows:

One preschool for every 4000 inhabitants and 2 preschools per primary school
The total area of the site is 25 - 30 square meters per child
The size of the classroom is 15-20 children
The walking distance from the residence to school by feet is no more than 500 m
Some academic The roofed area is 2.5 - 3 square meters per child
Despite the fact that preschooler needs space where he/she can play with his/her peers, smaller and quiet areas are essential for his/her own solitary activity (ergonomic) [1]. In a similar vein, classroom space should be large enough to accommodate a desired number of preschoolers. Jaclynn Shaw stated that "children are exceedingly sensitive to space; they respond to many kinds: big and small spaces, open spaces, cozy spaces, and especially hidden private spaces"[6]. Thus, the zoning of activity areas is very important. Recently, moving towards a classroom flexible in its design is a current trend within the design of preschool facilities. Therefore, designating spaces for classroom work such as reading and writing should be implemented. Besides the functional demands of the classroom, the question for design should be how the children feel inside it and how they are going to experience the space.

5.2. Case Studies

Three preschools has been selected (Figure 1). Two of them are basically residential buildings and the third one is designed as preschool (only one in the study area). However, its design similar to a residential building because there are no architectural design considerations have been applied in its design as preeschool. The selected case studies are:

- Azzohoor Preschool (Public Preschool)
- Almnahel Preschool (Private Preschool)
- Annabega Assageer Preschool (Private Preschool)

5.2.1 Azzohoor Preschool (Public Preschool)

Figure 2: A classroom in Azzohoor Preschool

Table 2: Main information about Azzohoor Preschool [7]

No	No of Preschoolers	Classrooms Size (m)				No of Windows			Size m² / child
		Area m²	Length	width	height	units	Size≈m²	Direction	
1.	45	32	8	4	3	2	2	East - West	**0.71**
2.	44	32	8	4	3	2	2	West	**0.72**
3.	43	32	8	4	3	2	2	East - West	**0.74**
4.	45	32	8	4	3	2	2	East	**0.71**

5.2.2 Almnahel Preschool (Private Preschool)

Table 3: Main information about Almnahel Preschool [7]

No	No of Preschoolers	Classrooms Size (m)				No of Windows			Size m² / child
		Area m²	Length	width	height	units	Size≈m²	Direction	
1.	18	24	6	4	3	2	1.5	West	**1.33**
2.	18	18	4.5	4	3	4	1.6	East	**1.00**
3.	12	9	3	3	3	3	1.6	North	**0.75**

5.2.3 Annabega Assageer Preschool (Private Preschool)

Figure 3: A classroom in Annabega Assageer

Table 4: Main information about Annabega Assageer Preschool [7]

No	No of Preschoolers	Classrooms Size (m)				No of Windows			Size m² / child
		Area m²	Length	width	height	units	Size≈m²	Direction	
1.	10	12.25	3.5	3.5	3	1	0.80	North	**1.22**
2.	10	9	3	3	3	1	0.80	South	**1.11**
3.	18	12.25	3.5	3.5	3	1	0.80	North	**1.22**

The three preschools that were part of this research their classes are small and did not have appropriate facilities. In public preschool, for instance, space was inadequate because classrooms were overcrowded. Approximately 44 preschoolers were enrolled per classroom. The tables in three of them were arranged in lines. In addition, there are no any materials, toys, bookcases, art activities, blocks and manipulatives/fine motor. It was very poor and space generally lacked adequate lighting. Very limited attention was paid to safety issues. In the three cases, there are no bathrooms or kitchen were located near the class. Even water source not existed. In general, there is lack in numbers of toilets.

5.3. Shape and Furnishings

In Libya, classrooms designs are usually rectangular or square shape. For example, in one of the selected preschools, all its classrooms are rectangles 8 * 3 m (table 1) and some classes are only 3 * 3 m (as shown in tables 2 & 3 and figure number 3 & 4).

Figures 3 & 4: classrooms are rectangular and square shape

In terms of classroom furniture, the classroom style seating is often rectangular desks that are arranged in horizontal rows which, in fact, were used in the middle of the last century. Whereas, an open classroom was implemented during the 1970s in the developed countries. This classroom type still used today [3]. Rearranging furniture in preschool classrooms may encourage classroom activities. In addition, in three examples, often only one style of furniture is used for all children. Desks and chairs in two of three preschools are the same sizes as primary schools. Moreover, the furniture characteristics are heavyweight and oversized for preschoolers. From previous tables, the size of the classrooms are not enough for carrying, lifting and turning desks.

5.4. Natural and artificial Light

There is no doubt that daylight and/or artificial light play a crucial role in the learning environment. The quality and quantity of light affect preschoolers' ability to see clearly, concentrate and learn effectively in the classroom. The light in all visited classrooms are very poor in both natural and artificial lighting (Figure5,6 & 7). In addition, windows orientations are not applicable to the standards, for instance, some classes windows are placing in the front and in the back of the classroom which could make glare. Furthermore, their number in each classroom are very few, for example, some classrooms have only one window and its area is only 0.70 m^2. Moreover, halogen and fluorescent bulbs (lamps) are only one or two in each classroom.

Figures 5, 6 & 7: Natural and artificial lighting in different classrooms

6. Conclusions

It is notable that most preschools in the study area are not standard and appropriately designed for children. They are mostly located in residential areas and apartment buildings that are painted to suit children. Recently, the Ministry of Education has focused on the educational progress of children in preschools. We hope that running the functional ideas of this study and considering the conditions, climate, and environment lead to a guideline for designing a standard preschool where children can learn, play, and grow up. This research can be generalized to other educational spaces such as elementary schools, training centres, and centres for Intellectual Development of Children and Adolescents. More studies in larger research fields are recommended for designing preschools environment, with a focus on indoor and outdoor elements, to improve children's learning.

References

[1]. Day, D. E. (1983). Early childhood education: A human ecological approach (T.W. Hipple, Ed.). Glenview, Illinois: Scott, Foresman and Company
[2]. B. E Şahin & N. Dostoğlu, "Evaluation of Kindergarten Group Rooms in the Context of Size: Children and Teacher's Perspective in Turkey. European Journal of Contemporary Education, 2014, Vol.(10), № 4
[3]. Amer, F. O (2018). Education in Libya and some other countries: A comparative study
[4]. Access online on 19 August 2018 at www.bing.com
[5]. Olds, 2001
[6]. The Libyan Urban Planning Department
[7]. Jaclynn, S
[8]. The Ministry of Education. Preschool management, Alkhums branch.

Solar Hydrogen Production System Simulation Using PSCAD

Matouk M. Elamari
Electronic department Engineering Academy Tajoura Libya
matoukelamari@yahoo.com

ABSTRACT

Hydrogen is a potential future energy storage medium to supplement a variety of renewable energy sources. It can be regarded as an environmentally-friendly fuel, especially when it is extracted from water using electricity obtained from solar panels or wind turbines. One of the challenges in producing hydrogen by using solar energy is to reduce the overall costs. It is therefore important that the system operates at maximum power.In this paper a PSCAD computer simulation based on a water-splitting, hydrogen-production system is presented. The hydrogen production system was powered by a photovoltaic (PV) array using a proton exchange membrane (PEM) electrolyser. Optimal matching between the PV system and the electrolyser is essential to maximise the transfer of electrical energy and the rate of hydrogen production. A DC/DC buck converter is used for power matching by shifting the PEM electrolyser I-V curve as closely as possible toward the maximum power the PV can deliver. The simulation shows that the hydrogen production of the PV-electrolyser system can be optimised by adjusting the converter duty cycle generated by PWM circuit.

Keyword— Renewable - photovoltaic- solar hydrogen- PEM electrolyser.

1. Introduction

In recent years, the central aim of world energy policy has been to develop renewable energy sources and share the energy they produce to reduce dependence on fossil fuels and to reduce the harmful emissions that result when they are burned. To fully take advantage of the environmental benefits of hydrogen, it must be produced from a renewable feedstock (renewable energy), but most of the hydrogen that is currently produced is derived from natural gas, which is a non-renewable fossil fuel.

Hydrogen produced from renewable energy sources offers the promise of a clean, sustainable energy carrier that can be produced from domestic energy resources around the globe. One method of hydrogen production using a renewable energy source is the electrolysis of water using renewable electricity, i.e., electricity generated from photovoltaic cells, wind turbines, hydroelectric turbines, or generators fuelled by biomass.

Several potential applications for electrolysis use solar- and wind-produced electricity. Solar PV cells and wind turbines convert solar energy and wind power, respectively, into electricity that can be used to produce hydrogen from water by electrolysis. Electrolysis using solar energy is a very attractive process to produce hydrogen .The exploitation of this important potential comes through the conversion of the solar energy to

an energy vector that is versatile, storable, transportable and ecologically acceptable. Today, hydrogen seems to be the best candidate

2. Components of the solar hydrogen production system

Hydrogen production through water electrolysis using solar photovoltaic cells to provide the required electricity is highly feasible. Both water and solar energy are available in huge amounts, and hydrogen provides an ideal means for storing and transporting electricity from solar energy. The PV uses light to generate DC electrical energy. The PV cell consists of one or two layers of a semi-conducting material (p-n junctions), usually silicon. When light shines on the cell, an electric field is created across the layers, which causes electricity to flow. The greater the intensity of the light, the greater the more power the PV cell delivers. The electric current produced by the PV cell is passed through water in an electrolyser, and the water molecules separate into hydrogen and oxygen. The most common electrolyser uses a proton exchange membrane (PEM) as a catalyst in the electrolysis process. In comparison to electrolysers that use a liquid electrolyte that must be replenished frequently, the PEM electrolyser has the advantages of producing very pure hydrogen, and requiring much less maintenance. In addition, it has easily scalable cells, and it can operate at much higher current densities than other types of electrolysers (1-2 A/cm2), with conversion efficiencies ranging from 50-90%. As mentioned earlier, electrolysers are thought to be a potentially cost-effective way of producing hydrogen locally. Electrolysers are compact and can realistically be located at existing fuelling places. Also, they offer a way to produce hydrogen with electrical power generated from renewable sources. Currently, renewable sources, such as solar, wind, and hydropower, produce only electricity, but the electricity they generate can also be used to produce hydrogen fuel through the use of electrolysers.

Figure 1 shows a PV hydrogen production system, which usually consists of the following main components: a PV array to supply the DC power to the system and PEM electrolyser; and DC-DC converter that consists of a control unit for power matching between the PV material and the PEM electrolyser and for providing the delivery of maximum power by PV material to maximize the hydrogen production rate.
Studies have been conducted on connecting solar PVs directly to an electrolyser (shown by the dotted path), thereby avoiding the need for a DC-DC converter. However, in this case, PV modules are not optimized to supply the most power the PV modules can deliver.

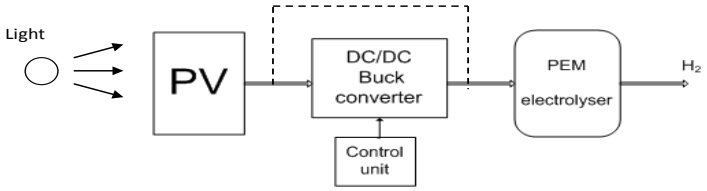

Figure 1: Block diagram of a PV hydrogen production system

One of the challenges in producing hydrogen by using solar energy (PV-Hydrogen system) is to reduce the cost. Therefore, it is important that the system operate at maximum power. This operation is usually achieved by matching the power generated by the PV cell with the power required to produce hydrogen.

3. PSCAD simulation

This part describes the use of PSCAD/EMTDC software to simulate the performance of a solar PV-PEM hydrogen production system.

System components:

Only the essential solar hydrogen production system components are included in this simulation programme. These components are the photovoltaic module, the DC-DC buck converter and the proton exchange membrane electrolyser.

The input data to the simulation programme are the solar irradiance hits the photovoltaic module, and the ambient temperature. The output results of the simulation are:

- Characteristics of the photovoltaic current, voltage, and power at standard test conditions (1000 W/m^{2}and 25 ^{o}C).
- Current and voltage readings at the input and output of the DC-DC buck converter
- Characteristics of the electrolyser's current and voltage
- Characteristics matching of the photovoltaic source and the electrolyser
- The operating current of the system
- Hydrogen production rate

3.1. PV Model

The PV solar cell was modelled in PSCAD/EMTDC, as shown in

Figure 2 There are two inputs and two outputs in this block. The inputs are terminal voltage and irradiance. The voltage varies from zero up to the open circuit voltage of the solar cell. The irradiance is assumed to be fixed at the standard test condition of 1000 W/m^2.
The two outputs are the current and power delivered by the solar cell. The maximum current is controlled by the irradiance. (More irradiance gives more current.) The power is the result of multiplying the voltage and the current.

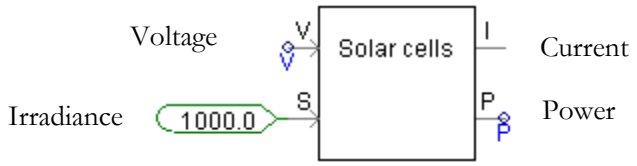

Figure2: Solar cell PSCAD block

Table 13: provides the parameters used in modelling a crystalline silicon solar cell [2] ,[7].

Symbol/Value	Description	Unit
q =1.602 x10^{-19}	Electron charge	C
k = 1.38x10^{-23}	Boltzmann constant	J/K
n = 1.792	Non-ideality factor	
Ta = 293	Ambient temperature	^{o}K
T_{ref} = 293	Reference temperature	^{o}K
$I\,sc$ = 2.0	Short circuit current at reference state	A
$NOCT$ = 49	Nominal Operating Cell Temperature	^{o}C
$J\,o$ = 1.6 ×10^{-3}	Temperature coefficient	A/^{o}K
S = 1000	Irradiance	W/m^2
$I_{do}\,do$ =71.1×10^{-9}	Diode reversal current	A

Table 10 Parameters used in modelling a solar cell based on a crystalline Silicon solar cell

The following equations were implemented in FORTRAN codes inside the block model:

$$T = T_a + S\frac{(NOCT - 20)}{800} \quad (1)$$

$$E_g = 1.16 - 7.02\times10^{-4}T^2(T + 1108) \quad (2)$$

$$I_0 = I_{do}(\frac{T}{T_{ref}})^3 \exp(\frac{qE_g}{nK}(\frac{!}{T_{ref}} - \frac{1}{T})) \quad (3)$$

$$I_{ph} = I_{sc}\frac{s}{1000} + J_o(T - T_{ref}).. \quad (4)$$

$$I_d = I_0 \exp(\frac{qV}{nkt} - 1)... \quad (5)$$

$$I = I_{ph} - I_d... \quad (6)$$

Where:

T = cell temperature.

T_a = ambient temperature.

I_0 = dark saturation current.

E_g = energy gap of cell semiconductor.

Id = diode current.

I_{ph} = photo current or light generated current.

V = cell output voltage.

3.1.1 Response of the solar cell to changes in irradiance

The characteristics of the solar cell at different levels of irradiance are shown below in Figure 3. The irradiance has a large effect on short-circuit current (the horizontal part of the I–V curves), while the effect on open-circuit voltage (the vertical part of the curve) is rather weak.

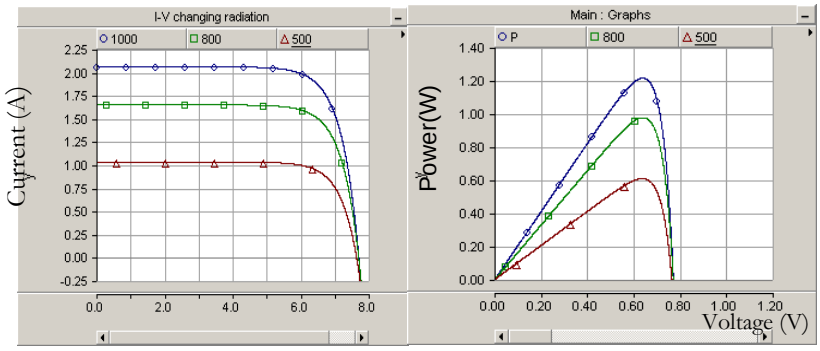

(a) I-V characteristics **(b)** V-P characteristics

Figure 3: the effect of irradiance on current and power in the solar cell

According to the voltage and power curves, the maximum output power of a photovoltaic cell changes with irradiance. When the irradiance is greater, the cell generates more power.

3.1.2 Response of the model PV solar cell to changes in temperature

As seen in Figure 4 as the cell temperature increases, the open circuit voltage decreases, whereas the short circuit current increases slightly. Increasing the temperature causes the voltage to decrease. This is a particularly severe problem, since the cell is often operated at the maximum power point, which is within the region.

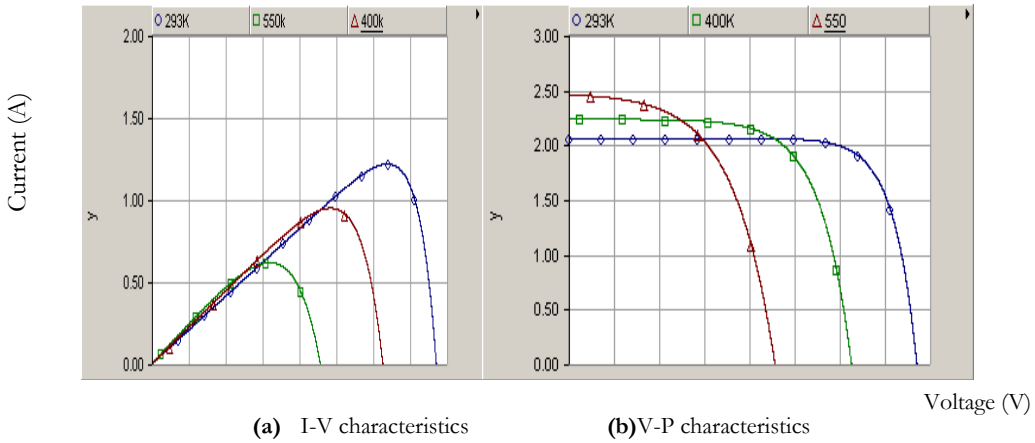

(a) I-V characteristics **(b)**V-P characteristics

Figure 4: the effect of temperature on current and voltage

The cell temperature varies because of changes in the ambient temperatures and because of changes in the levels of irradiance. Since only a small fraction of the irradiance on a cell is converted to electricity, most of that incident energy is absorbed and converted into heat.

From the simulation curve for the solar cell's I-V characteristics, we can see that the two values used to characterise the output of solar cells for a given irradiance level and operating temperature are:

1. Short circuit current, Isc, is the maximum current when the voltage is zero, i.e., the terminal points of the photovoltaic module are short circuited. The short circuit current is directly proportional to the available sunlight.
2. Open circuit voltage, Voc, is the maximum voltage when the current is zero, i.e., terminal points of the photovoltaic module are open circuited. The open circuit voltage increases logarithmically with increasing sunlight.

These two parameters are usually provided in the data sheets of PV modules. These parameters establish the operating point of the PV module along the I-V curve, i.e., the operating point moves along the I-V curve. It is desirable for the operating point to be at the point where maximum power from the PV module is generated. This is known as the maximum power point (MPP; $P_{mp} = V_{mp} \times I_{mp}$). V_{mp} and I_{mp} are the operating voltage and operating current at the maximum power point.

In practical applications, solar cells do not operate under standard conditions, because they are affected irradiance and temperature. Often, manufacturers provide plots that show the I-V curves shifting with irradiance and cell temperature changes.

3.2. Model of the PEM electrolyser

PEM water electrolysis is one of the most popular ways of producing pure hydrogen with compact equipment at a comparatively high level of efficiency. PEM is composed of a membrane, cathode, and anode, which produce hydrogen by providing pure water to one side of the polymer ion exchange film, which is placed between the anode and cathode.

The PEM cell is capable of high efficiency electrolysis under high current density conditions. The power consumption is proportional to the instantaneous current density, so the main consideration is the amount of current that can flow to the PEM cell from the DC-DC converter.

A unit PEM cell for water electrolysis was modelled by PSCAD/EMTDC block, as shown in Figure 5 the specifications for the cell are as follows:

- the operating temperature is 294 ^{o}K
- the effective area is 50 cm ^{2}
- the maximum electrolyte current is 50 A
- the electrolyte voltage is 2 V

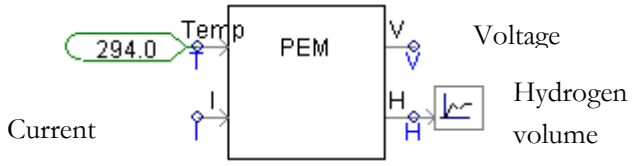

Figure 5: PSCAD PEM electrolyser block

The PEM model has two inputs and two outputs. The two inputs are current and temperature and the two outputs are voltage and the volume of hydrogen. The equations below govern the relationships between input and output variables.

The V-I relationship of a PEM cell is given by the following equations from [3],[4].

$$V = V_0 + \eta_c + \eta_a + IR, \quad (7)$$

where V is PEM cell voltage, V_0 is the theoretical dissociation voltage, which depends on absolute temperature T (°K), as shown:

$$V_0 = 1.5 - 1.5e^{-3}T + 9.5e^{-5}T\ln(T) + 9.8e^{-8}T^2 \quad (8)$$

The term η^0 is an excess voltage on the cathode side, and its value varies from 0.05 to 1 V.

The term η^a is an excess voltage on the anode side, with a maximum value of 0.3 V.

R is the electrical resistance of PEM. In the simulation, the value of R is set to 0.037 ohm. The current (I) represents the current that flows through the PEM electrolyser.

Figure 6 shows the V-P characteristics of the PEM cell electrolyser model. The voltage-current graph shows that, for the PEM (Proton Exchange Membrane) electrolyser, the current only starts to flow at a certain voltage, after which it rises continuously. The slope of the curve is dependent on its equivalent ohmic resistance.

The applied voltage must be at least as large as the theoretical cell voltage in order for current to flow, which leads to a release of hydrogen at the cathode and oxygen at the anode.

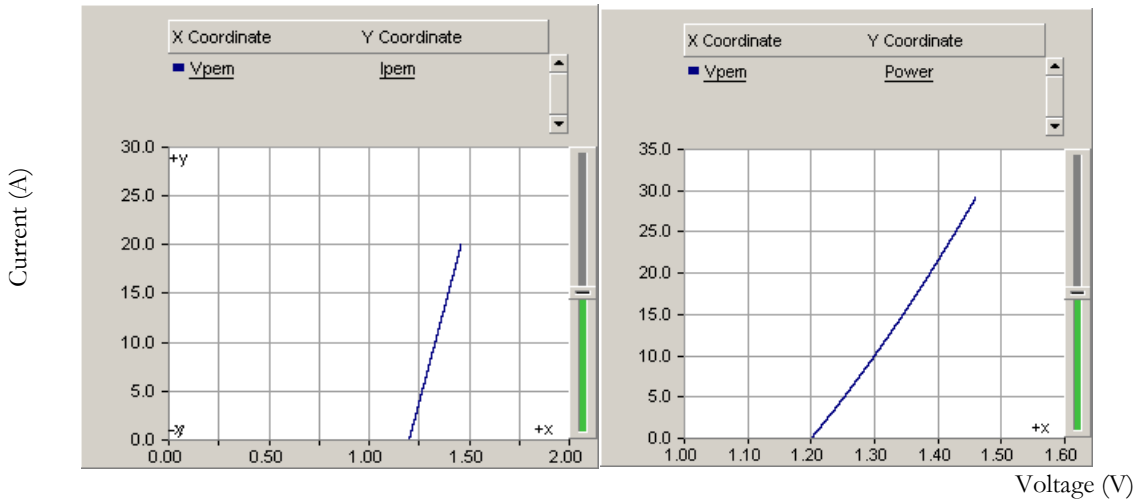

Figure 6: I-V and V-P Curves for the PEM electrolyser PSCAD model

4. PV–PEM electrolyser power matching using a DC-DC buck converter

The need for optimal power matching in the PV–PEM hydrogen production system is essential for maximum power transfer between the PV generator and the PEM electrolyser. The DC-DC buck converter is used for matching the power characteristics of both components.

Figure 7 shows the PSCAD/EMTDC simulation for the PV-PEM hydrogen production system using a DC-DC buck converter. The PV generator generates the DC power at standard conditions(1000 W/m^2 and 25 ^{0}C).

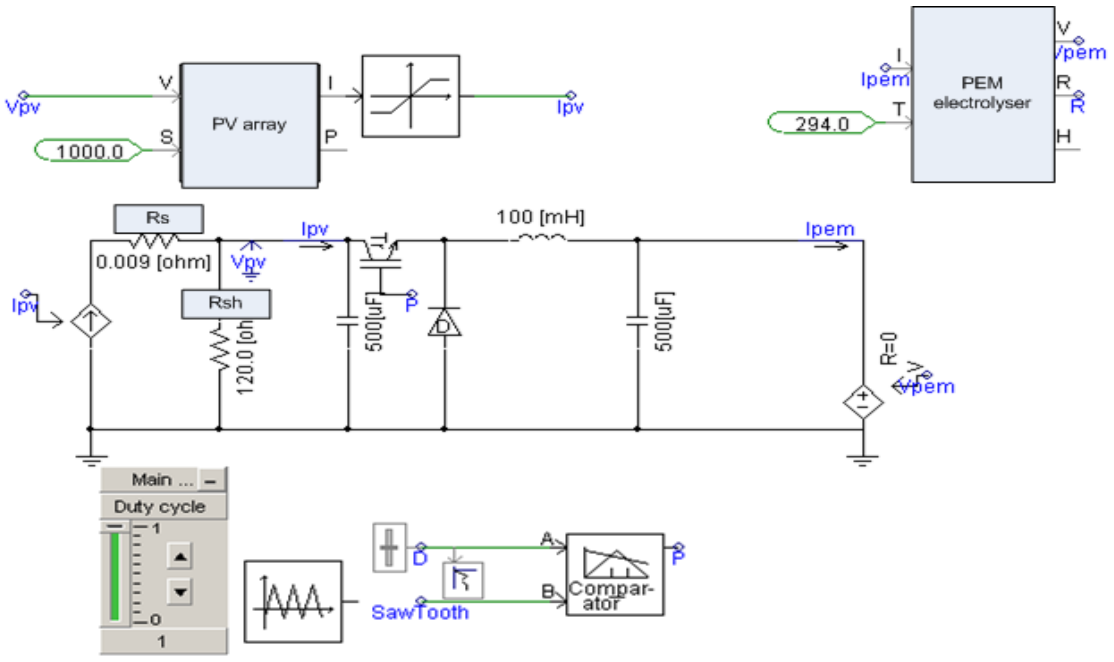

Figure7: PSCAD simulation of the PV-PEM electrolyser hydrogen production system using a buck converter

The series resistance Rs and shunt resistance Rsh are calculated as follows:

$$Rs\langle\frac{0.01V_{oc}}{I_{sc}} \text{ and } Rsh\rangle\frac{100V_{oc}}{I_{sc}}$$

To generate different duty cycle values, a fixed-amplitude, saw tooth signal is compared with a changeable voltage level. A comparator produces pulses with different duty cycles. The pulses switch the buck converter switch on and off , and the durations of the on and off states control the relationships between the PV voltage Vpv and current Ipv and the PEM electrolyser voltage Vpem and current Ipem, as follows:

$$D=\frac{Ton}{Ton+Toff}=\frac{Vpem}{Vpv}=\frac{Ipv}{Ipem} \quad (9)$$

From equation (9), it is apparent that there is a different operating point for every duty cycle of the switch of the DC-DC converter.

The following PSCAD simulation results were obtained under standard irradiance (1000 W/m^2) and standard temperature (25 ^{0}C), and the measured values are volts for voltage readings and amperes for current values.

The power supply of the circuit is a PV module, and its characteristics are shown in Figure 8. The short-circuit current is 0.7 A, and the open-circuit voltage is 20 V; the operating voltage of the two-cell PEM electrolyser is approximately 5.8 V.

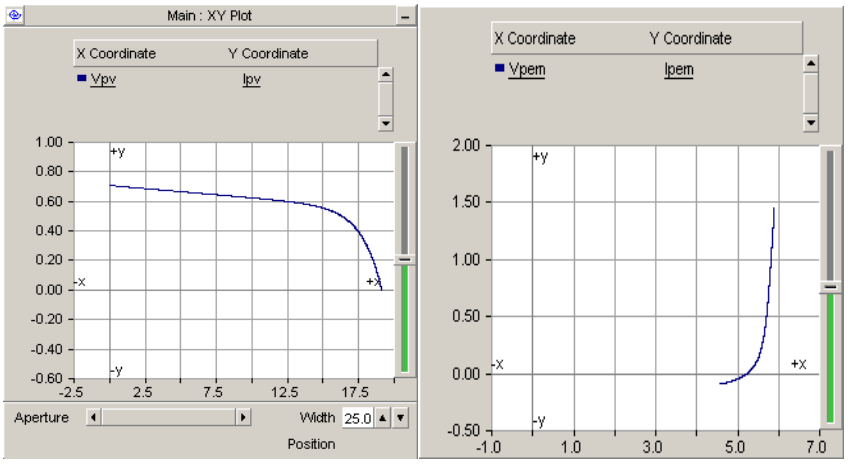

Figure 8: I-V characteristics of (a) PSCAD model of the PV module and (b) PSCAD model of the PEM electrolyser

Voltage, current, and power readings were taken at the terminals of the buck converter by varying the duty cycle value from 0.05 to 1 with scale of 0.5. As shown in Figure 9 , the operating voltage of the PEM electrolyser is considered to have an exponential shape with a maximum value of 5.8 V. The graphs show the power matching between the PV generator and the PEM electrolyser,

Voltage, current, and power readings were taken at the terminals of the buck converter by varying the duty cycle value from 0.05 to 1 with scale of 0.5. As shown in Figure , the operating voltage of the PEM electrolyser is considered to have an exponential shape with a maximum value of 5.8 V. The graphs show the power matching between the PV generator and the PEM electrolyser,

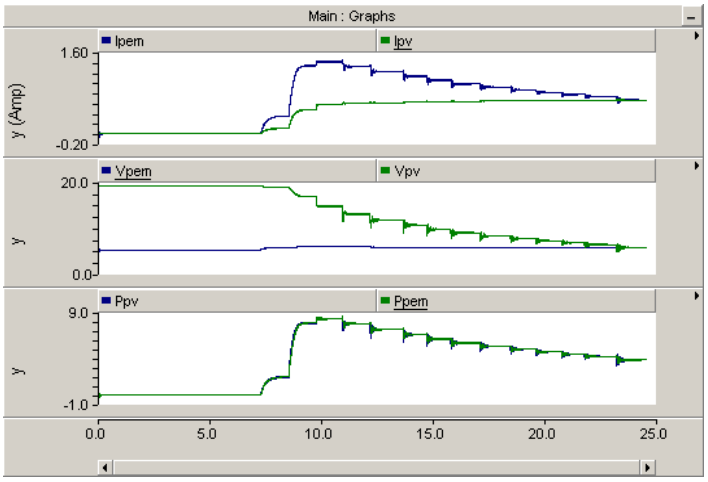

Figure 9: PSCAD simulation results for the PV-PEM electrolyser

where:

Ipem and Ipv are the PEM electrolyser and PV current values in (A), respectively

Vpem and Vpv are PEM electrolyser and PV voltage values in (V), respectively

Ppem and Ppv are yjhe PEM electrolyser and PV power in (W), respectively

From the previous results, it is apparent that the duty cycle governs the voltage and current on both sides of the buck converter, keeping the output voltage fixed at the PEM operating voltage. Current measurements at the power matching duty cycle (D = 4) show that the electrolyser current will be increased by about 2.5 times the PV operating current. This will increase the hydrogen production rate of the system while minimizing the solar PV area and decreasing the hydrogen production cost.

The power matching duty cycle D can be calculated, by using voltage and current values as follows:

$$dutycycleD = \frac{Vpem(V)}{Vpv(V)} = \frac{5.88}{14.71} = \frac{Ipv(A)}{Ipem(A)} = \frac{0.56}{1.40} = 0.4$$

The duty cycle needed to achieve maximum power point operation is equal to the ratio between the voltage of the PEM electrolyser and the PV array voltage at its maximum power point.

$$Dutycycle = \frac{V_{PEM}}{V_{mpp}}. \qquad (10)$$

The observation that the PV maximum power point voltage (Vmpp) has an almost linear relationship with the open-circuit voltage (Voc) of the solar photovoltaic module is apparent in the equation:

$$V_{mpp} = KV_{oc}.. \quad (11)$$

Where K is a constant that has different values for different solar panels, and$V_{oc}$is the open-circuit voltage. The open-circuit voltage (Voc) can be measured by disconnecting the PV at regular intervals.
AQ

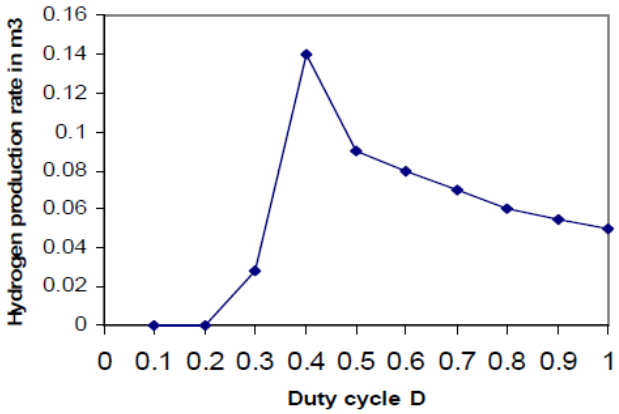

Figure 10: Hydrogen production rate at different converter duty cycle

The simulation shows that the hydrogen production of the PV-electrolyser system can be optimised by adjusting the converter duty cycle generated by PWM circuit. The strategy used was to fix the duty cycle at the ratio of the PV maximum power voltage to the electrolyser operating voltage.

5. Conclusion

A PSCAD software computer model was developed that was capable of exploring modelling for a photovoltaic-hydrogen production system with power matching using a DC/DC Buck converter. The evaluation took into account the different factors that affect the I-V characteristics of a PV array. The simulation proved that the operating voltage of the electrolyser and the PV voltage at maximum power were the key elements in power matching. The results show that the hydrogen production of the PV-electrolyser system can be optimised by adjusting the switch converter duty cycle generated by PWM circuit, the strategy used was to fix the duty cycle at the ratio of the PV maximum power voltage to the electrolyser operating voltage.

References

[1]. The International Energy Agency, World Energy Outlook 2007, http://www.iea.org/weo/2007.asp
[2]. B. S. Borowy, Z. M. Salameh; "Methodology for Optimally Sizing Combination of Battery Bank and PV Array in a Wind/PV Hybrid System", IEEE Transactions on Energy Conversion 11(2), pp. 366 – 373, 1996

[3]. M. Park, D. Lee, and I. Yu; "PSCAD modelling and simulation of solar powered hydrogen production system", Renewable Energy 3, pp. 2342-2355, 2006.

[4]. R. Muhida, M. Park, and M. Dakkak; "A maximum power point tracking for photovoltaic-SPE systems using a maximum current controller", Solar Energy Materials and Solar Cells 75, pp. 697-706, 2003.

[5]. G. E. Ahmed, E.T. El Shenawy; "Optimal photovoltaic system for hydrogen production", Renewable Energy 31, 2006.

[6]. J. Bockris Hogbin; "The solar hydrogen alternative", Pool Pty Ltd., Redfern NSW Australia, 1976.

[7]. Abd El-Shafy A. Nafeh; "Hydrogen production from a PV/PEM electrolyser system using a neural-network-based MPPT algorithm", International Journal of numerical modelling, vol. 24, issue 3, pp. 282-297, Wiley, InterScience,2010.

[8]. K. Rajeshwar, R. McConnell, S. Licht, "Solar hydrogen generation: Toward a renewable energy future," ISBN 978-0-387-72809-4, Springer, 2008

[9]. T. L. Gibson, A. Nelson; "Predicting efficiency of solar powered hydrogen generation using photovoltaic-electrolysis", International Journal of Hydrogen Energy 35, pp. 900-911, 2010.

Performance Analysis of a Solar Driven Single Stage LiBr/H_2O Absorption Refrigeration system

Islam Kamel Shahboun[1], Salem Omran Adeilla[2]
[1]kamel20122011@gmail.com, [2]Salem_279@yahoo.com
[1]Department of Mechanical Engineering, College of Engineering, University of Gharyan, Libya
[2]Department of Mechanical Engineering, Higher Institute For Sciences and Technology, Libya

ABSTRACT

The solar-assisted combined ejector was configured with the basic cycle of solar absorption refrigeration system to evaluate the performance of this cycle which using LiBr/H_2O as a working fluid and operating under steady-state conditions. In this paper, the improvement of the system is achieved by utilizing the potential kinetic energy of the ejector to enhance refrigeration efficiency. However, the first and the second law of thermodynamics are used to analyze the performance of a single-stage water-lithium bromide absorption refrigeration system (ARS), whereas some working parameters are varied. Moreover, a mathematical model based on the exergy method is introduced to evaluate the system performance, exergy loss of each component and total exergy loss of all the system components. As well as, Parameters connected with performance of the cycle–circulation ratio (CR), coefficient of performance (COP), exergetic efficiency are calculated from the thermodynamic properties of the working fluids at various operating conditions. In addition, Minimum generator temperature that required to operate the system was evaluated. The results showed that, the evaporator, condenser loads and post-addition of the ejector are found to be permanently higher than that in the basic cycle. As well as, The COP of the modified cycle is improved by up to 60 % compared with that in the basic cycle at the given condition.

Keyword— LiBr-H2O, COP, Exergy, Optimization, Generator temperature, Combined ejector absorption cycle.

1. Introduction

Absorption refrigeration systems (ARSs) have been gaining popularity because, firstly, they operate on environment friendly refrigerants. Secondly, they harness cheap alternative energy sources, such as geothermal, bio mass, solar energy or a waste by product heat source. Therefore, in recent years, research has been devoted to the improvement of ARSs. The main way of improving efficiency is through thermodynamic analysis and optimization [1–4].

The basis of thermodynamics is stated in the first and second laws. The first law describes the conservation of energy, while the second law is used to describe the quality of energy and material. The first law optimization should result in maximizing the coefficient of performance (COP),thus providing maximum heat removal for minimum power input, while the second law optimization should result in maximizing the

exergetic efficiency and minimizing entropy generation within the system, hence providing maximum cooling for the smallest destruction of available energy (exergy).

The exergy method, known as the second law analysis, calculates the exergy loss caused by irreversibility, which is an important thermodynamic property that measures the useful work that can be produced by a substance or the amount of work needed to complete a process [5]. The exergy analysis is a powerful tool for thermodynamic analysis of energy-conversion systems. The concept ofexergy is extensively discussed in the literature by Kotas [6], Szargut et al. [7] and Bejan [8]. Aphornratana and Eames[9] reported that the heat operated absorption refrigeration systems are attracting increasing interest, as they can be driven by low-temperature heat sources and employ environment friendly working fluids. Furthermore, they estimated the specific entropy field for temperatures ranging from 10 to 200 1C and concentrations ranging from 20% to 70%. Furthermore, some of the papers include economic analysis [10,11].

Many researches are recently interested in applications of solar-assisted absorption cooling/refrigeration systems and the improvement of their corresponding performance as it saves energy and is environmentally friendly. Solar energy is available in most areas and regarded as a good source of thermal energy. For many solar absorption cooling systems, LiBr/ Water and Ammonia/Water is a major working fluid pair in the context of these systems. The absorption performance of a cooling system is critically dependent on the chemical and thermodynamic properties of the working fluid[3]. Insolarapplications,the$LiBr–H_2O$ systemissuperiortothe$NH_3–H_2O$system, due to its simpler design and operation and low cost. Moreover, itisfunctionalunderlowgeneratortemperatureandperformbetterthanthatof $NH_3–H_2O$, due to its simpler design and operation and low cost. Moreover, it is functional under low generator temperature and perform better than that of $NH_3–H_2O$The LiBr/water system has been widely used for many years and their properties are well established. Many types of absorption cycles have been developed, however, the system's complexities increased over a conventional single- effect absorption system. The double-effect absorption systems using lithium bromide/water seem to be a high performance system, which is available commercially. The (single-effect) cooling system using $LiBr/H_2O$ as its working fluid system can provide COP as high as a double-effect system at minimal increase of system complexity. Thus, research has focused on improving these absorption cooling systems by enhancing the coefficient of performance (COP) of these systems with respect to both heating and cooling applications [5,6]. Ventas et al. [7] numerically studied single-effect absorption cycles and utilized ammonia-lithium nitrate solution as its working pair to determine the effect of mass flow rate recirculating through the absorber, as well as system performance. Numerous works also aim to optimize the operating parameters to enhance performance and minimize energy consumption in ARS

This work conceptualizes and analyse the single effect absorption refrigeration system combined with the ejector and an upgraded system that considerably lower the energy footprint. This paper aims to improve the system's performance by using the potential kinetic energy from the primary streamlines to drive the low pressure secondary streamlines to produce a quieter flow with more thrust and lower temperature. The proposed cycle will be evaluated via the entrainment ratio and the effect of the operation temperature on the

thermal loads and the system's performance. A general description of the proposed system will be presented, and further analysis on its performance is conducted based on a corresponding mathematical model.

2. Description of Absorption Cycle

There are many types of absorption cycles, single and multiple effect absorption cycles, the most commonly one is a single effect absorption cycle.

2.1. Description of Solar Single effect Absorption Cycle:

The basic cycle consists of generator, absorber, a condenser, an evaporator, solution heat exchanger, circulating pumps, and a solar collector. The cycle works between two pressure levels: low pressure at the evaporator-absorber, and high pressure at condenser-generator. The emitted vapours in the generator consist of pure water, while LiBrsal remained in the solution.

2.2. Description of Modified Single Effect Combined Ejector Absorption Refrigeration system:

The main part of the single effect absorption cooling system is shown schematically in Figure. 1.a The solution heat exchanger is advantageous, because it cools down the solution coming from the generator, which then heats up the solution entering the generator . An ejector was added between the generator and the condenser. The primary high-pressure water vapour from the generator enters the ejector, then from the secondary inlet of the ejector, the entrainment low pressure water vapor from the evaporator is mixed with the primary flow at the mixing chamber, passing the diffuser, then entering the condenser. In this new design, the lithium bromide mixture leaves the absorber (state 1) in the form of a saturated solution at low pressure. It is pumped to the system at high pressure (state 3). The generator operates from a high temperature source to separate the binary solution of water and Lithium bromide (strong solution comes from absorber). This two-phase mixture is separated, and the weak liquid flows through SHE (state 4 to state 5) than throttled to the low pressure system and sprayed into the absorber (state 6). On the ejector, the secondary flow (water vapour from evaporator (state 10A)) and the primary flow of water vapour from the generator are mixed and passed to the condenser (state 7).

3. Simulation and Analysis of Proposed Cycle

For the purpose of simulation and analysis, the following assumptions are made:

- The system operates under a steady state condition.
- The refrigerant leaving the condenser and evaporator is saturated (state points 8 and 10).
- $LiBr/H_2O$ solution in the generator, solution heat exchanger, and absorber are assumed to be in the equilibrium state at their respective pressure and temperature and assumed saturated state.

- The frictional pressure drop in the cycle is neglected except through the expansion device.
- The flow inside the ejector is steady and one-dimensional. The ejector walls are adiabatic.
- The primary flow and the secondary flow are saturated and their velocities are negligible before entering the ejector (states 7 and 10B in Figure. 1a respectively). The velocity of the mixed flow leaving the ejector (at state 7′) is also neglected.

In order to calculate the heat and mass balance for the proposed cycle, the thermodynamic properties (pressure, temperature, concentration, enthalpy and density) are necessary for the simulation. The binary mixture of LiBr/H_2O and pure H_2O are used in the proposed system. The detailed thermodynamic property equations of LiBr/H_2O are found by Engineering Equation Software.

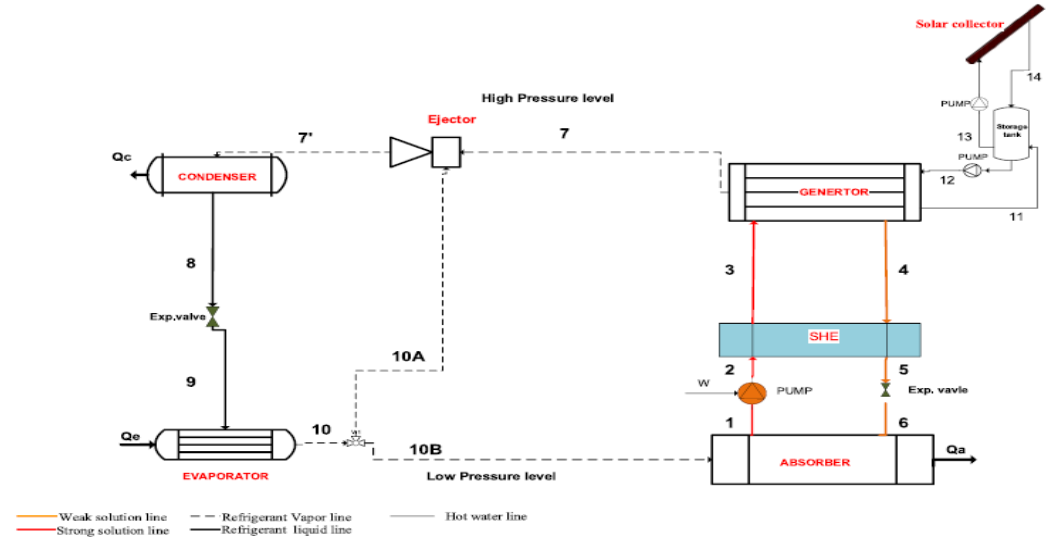

(a)

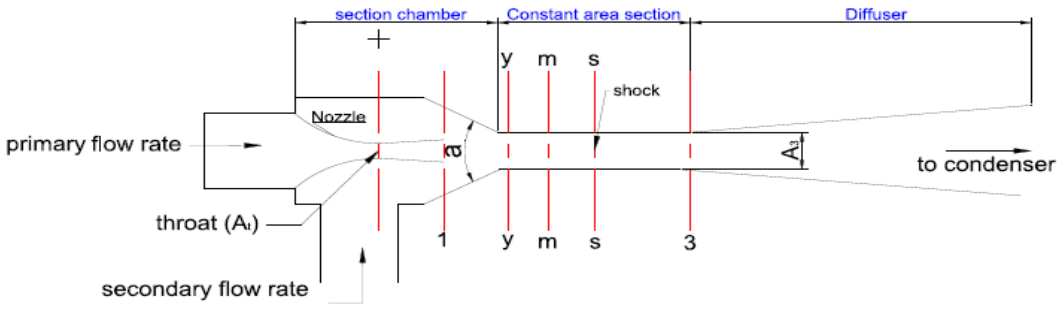

(b)

Figure 1:(a)System schematic of single effect combined absorption–ejector cooling system, (b)schematic diagram of the ejector

3.1. Thermodynamic Analysis

The thermodynamic analysis mainly aimed at assessing the thermodynamic imperfections and suggested possible ways of improving these imperfections. Here the system is analysed based on mass, energy and exergy balance. Each component of system can be assumed as control volume having inlet and outlet flow, work interactions and heat transfer. For analysing vapour absorption system circulation ratio is one of the most important parameter, it is defined as ratio of strong solution flow rate to refrigerant flow rate,

$$CR = \frac{\dot{m}_{ss}}{\dot{m}_r} = \frac{X_{SS}}{X_{SS} - X_{WS}} \quad (1)$$

The coefficient of performance (COP) is used to measure the system performance:

$$COP = \frac{Q_{eva}}{Q_{gen} + W_{pump}} \quad (2)$$

In order to use previous equation, mass and energy conservation should be determined at each component.

3.1.1 For the Generator – SHE – Absorber Loop:

The mass and energy balances around the generator

$$\dot{m}_3 = \dot{m}_4 + \dot{m}_7 \quad \rightarrow \quad \dot{m}_3 x_3 = \dot{m}_4 x_4 + \dot{m}_7 x_7 \quad (3)$$

$Where: \quad x_3 = x_1, \quad x_4 = x_6$

$$Q_{gen} = \dot{m}_4 h_4 + \dot{m}_7 h_7 - \dot{m}_3 h_3 \quad (4)$$

The fluid properties in this loop can be derived and developed as:
The liquid weak solution at state (4):
$T_4 = T_{gen} \quad , \quad P_4 = P_{gen}$
Exergy balance formulation for generator can be written as:

$$\Delta E_G = \dot{m}_{ws}(h_3 - T_0 s_3) + \dot{m}_{ss}(h_4 - T_0 s_4) - \dot{m}_r(h_7 - T_0 s_7) + \dot{m}_G(h_{11} - T_0 s_{11}) - \dot{m}_G(h_{12} - T_0 s_{12}) \quad (5)$$

3.1.2 Heat Exchanger:

SHE performance is expressed in terms of effectiveness ϵ_{she}..
The solution and refrigerant heat exchanger performance, expressed in terms of an effectiveness ϵ_{she}

$$\epsilon_{she} = \frac{T_4 - T_5}{T_4 - T_2} \quad (6)$$

$$C_{hot} = \dot{m}_4 \left(\frac{h_4 - h_5}{T_4 - T_5}\right) \quad , \quad C_{cold} = \dot{m}_2 \left(\frac{h_3 - h_2}{T_3 - T_2}\right) \quad (7)$$

$$Q_{hx} = \dot{m}_2(h_3 - h_2) \quad , \quad Q_{hx} = \dot{m}_4 (h_4 - h_5) \quad (8)$$

where,

$\dot{m}_1 = \dot{m}_2 = 0.05\ \frac{k}{s}$, $T_1 = T_{abs} = T_2$

Exergy balance formulation for solution heat exchanger can be written as:

$$\Delta E_{SHX} = \dot{m}_{ws}(h_2 - T_0 s_2) - \dot{m}_{ws}(h_3 - T_0 s_3) + \frac{Q_{SHX}}{T_b} \quad (9)$$

3.1.3 Solution Expansion Valve Model:

$h_5 = h_6$, $\dot{m}_5 = \dot{m}_6$, $x_5 = x_6$

Exergy balance formulation for expansion valve can be written as:

$$\Delta E_{REXP} = \dot{m}_{ss}(h_5 - T_0 s_5) - \dot{m}_{ss}(h_6 - T_0 s_6) \quad (10)$$

$$\Delta E_{SEXP} = \dot{m}_{ss}(h_8 - T_0 s_8) - \dot{m}_{ss}(h_9 - T_0 s_9) \quad (11)$$

3.1.4 Pump Calculation:

$$h_2 = h_1 + \frac{W_{pump}}{\dot{m}_1} \quad (12)$$

$$W_{pump} = \dot{m}_5 v_1 \frac{P_{hight} - P_{low}}{1000} \quad (13)$$

Exergy balance formulation for pump can be written as:

$$\Delta E_{pump} = \dot{m}_{ws}(h_1 - T_0 s_1) - \dot{m}_{ws}(h_2 - T_0 s_2) + \dot{W}_P \quad (14)$$

3.1.5 Absorber:

$$Q_{abs} = \dot{m}_{10} h_{10} + \dot{m}_6 h_6 - \dot{m}_1 h_1 \quad (15)$$

Exergy balance formulation for absorber can be written as:

$$\Delta E_{abs} = \dot{m}_r(h_{10} - T_0 s_{10}) + \dot{m}_{ss}(h_6 - T_0 s_6) - \dot{m}_{ws}(h_1 - T_0 s_1) + \frac{Q_{abs}}{T_b} \quad (16)$$

3.1.6 Condenser:

$$Q_{cond} = \dot{m}_7(h_7 - h_8) \quad (17)$$

Exergy balance formulation for condenser can be written as:

$$\Delta E_{cond} = \dot{m}_r(h_7 - T_0 s_7) - \dot{m}_r(h_8 - T_0 s_8) + \frac{Q_{cond}}{T_b} \quad (18)$$

3.1.7 Refrigerant Valve:

$h_8 = h_9$, $x_8 = x_9$

3.1.8 Evaporator:

$$Q_{eva} = \dot{m}_9(h_{10} - h_9) \quad (19)$$

Exergy balance formulation for evaporator can be written as:

$$\Delta E_{eva} = \dot{m}_r(h_9 - T_0 s_9) - \dot{m}_r(h_{10} - T_0 s_{10}) + \frac{Q_{eva}}{T_b} \quad (20)$$

The total rate of exergy destruction of absorption system is the sum of exergy destruction in each component and can be written as:

$$\Delta E_{Sys} = \Delta E_G + \Delta E_{abs} + \Delta E_{eva} + \Delta E_{cond} + \Delta E_{SHX} + \Delta E_{REXP} + \Delta E_{SEXP} + \Delta E_P \quad (21)$$

3.2. Nozzle Equations

For a given pressure $P_{gen} = P_7$, tempertature $T_{gen} = T_7$and $\dot{m}_p = \dot{m}_7$ the nozzle throat area required for choking condition follows the gas dynamic equation:

$$A_t = \frac{\dot{m}_p\sqrt{T_{gen}}}{P_{gen}\sqrt{\eta_P}\sqrt{\frac{k}{R}\left[\frac{2}{K+1}\right]^{\frac{K+1}{K-1}}}} \quad (22)$$

where η_p is a coefficient relating to the isentropic efficiency of the compressible flow in the nozzle. The relations between the Mach number at the exit of nozzle Mp1 and the exit cross section area AP1 and pressure Pp1 are, using isentropic relations as showing in the following equations:

$$\frac{A_{p1}}{A_t} = \frac{1}{M_{p1}}\left[\frac{2}{k+1}\left(1 + \frac{k-1}{2}M_{p1^2}\right)\right]^{\frac{K+1}{K-1}} \quad (23)$$

4. Results and Discussions

Table 1 shows that the highest heat load occurs in the generator(approximately 13kW) and the heat transfer rate of the refrigerant heat exchanger is lower than that of the solution heat exchanger due to mass flow rate and temperature difference between the fluids.

Table 1 : Heat transfer rates of components and performance parameters of the system

Components	Heat transfer rates (KW)
Generator	12.985
Condenser	10.483
Evaporator	10.000
Absorber	12.502
Pump	0.00012
Solution heat exchanger	2.254

Refrigerant heat exchanger	0.165

Table 2 shows the simulation results of the second law analysis of the ARS. The generator has the highest exergy loss rate (approximately 2 kW), and the next largest exergy loss rate occurred in the absorber (approximately 1.5kW). Since exergy loss rates in the pump and expansion valves are very small, their effects on the total exergy loss rate are inconsiderable. The exergy losses of the generator and absorber are important fractions of the total exergy loss in the system.

Table 2 : Exergy loss rates of the components

Component	Exergy loss rate (KW)
Generator	2.002
Condenser	0.048
Evaporator	0.685
Absorber	1.533
Pump	0.00015
Solution expansion valve	-----
Refrigerant expansion valve	0.013
Solution heat exchanger	0.093
Refrigerant heat exchanger	0.008
Total	**4.383**

4.1. Comparison Between the Basic and the Modified Cycle:

Figure. 2(a–d) depicts the COP of basic cycle and the modified absorption cycle under various operating temperatures. Comparison of COP values vs. generator temperature for (basic and modified cycles) are shown in Figure. 2(a). It is noticed that for the two absorption cycle, there is an optimum value of COP. This value of COP increases with generator temperature until it reaches the optimum value. This value depends on the type of the cycle. Moreover, there is a low generator temperature limit, where the cycle cannot operate at a generator lower than this. This is an important point for the utilization solar energy, since the fluid temperature for solar collector are generally below 100 °C. Therefore, the simulation exhibited in this figure reveals that modified cycle has a higher COP value than the basic cycle. The effect of evaporator temperature on the COP of the cycles is shown in Figure. 2(b). It is evident that the COP value of two cycles increases as the evaporation temperature increases, as shown in Figure. 2(b). It also can be seen that the highest value of the COP is obtained from the modified cycle. Figure. 2(c and d). illustrate the comparison of COP value vs. condenser and absorber temperature for two cycles. Increase condenser and absorber temperature causes a decrease in COP for each cycle. For modified cycle operation under choked conditions, the cycle is

independent of condenser pressure when the condenser pressure is less than a certain critical value; however, the cycle falls to similar values to the basic cycle when the condenser pressure is greater than this critical value, as shown in Figure. 2(c). It is observed that the absorber temperature of 44 °C and above the performance of the system tend to lean towards zero. This is due to the fact that the concentration of the liquid leaving the absorber has dropped to the same concentration as the liquid coming back from the generator. From this figure, it could be determined that the COP of the modified cycle is higher than that of the conventional cycles at all simulated working conditions. This is due to the fact that the performance of a refrigeration system is influenced by adding an ejector to the basic cycle.

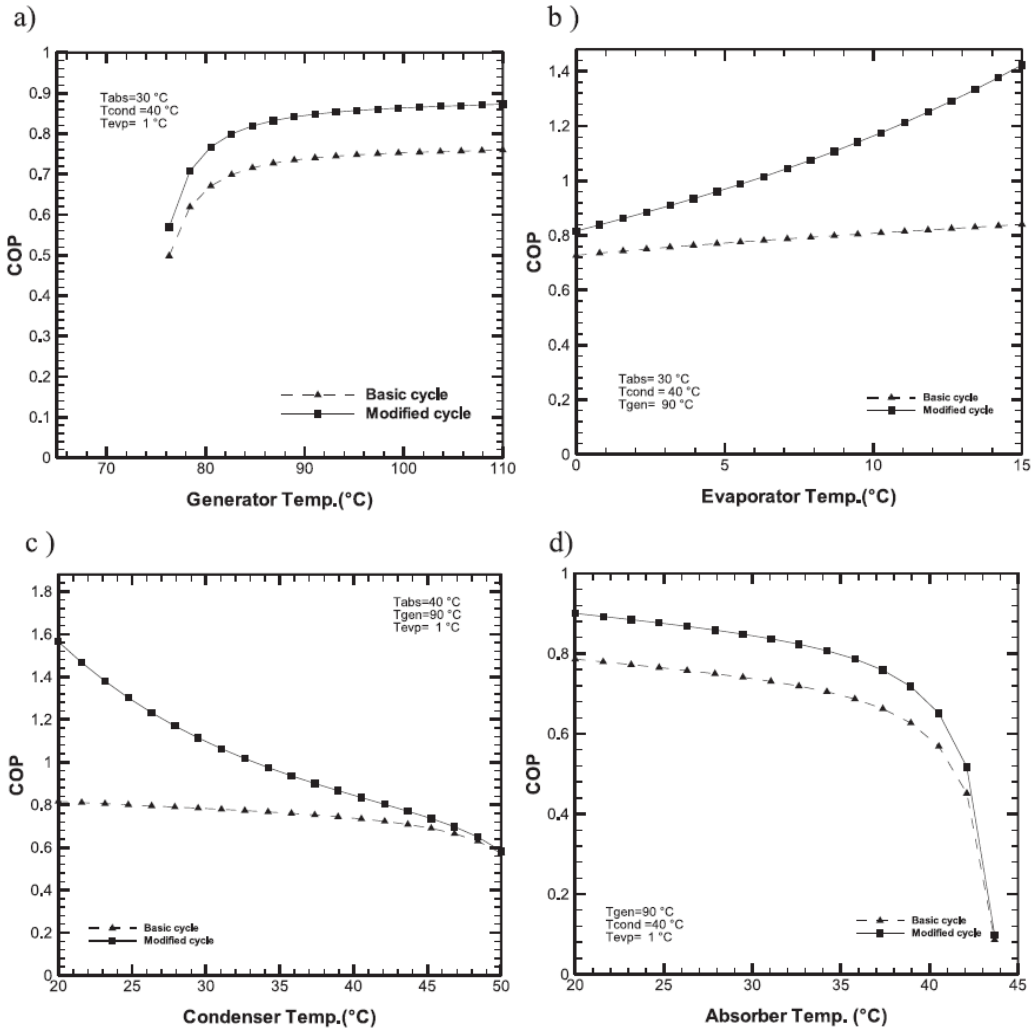

Figure 2:(a–d) Comparison of influence of operation temperature on the COP values for basic and modified cycle

4.2. Effect of Generator Temperature:

Variation of COP and total exergy destruction rate of system with generator temperature is depicted in Figure.3.a. It is observed that COP of system increase with generator temperature up to certain value and then after very negligible variation is observed. With increasing generator temperature, strong solution concentration increases hence mass flow rate of weak and strong solution decreases while refrigerant mass flow rate remains unchanged. Enthalpy of superheated refrigerant stream marginally increases with generator temperature while enthalpy of weak and strong solution increases rapidly hence lowering generator heat load. Therefore, COP of system increases with generator temperature.

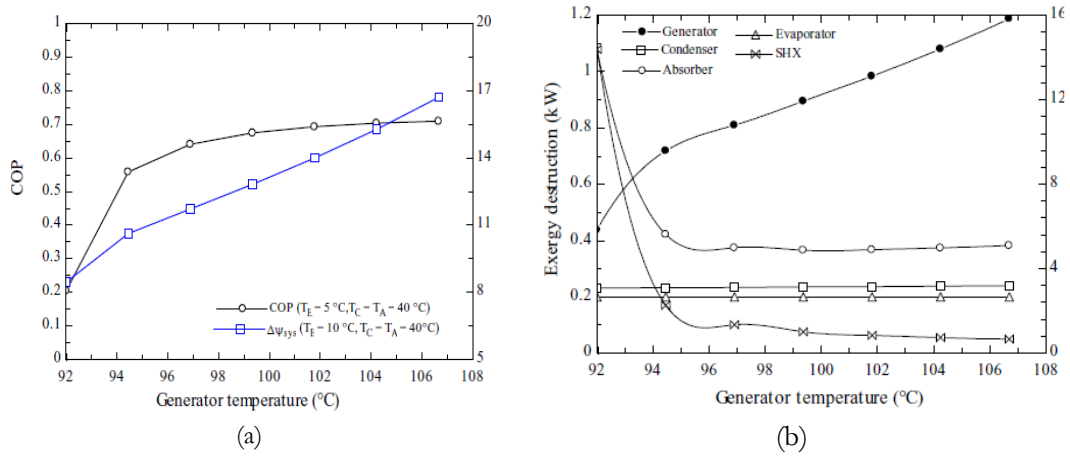

Figure 3: a) Variation of COP and total exergy destruction of systemwith generator temperature**, b)** Variation of exergy destruction of variouscomponent system with generator temperature

From Figure.3.a. it is found that with increasing generator temperature, total exergy destruction of system increases. This can be understood by Figure.3.b. It is observed that exergy destruction in condenser and generator increases with increasing generator temperature while in SHX and absorber it decreases. It is clear that with increasing generator temperature total exergy destruction of system increases rapidly so it is necessary to optimize the generator temperature for minimization of exergy destruction of system. From Figure.3.a it is observed that optimum generator temperature corresponding to minimization of exergy destruction rate found lower than that for maximization of COP.

5. Conclusion

The results show that COP of the cycle increases with increasing generator and evaporator temperatures, but decreases with increasing condenser and absorber temperatures. Moreover, exergy losses in the expansion valves, pump and heat exchangers, especially in refrigerant heat exchanger, are very small fractions of the

total exergy loss in the ARS. Three components that obtained the highest exergy loss are the generator, the absorber and the evaporator.

In the parametric analysis of the system, it is shown that a low condenser temperature yields a higher cooling COP and higher exergetic efficiency. The system operating with relatively high evaporator temperatures has better cooling COP and experiences smaller exergetic efficiency than the one having low evaporator temperatures. Increasing the generator temperature can improve the cooling COP of the absorption system, but as the heat source temperature further increases, the COP of the system levels off. This negative effect of increasing the heat source temperature is more dominant on the exergetic efficiency of the system. Consequently, this negative result on the exergetic efficiency and the COP removes the beneficial effect of a high heat source temperature.

In this study, an improved system of the single-stage absorption cycle operated with $LiBr/H_2O$ as its working fluid was conducted. Thermodynamic analysis of ejector–absorption refrigeration system has been carried out, and the theoretical performance of the cycles were compared. The results show that the modified combined absorption cycle is superior to the basic cycle over a wide range of operating conditions. The results also show that the thermal load of the condenser and the evaporator increase as the generator and evaporator temperature increases, while it decreases as the condenser temperature increases. The results in dicated that the overall COPs increments of the modified cycle was 8–60 % at a condenser temperature of 25–45 °C, and by 30–85% at evaporator temperature of 0–10 °C over the basic cycle.

References

[1]. Misra RD, Sahoo PK, Gupta A. Thermoeconomic evaluation and optimization of an aqua-ammonia vapour-absorption refrigeration system. Int J Refrig 2006;29(1):47–59.

[2]. So¨ zen A. Effect of heat exchangers on performance of absorption refrigeration systems. Energy Convers Manage 2001;42(14):1699–716.

[3]. Saravanan R, Maiya MP. Thermodynamic comparison of water based working fluid combinations for a vapor absorption refrigeration system. Appl Therm Eng 1998;18(7):553–68.

[4]. Sun DW. Comparison of the performance of NH3–H2O, NH3–LiNO3 and NH3–NaSCN absorption refrigeration systems. Energy Convers 1998;39(5/6):357–68.

[5]. Talbi MM, Agnew B. Exergy analysis: an absorption refrigerator using lithium bromide and water as the working fluids. Appl Therm Eng 2000;20(7):619–30.

[6]. Kotas TJ. The exergy method of thermal plant analysis. Florida: Krieger Publishing Company; 1995.

[7]. Szargut J, Morris DR, Steward FR. Exergy analysis of thermal, chemical, and metallurgical processes. New York: Hemisphere Publishing Corporation; 1988.

[8]. Bejan A. Advanced engineering thermodynamics. New York: Wiley;1988.

[9]. M.M. Talbi, B. Agnew. Exergy analysis: an absorption refrigerator using lithium bromide and water as the working fluids. Applied Thermal Engineering 2000;20: 619-30.

[10]. G. Gutiérrez-Urueta, A. Huicochea, P. Rodríguez-Aumente, W. Rivera. Energy and Exergy Analysis of Water-LiBr Absorption Systems with Adiabatic Absorbers for Heating and Cooling. Energy Procedia 2014;57: 2676-85.

[11]. Arora, S.C. Kaushik. Theoretical analysis of LiBr/H2O absorption refrigeration systems. International Journal of Energy Research 2009;33: 1321-40.

[12]. R. Gomri. Second law comparison of single effect and double effect vapour absorption refrigeration systems. Energy Conversion and Management 2009;50: 1279-87.

[13]. J.D. Marcos, M. Izquierdo, E. Palacios. New method for COP optimization in water-and air-cooled single and double effect LiBr–water absorption machines, International journal of Refrigeration 2011;34: 1348-59.

[14]. R. Saravanan, M.P. Maiya. Thermodynamic comparison of water-based working fluid combinations for a vapour absorption refrigeration system, Applied Thermal Engineering 1998;18: 553-68.

[15]. Y.A. Cengel, M.A. Boles, M. Kanoglu. Thermodynamics: an engineering approach. Eight ed., McGraw-Hill, New York, 2015.

[16]. R. Palacios-Bereche, R. Gonzales, S.A. Nebra. Exergy calculation of lithium bromide-water solution and its application in the exergetic evaluation of absorption refrigeration systems LiBr-H2O, International Journal of Energy Research 2012;36: 166-81.

[17]. S.A. Klein, F.L. Alvarado. Engineering equation solver, F-Chart Software, Madison. WI 2002: 1.

Preserving Architectural Heritage within the International Covenants and its Reflection in the Libyan Case

Husein AL derawe[1],Ashraf Laswad[2], Latefa Wafa3
[1]architect.of.libya@gmail.com, [2]Ashraflaswad@yahoo.com, [3]Lwafa@yahoo.com
[1]Department of Architecture, College of Engineering, Elmergib University, Libya
[2]Department of Architecture, College of Engineering, Elmergib University, Libya
[3] Department of Architecture, College of Engineering, Tripoli University, Libya

ABSTRACT

The architectural and archeological heritage are exposed to many damage factors that differ in terms of origin; act of nature , others because of the human works and the most serious infringements represented in the wrong and not well studied restoration process.

In the case of Libya; despite the historical and artistic diversity of its architectural heritage the preservation of which remains outside the priorities of legislators, which has led to cause various damage factors. In particular, the erroneous and misguided restoration processes , to distort many important architectural monuments which stood witness to many historical periods.

The purpose of this research is to emphasize that the international conventions of conservation are generate constitution of achieving their preservation and the importance of issuing a Libyan Charter that regulates the processes of architectural heritage in Libya according to the specificity of each case . This will be done through of a previous restoration study carried out on a single building at Leptis-magna for ensuring its valuation within parameters of international conventions. Furthermore, the same situation should highlight on the distortion due to the miss-performed conservation processes.

To sum up, the study tried to ensure the priority of the conservation operations that were done according to the international conventions, and highlighted the failure of other operations that were done neither scientifically nor well-prepared. Therefore, this problematic issue was reflected negatively on the origins and value of the undertaken case study. In addition, the study highly recommended that the Libyan local authority should establish its own Libyan charter to deal with every individual restoration case with its specialty. The study also insisted that Libyan authority should establish a specific law(s) and penalties that should deal to stop later similar operations.

Keyword— Restoration, preservation, charters.

1. Introduction

Architectural heritage is of great historical value as a living conveyor of history as well as its artistic value. it has become a major source of income in many countries of the world. But this heritage is like any ancient monuments are exposed to many factors that lead to deterioration and distortion, but the archaeological holdings can be saved in museums that limit of its damage, unlike the archaeological buildings that are difficult to protect.

Accordingly , the specialists and who are interested in the fields related to antiquities on the world level with different opinions and directions to support their efforts to develop laws and regulations to control the processes for the restoration of architectural heritage to give it sustainability, and emerged the international conventions and treaties related to the preservation of the material human heritage as the fruit of their efforts.

2. International Conventions Related to the Preservation and Restoration of Monuments:

Improper and unthought restoration is one of the most serious aspects of damage to any archaeological building, therefore, before any restoration work, it was necessary to study carefully to the legislation items concerning the preservation and restoration of archaeological buildings to get it out of it a summary that enable us to develop a sound and legal methodology to carry out a successful restoration process for the purpose of preserving the original character of archaeological buildings. Likewise, the development of appropriate solutions to treat what can be cured of the previous faulty operations and damages to the archaeological buildings.

The beginning of these covenants began with the beginning of the 20th century, after the destruction of large architectural monuments as a result of the nineteenth centuries.

There have been numerous national efforts to deal with architectural and urban heritage during the 18th and 19th centuries. However, they were aimed at serving local objectives . There were fundamental difference between the approaches to dealing with architectural and urban heritage during the 19th century, which ranged from the rejection of any form of restoration to the preservation of the inherited reality, and interfering with it in the same contemporary thought which it was designed for it to confirm its continuity.

There was also the need to protect the fixed and moveable heritage of destruction due to the different wars in Europe during 18th and 19th century. Perhaps the first ideas developed in this direction are "the law of states "developed by the Swiss judge "Emanerich de Vattel" 1758 , who decided that ,if any country is destroyed for any reason, care must be taken to preserve those objects that glorify human society and do not add to the enemy's strength, such as temples Cemeteries and public buildings. It was followed by the draft international declaration of laws and customs of war adopted by the conference called by the Russian Emperor “Alexander II after the Russo-French war the main idea of these efforts was that the antique is a general human property, not just the surrounding community, and that it must be protected even during wars and armed conflicts so that the invading forces became responsible for its protection [1].

The second half of the 19th century witnessed a national effort to preserve the urban heritage in different parts of Europe with different concepts between the reconstruction in France, the preservation of whole areas with the permission of new facilities as in Italy and the preservation of heritage in its historical state as in England. And there was a need for on international understanding on how to deal with unban and architectural heritage.

The most important of these efforts was the conference in "The Hague city " in 1899,1907, however these conferences did not place a specific collective responsibility on the international community that their application come be continued [1].

But that was not enough to lay the bases for limiting abuses that often occur unintentionally. The emergence of international conventions appeared in the decisions of the sixth international conference of Architects, held in Madrid in 1904. This was followed by the international scientific efforts in several conferences, which led to the issuance of a large number of charters. Where the charter of Athens was issued in 1931, which is the beginning of the existence of international conventions and recommendations agreed upon by experts and specialists in dealing with the heritage and the real beginning of the development of the thought of preserving the architectural and urban heritage, because of the great shortness of Athens document and the lack of defaited methodology through which to deal with the heritage and ted to the need for more effort as the charters followed and associations and organization were established that have been concerned with the protection of human heritage of all kinds where the "International center for the study of the preservation and the restoration of cultural property " ICCROM"was established in 1956.

Efforts of UNESCO have continued through its General Assembly and the recommendations emanating from the seminars it calls for the establishment of the "International council on monuments and Archeologicalsites" ICOMS in 1964, while who shared in the conference considered that many of the problems encountered by the restorer were not addressed in the Athens charter. It was therefore necessary to review the principles of the Athens charter with a view to deepening them and expanding their powers in a new document to solve these problems therefore, the second conference of architects and technicians specialized in archeological sites was held in VENICE 1964 under the auspices of UNESCO and came out with 13 documents most notably the first charter Known as the International document for the restoration and reservation of monuments and historical sites, which constituted a qualitative and important leap forward in establishing clear and specific foundations and rules for any restoration work. Also, it becomes the most important documents related to the preservation of historical and archaeological sites and areas. Also, it becomes the main reference for the restoration and maintenance operations and the basis on which many international conferences and conventions were built, which have woven a clear scientific and technical approach to the restoration process [1].

3. The Most Important Issues Covered by International Conventions on the Restoration of the Historic Building

The international conventions provided a set of specific laws which organize the restoration processes of archeological buildings in order to avoid any damage that may result from faulty and unplanned restoration operations :

a. The architectural heritage represents a wealth that is a common property of the people, and these peoples must protect it from the dangers that threaten it [7].

b. Historical sequence must be respected[4].
c. The role and priority of sciences and techniques for studying and rescuing the antique monuments[5].
d. Conservation and restoration must only be limited to authorized and specialized architects[3].
e. Local authority should establish a general policy for the conservation and restoration of cultural and natural heritage[6].
f. Documentation and proven methods[5].
g. The decision of what must or must not be removed should not be a single decision, Venice [5].
h. The selection of proper materials and techniques for later replacement and/or modification restoration operations[8].
i. The restoration must be carried out strictly according to precise analytical study. In another words, restoration must be carried out away from assumptions and probabilities[5].

From the above mentioned, we conclude that the international conventions have confirmed the importance of heritage and set the specific criteria and control of the conservation process within the stages and priorities of the restoration process in all its aspects, so as to result in a process of preservation as successful as possible with emphasis on the specificity of each case. However, the application of these covenants remains a non-binding literary responsibility, particularly terms of faulty repair operations. This will be evident in the case of study.

4. Articles of the Libyan law Regarding Archaeological Restoration Operations:

The last updated Law on the Protection of Monuments, Museums, Old Cities and Historical Buildings in Libya is Law No. (3) of the year 1993 AD, which confirmed some of the articles issued in the previous laws. It contains six articles concerning the restoration of ancient cities and historical buildings. nevertheless, these articles are considered gelatinous and insignificant without the existence of technical determinants and criteria that determine and assess restoration processes according to the specificity of each restoration case. The fourth chapter of the same law is related to penalties. Accordingly, the mentioned penalties were not deterrent, and without exaggeration they're not encouraging, since the maximum penalty is not more than twenty thousand dinars, and the maximum sentence of imprisonment not exceeding one year.

5. The Case Study:

The selection was done of an important historical monument from the archaeological city of Libya as a campaign of restorations were carried out at different periods of time and the result were clearly different, and it was chosen to examine the scope of the commitment to what it contained in international conventions to maintain and reflect on the results of restoration operations.

In summary, all international legislations combine with the need to protect cultural property and lay the foundations and legal principles for implementing this.
The executive authorities should therefore put in their programs hew to activate this legislation and enact laws and implement them in cooperation with the security and judicial services.
As a field study, The Augustical theater was chosen from the ancient city of Leptis which mainly support the above mentioned criteria of the case study. Therefore, a number of the restoration operations has been done on different periods of time and the results were clearly different. Accordingly, these restoration operations were chosen to examine the scope of the commitment to what is contained in international convention to maintain and reflect on the results of restoration operations.

5.1. The Augustical theater historical background:

it was built by one wealthy man from city of Leptis named "Hanbal Rufus " between 1-2 , and presented as a gift to Emperor Auguat. The theater in the imperial era is only a listening room to hear the music, but was using a little for playing drama, (figure 1).

5.2. Its architectural and historical importance:

The importance of the historical theater is built one of the wealty Libyans of the time , which confirms that Leptis is not purely Roman city , but Libyans have a great role in its construction. And concerning its architectural importance is the creativity in the architectural configuration of the building in addition to being one of the largest buildings in the city of Leptis and performing its function until today.

Figure1: general view of the Augusti theater(Authors,2018)

5.3. Factors of damaged suffered and resulting deterioration:

the Augusti Theater is considered to be one of the building close to the sea, which has been exposed to many destructive factors such as erosion caused by winds and weathering, growing of vegetation and shrubs, as well as seawater filtration, which lead to deterioration of the building and damage its basic structure.

All these factors make it necessary to pay attention to its restoration and maintain it periodically and continuously, making it susceptible to wrong and unskilled restoration.

5.4. The restoration works that were carried out on the monument:

The stages of restoration can be divided according as its history to three historical stages starting from 1937 – 2001.

Note: (the most we can talk about in this regard, that there not monitoring … these monuments for the area of Leptis and the ministry of reports or documents of the restoration operations that have been conducted on the monument whether old or modern and these is only one book in the scientific library in Italian Language detailing the exploration & restoration carried out from 1937 – 1951.As for the modern restoration it has no documents except for some photographs).

Figure 2: The part found from the theater during the excavation and exploration[5].

- The first restoration process: began with excavation in 1937 the theater works continued for 14 years until 1951, in which the general shape of the building was substituted according to the materials found. The excavation of the building, which was prepared by the Italian team was commissioned to prepare preliminary studies of the restoration process. This is because most of the building materials disappeared & were destroyed as a result of the damage factors and thefts that the city exposed to it during different ages (figure 2), which forced these who are responsible for restoration process to make the decision to using building materials from the residential and service buildings in the city. As for the materials found it has Lost large parts of its features and therefore the team specialized in restoration and maintenance of the stones has paid effort to repair them and trying to restore their original form to be returned to their place [2], (figure 3).

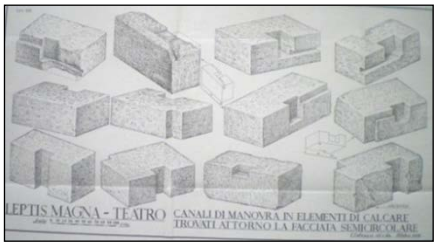

Figure 3:restoration of the building stores found in the excavations[5].

Despite the preparation of preliminary studies and perception of the architectural form of the theatre, it was not delivered from some of the violations to the restoration although a few in total and do not violate international conventions. The use of cement was warned only in the Venice convention in 1964. We note the use of cement mortars in the rear entrances and their negative effect on the finishing layers and building stones. The chemical reactions that occur in the cement mix change the colors of the building materials and the finish formed over time as well as the erosion of the stones and the deterioration of the stones, (Figures 4).

Figure 4:Effect of using cement mortar on building blocks[5].

As well as the restoration of the vaults and the collapsed arches. The parts that found materials were rebuilt and the materials lost were replaced with good materials that fit in shape with the original materials. Materials of the same building were used, and white cement with sand was used, therefore these processors still exit so far after more than fifty years (Figure 5, 6).

After the reconstruction of the theater on the situation in(Figure 7), although some of the distortion of the area under the upper columns restored in a way that acquired a modern appearance, work processes were stopped at this point because the building materials are no longer available and continue to work to get the building to the situation as it was put into the study, which will somehow lead to the production of a building that may be a monster for the original building. This is stated in Article 9 of the Venice charter of 1972, which stipulates that "the repair should stop when the guesswork begins".

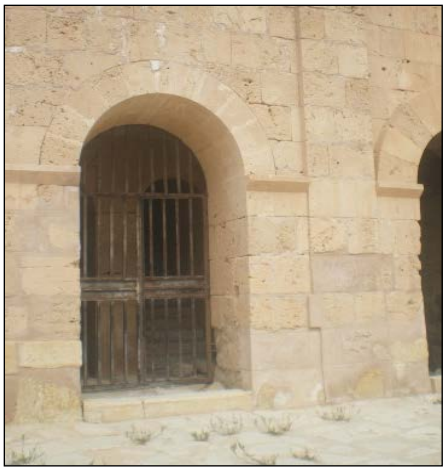

Figure 5:Treatment of arcs using materials of the same original building material [5].

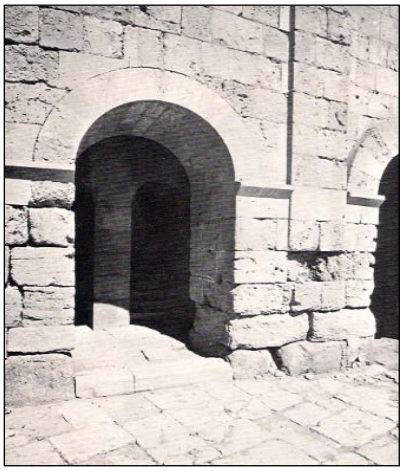

Figure 6:The current appearance of the arc with same old treatment,(Author-2018).

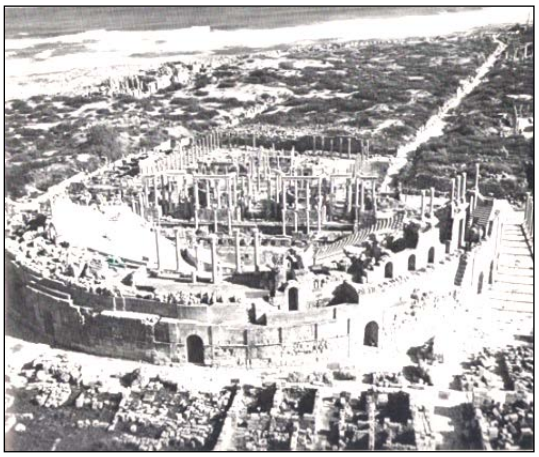

Figure 7: The situation in which the first restoration process has stopped [5].

- The second restoration process: after the completion of the initial restoration, did not occur any important restoration operations, but were cases of treatment to the existing situation as a result of the factors of degradation that did not stop to this monument. We do not exaggerate if we said that it is sabotage rather than restoration, as it was not in the hands of specialists, no appropriate materials was used and was not documented, mostly using mortars and cement concrete, where many of the walls and stones that suffered from sludge and crumbled were restored by using black cement, which in turn led to worse situation by occurring holes in these stones. This was because of destroying and dispersing the remaining finishing layers over time. The worst was the distortion of the architectural character of the monument by the color of the materials used in the restoration, which appear to be irregular to the building, (Figures 8,9).

Figure 9: The use of black cement and paint it with a contemporary paint,(Authors,2012)

Figure 8: Using concrete in the floors and surfaces,(Authors,2012)

- The third restoration process: it was the last restoration operations carried out on the theatre and it was in 2001. It was decided by the tourism sector, and the administration decision was not subject to any of the scientific and technical conditions. No preparatory studies were done, and it was carried out by non-specialists or trained stuff where the roof of the eastern entrance of the theatre and the vault leading to the orchestra area was restored using concrete block and reinforcing steel, (Figures10,11).

After restoration of the eastern entrance to the theater, there was a great controversy by the interested and specialists in the field of archeology to the extent of submitting complaints to UNESCO, but the process of restoration did not stop, and the restoration of the western entrance continued by using the limestone block and cement mortar as a bond and then poured concrete above it as a different treatment from was carried out on the eastern entrance, but these treatments were the implantation of cancerous tumor within the body of the building, even the attempt to replace it will lead to collapses and smash in the structure of the building, (Figure12),*[10]*.

Figure 12: Using the limestone bricks to roof the western entrance of the theatre [10].

Figure 11: Using concrete and reinforcement steel in the roof of the eastern entrance of the theatre[10].

Figure 10:Using the cement block in the theatre [10].

The wall of the external walls of the theater were reconstructed with cement blocks and was covered with black cement mortar and was decorated with random lines without taking in consideration the old lines of stones and treatments as a kind of an attempt to dive the impression that it was a building of stones and then painted with colors compared to the stone color and then the crystallized salts appearing on the wall surfaces and the building turned into a monster that had nothing to do with the original form, (Figures 13,14,15 and 16).

Figure 14: The outer wall of the theater after its restoration (Authors, 2012)

Figure 13: The outer well of the theater before its restoration[10].

Figure 16: Thatproduced by using cement material(Authors, 2018)

Figure 15: Using the cement blocks in the restoration of outer wall(Authors, 2018)

6. Summary of the case study

Through the previous presentation regarding the restoration process of the Augusti theater in the archaeological city of Leptis, the evidence that the first restoration of the monument after the completion of excavation and exploration, which although it was in an advanced time in 1937 where did not appear except some of the conventions and agreements, but it was according to a scientific approach based on steps and stages predetermined for all aspects that would affect the process of restoration. But later there were no

major restoration, where most of the operation that are taking place were restoration for the purpose of prevention, and it was more destructive than restoration and has not been subjected to any scientific and technical basis, although it was at a later period after the emergence of the most international conventions to preserve the relics. The last major restoration operations that the monument subjected to was in 2001, which was not based on any scientific or technical study, but was a decision by the tourism sector which was performed by one of the construction contractors.

7. Conclusions

All international legislation agreed to the need to protect cultural properties. Also, it emphasized the importance of the heritage and set criterion to evaluate it.

In addition to establishing the principles and technical bases to protect and preserved it in the form of international charters in order to control the preservation process within the stages and priorities of the restoration process in all its aspects with emphasis of each case. However, the Libyan Antiquities Law, despite the obvious infringements of the architectural monuments due to the erroneous and un thought restoration processes, which has distorted and lost some of its features, is still limited to the development of legal texts that impose deterrent penalties to limit these infringements. International covenants remain a literary responsibility and not mandatory to apply, especially with regard to faulty repair operations. Moreover, the articles of the law relating to antiquities remain loose unless the competent technical authorities referred to in the articles o the Libyan antiquities law in its articles regarding the restoration operations set clean technical parameters and standard which can be invoked according to the specificity of each case.

References

[1]. JukkaJokilehto, "A History Of Architectural Conservation,"D.Phil.University of York, England, pp.283-284, 1986.

[2]. Giacomo Caputo, "Mnongrafie Di ArcheologiaLibica," *L`erma Di Bretschneider - Roma*, vol. III, pp. 5,11,22,133, 1987.

[3]. International Congress Of Architects ,Madrid, Article 5, 1904.

[4]. The Athens Charter, "for the Restoration of Historic Monuments", Article 2, 1931.

[5]. The Venice Charter, "International Charter for the Conservation & Restoration of Monuments & Sites," Article 2,9,11,16, 1964.

[6]. Paris Charter, "International Convention for the Protection of the World Cultural and Natural Heritage," Article 5, 1972.

[7]. Europian Charter, "the Architectural Heritage, declaration of Amsterdam" Article 3, 1975.

[8]. Appleton Charter, ", for the Protection & Enhancement of the Built Environment" Article 4, 1983.

[9]. Libyan Law (No. 3), "For the Protection of the monuments, museums, ancient cities and historic buildings" Article 14,18,23,36,39,49, Libya, 1994.

[10]. Antiquities monitoring of Leptis, "Reports of restoration works of the Augustic theater", 2001.

قياس الوضوح الحضري للبيئة المبنية

Measuring urban clarity of the built environment

د. فوزي محمد علي عقيل
Fawzi Mohamed Agael
fawzi6664@gmail.com
قسم العمارة , كلية الهندسة , جامعة المرقب , ليبيا
Department of Architecture and urban planning, College of Engineering, Elmergib University, Libya

الملخص

من وقت قصير جدا كانت كيفية قياس الفراغات العمرانية قضية غير محددة في النقاش العلمي , وقد اعتمدت في جلها على نظريات نتائجها في الغالب انتقائية تعتمد على متغيرات معقدة قلما تتوفر مجتمعة في آن واحد في البيئة المبنية والعنصر الإنساني معاً .

تهدف هذه الورقة إلى تناول مؤشر الوضوح "intelligibility" للفراغات العمرانية والبيئة المبنية والعلاقة بين قياس "integration" التكامل و "connectivity" الترابطية للفراغات من خلال التحليل المحوري axial line analysis , ومن وجهة نظر نظرية التركيب الفراغي أو (الحيز الفراغي) space syntax .

ويساعد هذا المؤشر "intelligibility " إلى سهولة فهم البيئة المبنية المحيطة , وهو أمر بالغ الأهمية لموضوع الملاحة الحضرية ويساعد في فهم إعادة التشكيل المكاني الحضري للبيئة المبنية وتسهيل فهمها للملاحظ .

الكلمات الدالة: الوضوح الحضري , الفراغات العمرانية , تكامل , ترابطية , تحليل محوري ,الملاحة الحضرية.

ABSTRACT

since a very short time, how to measure urban spaces was an undefined issue in the scientific debate. Most of them have relied on theories that their results often selective; they based on complex variables that are rarely available simultaneously in the built environment and the human element**.**

This paper aims to explain the "**intelligibility**" indicator of Urban Spaces, Built Environment and the relationship between **Global Integration** measurement and **Connectivity** measurement of spaces through the **Axial Line Analysis** from the point of view of **Space Syntax theory.**

This indicator helps to understand the surrounding Built Environment, which is critical to urban navigation and helps to understand the urban spatial restructuring of the Built Environment and facilitate its understanding of the observatory**.**

Keyword— Urban clarity, Intelligibility, Urban spaces, Integration, Connectivity, Axial Analysis, Urban navigation.

1. مقدمة

لقد اهتم البحث العلمي بشكل كبير على معرفة مدى وضوح البيئة المبنية وكيف يؤثر هذا الوضوح سواء كان ايجابيا أو سلبيا على الصورة الذهنية للمستعمل وبالتالي على تحسين سلوكه . لقد جاء هذا الاهتمام لمحاولة استخدام هذا الوضوح وبشكل استباقي للتأثير على سلوك معين كتحسين التفاعل الاجتماعي او تناقص الجرائم على سبيل المثل.

التصميم الحضري والجغرافيا و علم النفس الحضري وعلم الاجتماع الحضري وعلوم الإنسان المختلفة وعلاقته ببيئته المبنية , كل هذه مجالات لها صلة عميقة ومهم جداً لها معرفة مدى وضوح البيئة التي يعيش فيها الإنسان ومدى تأثير نسبة وشكل هذا الوضوح عليها.
إن التحسن والتقدم في المناطق الحضرية القريبة من التغيرات الاجتماعية المختلفة قد وسع بشكل كبير من التصميم المتعدد الأوجه [**20**].
لقد ركز المعماري كيفن لينش (Kevin Lynch) في نظريته الصورة الذهنية للمدينة , في كتابه (The image of the city, 1960) على الجودة البصرية للمدينة الأمريكية, وخاصة جودتها المرئية المحددة ,وقد ظهر آنذاك مصطلح (Legibility) للتعبير عن مدى وضوح البيئة المبنية , ولا يعتبر الوضوح (Legibility) هو الخاصية الوحيدة لجمال المدينة , لكن له معنى هام جدا في البيئات المبنية ومقياسها وحجمها الحضري و مدى وضوحها أو تعقيدها .
إن بساطة إدراك منطقة ما وتأثير البيئة في توجيه المستخدم والملاحة الحضرية قد تمت مناقشتها بفكرة "الفهم" او الوضوح (Intelligibility) التي وضعها بيل هيلير (Bill Hillier) في كتاب نظريته الشهيرة الفضاء هو الآلة (Space is the machine, 1996) وفي الأبحاث المتعلقة بنظرية التركيب الفراغي (Space Syntax)
يتميز هذا المفهوم (Intelligibility) بأنه يعني درجة الوضوح التي نراها من الفراغات التي تشكل النظام أو البيئة المبنية .
في هذه الدراسة يتم توضيح أسلوب تحليل (هيلير) وقياسه للوضوح الحضري وتطبيق ذلك كل حالة دراسية متمثلة في مدينة الخمس ومقارنتها بأشهر المدن المدروسة.

2. معنى الوضوح "intelligibility" :

تم تقديم فكرة الوضوح أو الفهم لأول مرة من قبل Bill Hillier, Hanson [**6**] وقد تم تقييم هذا المصطلح كإجراء من الدرجة الثانية , وهو ناتج من العلاقة بين مقياسي الترابطية (Connectivity) مع قيم التكامل الشامل (Global Integration) للخطوط الحورية للتكوين المكاني .
وقد فرض (Hillier) أن العلاقة بين الخطوط المحورية للشبكة ستكون واضحة وان الاعدادات المكانية منطقية وغير مستغربة بالنسبة للمتجول على الأقدام أو راكب المركبة على حد سواء .
إن خاصية الوضوح أو الفهم (Intelligibility) في الشبكة تعنى ما يمكن أن نراه من الفراغات التي تشكل الإطار الذي يرتبط به عدد الفراغات المختلفة وهو دليل واضح لما نستطيع رويته, وهو يمثل مزيج كل فراغ في إطار الفراغات ككل [**9**],[**11**] لتوضح خاصية الشمولية (Global) وأجزاء من التميز المكاني الذي يتعلق بالطريق واكتشاف الطريق و الحركة والمرجعية المكانية والذاكرة والعلاقات المكانية . إن أغلبية الدراسات الحالية أكدت أن الوضوح أو الفهم (Intelligibility)هو خاصية مرتبطة بسمات فهم الفراغات والاستخدام المكاني وتضمن إمكانية التبوء بنظام الفراغات .

3. التركيب الفراغي space syntax :

تعتبر نظرية التركيب الفراغي (space syntax) فرضية كبيرة وأداة دقيقة لتحليل كيف تؤثر الفراغات على التنمية البشرية من خلال قياس التكوين المكاني (spatial configuration) [**6**] ,كما أصبحت لغة الكمبيوتر مهمة جدا لوصف النمط المكاني للحيز الحضري .
تنقسم الفراغات الحضرية إلى فئتين من منظور الحركة البشرية ; فراغات مغلقة وفراغات حرة وتتكون الفراغات المغلقة من عوائق مكانية مثل الأبنية وفي هذه الفراغات لا يستطيع الأشخاص التنقل بحرية من موقع إلى آخر , على عكس ذلك المساحات الحرة هي جزء من الحيز الفراغي الحضري حيث يمكن للناس حرية وسهولة الحركة.
تعني هذه النظرية بدراسة المساحات الحرة , والفراغ هنا ليس كائن يقاس بالمسافات الأقليدية . [**11**] , وتركز النظرية على العلاقة الطوبولوجية للفراغات بما في ذلك الترابطية بين الفراغات والتفاعلية وليس المسافات الطبيعية. في دراسة التركيب الفراغي تتمثل

المنهجية الأساسية في تقسيم المساحة حسب الحجم والقدرة البصرية البشرية ومن هذه النقطة ينقسم الفراغ إلى مساحة واسعة النطاق وقليلة الحجم. [17] ,[26]

إن مقياس المساحة الواسعة مثل المدينة الكاملة تتعدى القدرة البصرية للإنسان , ولا يمكن رؤيتها من وجهة نظر فردية في حين ان مساحة صغيرة الحجم مثل جزء من حجرة هي اكبر من حجم الإنسان إلا انه يمكنه فهمها بشكل أسرع ومميز [18] .

يمكن دراسة الفراغات الواسعة من خلال تقسيمها إلى عدد محدود من الفراغات, وقد اقترحت نظرية التركيب الفراغي لأول مرة بواسطة (Hanson & Hillier) في كتاب المنطق الاجتماعي للفراغ (Social logic of space) بان يقوم بتحليل فراغات حرة مقسمة إلى أجزاء صغيرة الحجم ليكون كل جزء واضحا من نقطة مراقبة منفصلة. [9] لقد تم تطوير تقنيات نظرية التركيب الفراغي بغرض البحث في العلاقة بين الفراغ والسلوك البشري , حيث يوفر الفراغ الشروط المادية اللازمة للعلاقات الاجتماعية , وتستخدم بنية الفراغ كمنهجية لقياس إمكانية الوصول النسبي لاماكن أفضل في إطار مكاني عن طريق تقسيمها إلى "فراغات مستقلة ولكن مرتبطة" .[6] ,[2] وتتبنى هذه النظرية هذا النهج لدراسة إلى أي مدى تتشابه السمات المكانية والاجتماعية للفراغات , وهي تدقق في الخصائص الطوبولوجية للمجموعة الحضرية التي تتضح من شبكات الشوارع الحضرية, ويقارن ذلك أيضا بحركة المشاة والمركبات, وتقدم النماذج العلمية بعيدة المدى بطوبولوجيا الطرق الحضرية التي تم ترتيبها وتحليلها ودعمها من خلال المعلومات التجريبية نتائج معمقة عن المعرفة في الأمثلة العلمية والمناطق الحضرية. [14]

1.3 التحليل ببرنامج Depthmap :

يهدف هذا التحليل إلى فهم العلاقة الأساسية بين كل من الفراغات المفتوحة الرئيسية والنمط المكاني وقد تم بناء نظرية التركيب الفراغي بشكل أساسي على فرضية المنطق الاجتماعي للفراغ الذي يقدم نظرة عامة حول كيفية تحديد الأفراد مع الفراغ في البيئات المبنية و تأثير الفراغ على السلوك الاجتماعي والعلاقات الاجتماعية وتكون الإجراءات على النحو التالي :-

- رسم خريطة الحالة المدروسة (أطول واقل الخطوط المحورية) للحصول على الخريطة المحورية Axial map بواسطة برنامج Auto cad .
- تصدير الملف بصيغة DXf إلى برنامج UCL Depthmap .
- تحليل الخرائط المحورية للحصول على القياسات والعلاقات المهمة .

1.1.3 التكامل (Integration) :

تتغير قيمة تكامل الخط وفقا لعدد المستويات التي تم اعتبارها في القياس إذا قمنا بحساب مدى عمق أو ضحالة كل خط من جميع الخطوط الأخرى, فإننا نسمي هذا التكامل , (تكامل شامل) (global Integration) في حين أن حساب مدى عمق أو ضحالة كل خط من جميع خطوط الشبكة حتى ثلاثة مستويات فقط يسمى (تكامل R3) أو (Radins3) أو (التكامل المحلي)(Local Integration) وإذا كان فقط على بعد مستوى واحد من كل خط من الشبكة فإذا هذا يسمى الترابطية أو الاتصالية (Connectivity) لخط (عدد الخطوط المرتبطة به مباشرة) لذا فإذا تحديد نوع التكامل تعتمد على نصف القطر R [11].

2.1.3 التكامل المحلي (Local Integration) :

يمثل هذا النوع من التكامل إمكانية الوصول والترابط ضمن جزء من النظام المكاني بأكمله , يتم احتساب هذه القيمة فقط عدة خطوات بشكل فراغ معين , عادة في حدود 3 خطوات عمق (R3) , وقد أشارت الأبحاث السابقة إلى أن التكامل المحلي يمكن تفسيره من خلال التسلسل الهرمي لإمكانية الوصول والحركة المحلية للمشاة.

يتميز التكامل المحلي (Local Integration) المتوسطي بتقديرات المزج للخطوط المحورية في نصف القطر 3 (الجذر إضافة إلى خطوتين طوبولوجيتين من الجذر) يمكن استخدامها لتظهر صورة مركزية للتكامل.

2.1.3 التكامل الشامل (Global integration) :

يشير التكامل الشامل إلى إمكانية الوصول والاتصال لكل فراغات الإطار المكاني كاملا والفراغ الذي يمكن الوصول إليه بشكل أكثر من الفراغات الأخرى يكون الفراغ الأكثر تكاملا . ويشكل أكثر وضوحا هناك فراغ ذو قيمة تكامل عالية يتمتع بفرصة جيدة ليصبح مكانا للتجمعات والتفاعل الاجتماعي بين الأشخاص.
يتميز التكامل الشامل المحوري بقيم التكامل للخطوط المحورية في دائرة نصف قطرها لانهاية له والتي يمكن استخدامها لتظهر صورة لأسلوب التكامل في أكبر مقياس .

3.1.3 الاتصالية أو الترابطية (Connectivity) :

هو خاصية للخط (الفراغ) الذي يمكن رؤيته من الخط (الفراغ) الآخر,في حين أن التكامل الشامل لا يمكن رؤيته من الخط (الفراغ) الملاصق لأنه يتطلب معرفة النظام ككل , فإن الاتصالية تعتبر العلاقة بين كل خط وكل الخطوط الأخرى بغض النظر عن كيفية استمراريتها إلى ابعد الحدود لذلك هو مقياس شامل (Global).

3.1.3 قياس الوضوح (Intelligibility) :

يوضح هذا المصطلح العلاقة المتبادلة بين مقياسيين مهمين جدا هما التكامل الشامل والاتصالية أو الترابطية (\ Global integration Connectivity) وهو يشير إلى الفراغات الأكثر وضوحا أو فهما (أسهل لتصميمات الأشكال المكانية إذا كانت العلاقات عالية) و يتم عرض هذا المؤشر في مخطط تشتت مع خطوط انحدار تظهر العلاقة بين قيم التكامل الشامل (Global Integration) والاتصالية او الترابطية (Connectivity)

4. حالة الدراسة ومناقشة نتائجها (مدينة الخمس) :

تقع المدينة ضمن إقليم طرابلس الرئيسي في الجزء الشمالي الغربي من ليبيا . ولها موقع رئيسي مهم كميناء بحري , وتعتبر مدينة الخمس عاصمة لإقليم الخمس الفرعي.
المدينة لها جذور فينيقية ورومانية متمثلة في آثار مدينة لبدة الكبرى والتي تقع ضمن مخطط مدينة الخمس وفي الجزء الشرقي منه.
مدينة الخمس الحديثة أسسها العثمانيون كحامية عثمانية وميناء رئيسي لتصدير نبات الحلفاء .هناك القليل من المباني العثمانية والإيطالية التي بقيت إلى الآن من تلك الحقبتين .الشكل (1)

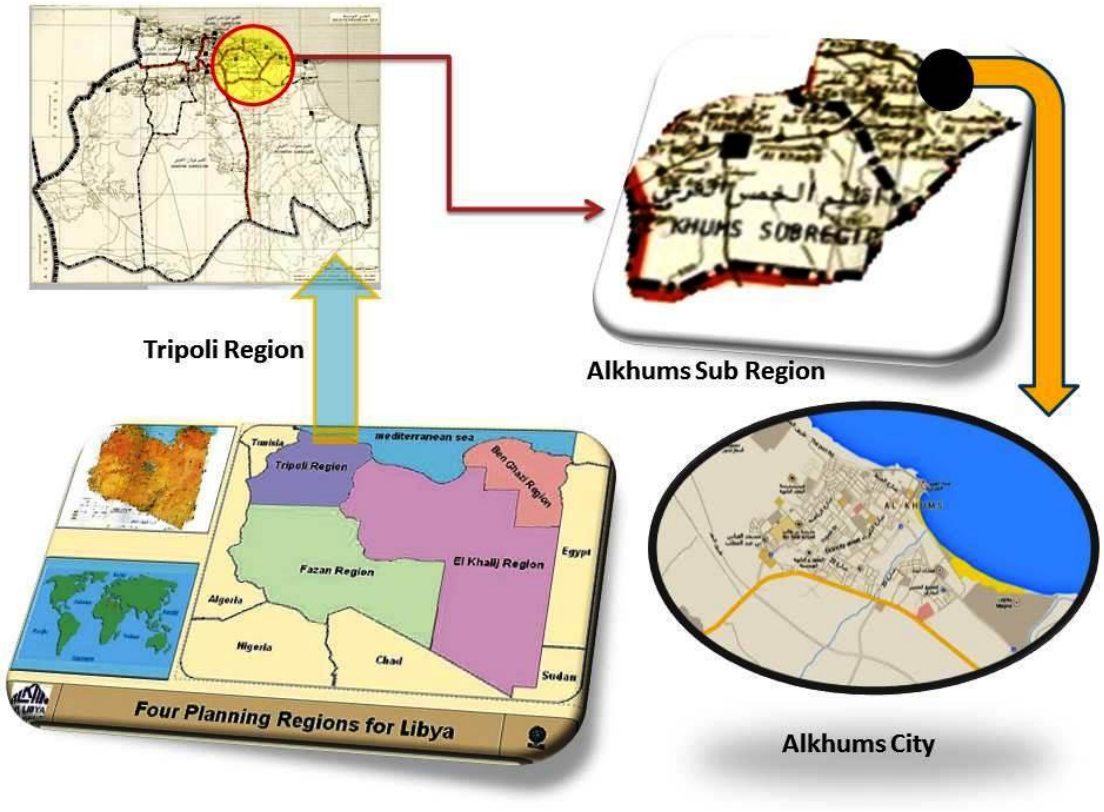

الشكل (1) : موقع مدينة الخمس

1.4 التحليل المحوري لمدينة الخمس النتائج و المناقشة :

من الواضح ان المدينة هي حاوية الأنشطة البشرية المختلفة وهي بالتالي تحوي العديد من سلوكيات البشر في فراغاتها المختلفة (أماكن للأكل , السكن , تجمعات ,اتصال مع الآخرين و مشي) هناك أيضا اتصال طبيعي بين فراغاتها , ويمكن استخدام الفراغ في العلاقة بين تكوين الأفراد وتكوين الفراغ. هذا التكوين هو ما وضحه هيلير (Hillier) في كتابه (الفراغ هو الآلة) (Space is the machine) كمجموعة من العلاقات المترابطة التي يتم تحديد كل منها خلال علاقتها بالآخرين . (Hillier 1996)

1.1.4 قيمة الترابطية (C) لمدينة الخمس (Connectivity) :

لقد بلغت قيمة الترابطية (connectivity) في مدينة الخمس من خلال التحليل المحوري (Axial line Analysis) "3.745" وهو رقم ضمن حدود المتوسط للمدن الأوروبية والإنجليزية , وتؤكد هذه القيمة أن نظام الكتل والشوارع المفتوحة يسيطر على مخطط المدينة . الشكل (2)

الشكل (2) : قيمة الترابطية (C) لمدينة الخمس (Connectivity)

2.1.4 قيمة التكامل المحلي (R3) (local integration) لمدينة الخمس :

تم حساب هذا القياس أساس 3 خطوات عمق R3 وقد كانت قيمة التكامل المحلي "1.842" وهو رقم أعلى قليلا من متوسط القيمة للمدن العربية, هذه القيمة تؤشر أن المدينة ذات شوارع مباشرة ومتصلة ومن خلال هذا المؤشر يبدو أن الفراغات الأكثر تكاملا محليا شبيهة جدا بالفراغات الأكثر تكاملا على المستوى الشامل.

ومن خلال التحليل كان شارع 17فبراير وشارع طرابلس وشارع 20 الأعلى تكاملا, وأن أفضل الخيارات للوصول إلى المدينة من خلال استعمال شارعي 17 فبراير وشارع طرابلس . الشكل (2)

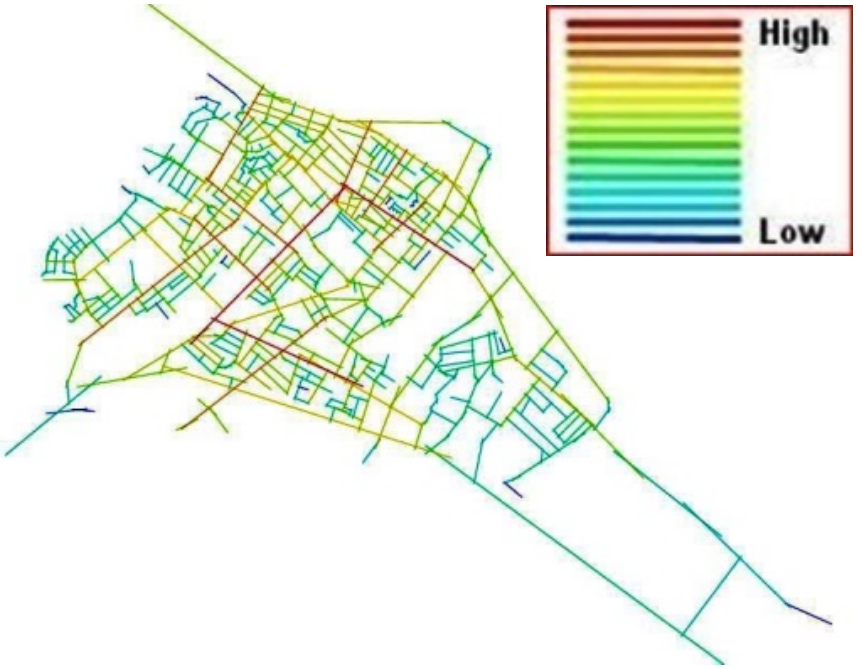

الشكل (2) : قيمة التكامل المحلي لمدينة الخمس (R3) (local integration)

3.1.4 قيمة التكامل الشامل (Rn) (global integration) لمدينة الخمس:

استنادا للتحليل المحوري والخريطة المحورية لمدينة الخمس فقد تبين أن قيمة التكامل الشامل Rn يقترب من متوسط المدن الأمريكية وقد بلغت قيمته "1.293" والفراغات الأكثر تكاملا تمثلت في جزيرة الدوران والشوارع الرئيسية والطرفية المتصلة بها , وقد كانت أيضا أكثر الشوارع تكاملا هي شارعي 17 فبراير وشارع طرابلس والشوارع المتصلة بهما , هناك أيضا شوارع سجلت قيما عالية مثل شارع الحاراتي. الشكل (3)

4.1.4 قيمة الوضوح أو سهولة الفهم Rn vs C (intelligibility) لمدينة الخمس :

من المميزات المهمة والمثيرة للاهتمام لمدينة الخمس هي مؤشر الوضوح وسرعة فهم المدينة (Intelligibility) بلغ هذا المؤشر قيمة (0.3286) الشكل (4) وهي تعتبر قيمة عالية جدا أكثر من العديد من المدن الجدول (1)
وتعني هذه القيمة أن المراقب أو المتجول في المدينة يستطيع فهم جميع فراغات المدينة من خلال حركته ورؤيته لفراغات قليلة جدا ومحدودة ,أي أن المدينة وفراغاتها تساعد الزائر والمتجول على سرعة الفهم لفراغاتها. وبالتالي فإن البنية المكانية لمدينة الخمس لا تحتاج إلى الكثير من الخطوات لفهم أجزاء المدينة بالكامل . وتعتبر العلاقة بين الترابطية Connectivity والتكامل الشامل Global Integration مؤشرا أساسيا لمدى وضوح النظام الحضري لمستخدميه . ويطلق على ناتج هذه العلاقة بين Rn vs C مصطلح الوضوح وسرعة الفهم Intelligibility وهذا المؤشر هو واحد من عدة مقاييس ومؤشرات أخرى أصبح من السهل إيجادها وقياسها من خلال التحاليل المختلفة لنظرية التكوين المكاني Space Syntax وبواسطة برنامج التحليل Dephtmap.

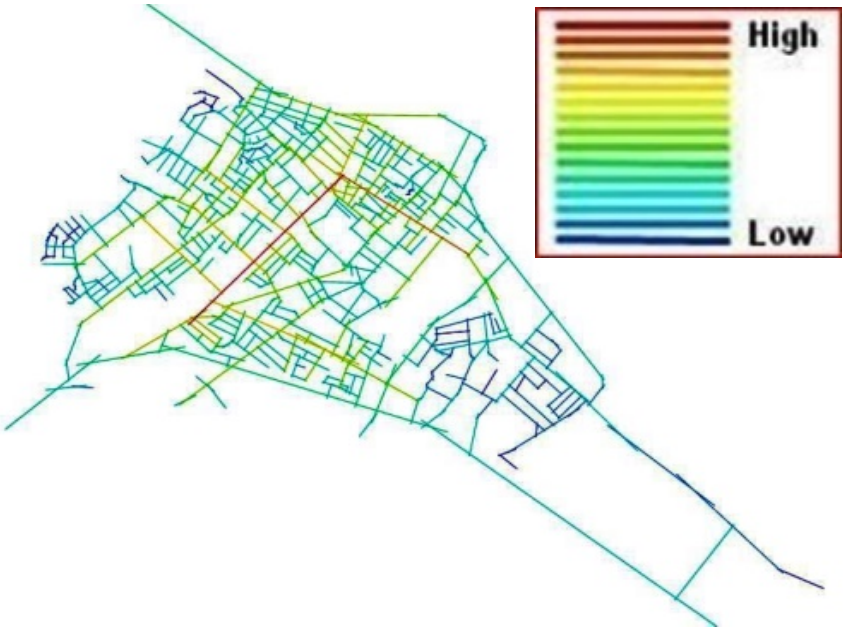

الشكل (3): قيمة التكامل الشامل لمدينة الخمس (Rn) (global integration)

إن المناطق الحضرية لمدينة الخمس تتمتع بقيم عالية لمؤشر الوضوح وسهولة الفهم , ويظهر تحليل التكامل الشامل Rn والمحلي R3 لمدينة الخمس أن الطرق الرئيسية المركزية قوية وهي ما يميزها في خريطة التحليل المحوري بألوان قوية وهذا يعني أن الهياكل المكانية وفراغات المدينة تدعم سرعة فهم مستخدميها مما يساعد على الوصول إلى كل الأماكن بسهولة أكثر, وهذه ميزة تخدم الزوار وتسهل من حركتهم , خاصة أن المدينة وجهة سياحية للزوار من كل الجنسيات.

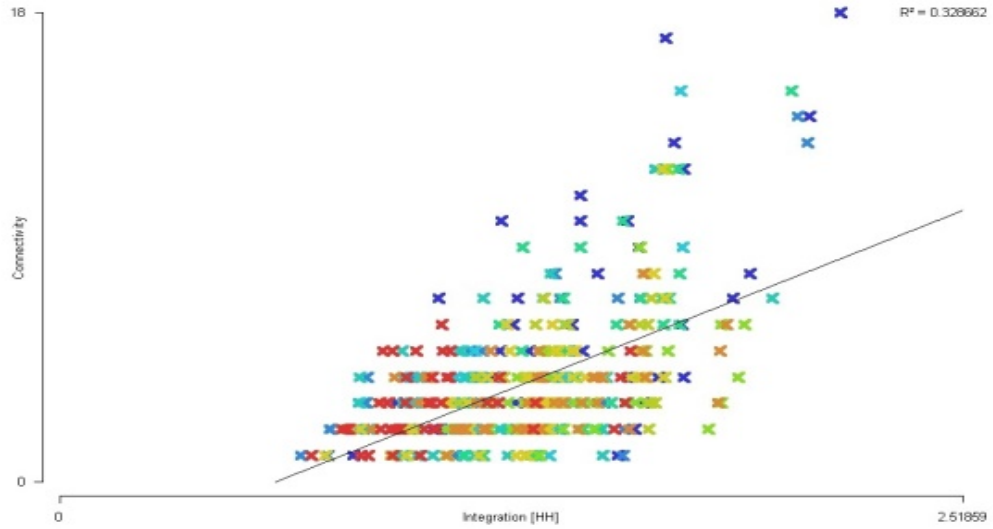

الشكل (4) : Rn vs C قيمة الوضوح أو سهولة الفهم لمدينة الخمس (Intelligibility)

الجدول (1): مقارنة لأهم قيم التحليل المحوري لمدينة الخمس واهم المدن المدروسة

Cities	Cases	Axial size	Connectivity C	Local integration R3	Global integration Rn	Intelligibility Rn / c	Synergy Rn /R3
U.S Cities	12	5420	5.835	2.956	1.61	0.224	0.559
Euro Cities	15	5030	4.609	2.254	0.918	0.137	0.266
English Cities	13	4440	3.713	2.148	0.720	0.124	0.232
Arabic Cities	18	840	2.975	1.619	0.650	0.231	0.160
Libyan Cities	6	1416	3.53	3.53	0.904	0.192	0.369
Ghadames City	1	744	2.7	2.7	0.558	0.122	0.227
						prepared by Alagori farag 2002	
Khums city	1	486	3.745	1.842	1.293	0.3286	0.7128

***Sources**: Blue part: Alagori farag ,2002 based Bill Hillier, theory of the city as object.& Orange part: prepared by researcher based empirical work, 2017.*

5. الخلاصة :

إن أهم عامل لتسهل الحركة وسرعة الفهم هي فهم التركيب الفراغي وارتباطه بباقي الفراغات , في هذه الورقة تم التركيز على التكوين المكاني للفراغات من كونه قواعد مكانية مخفية لم يكن يسهل قياسها ومعرفة قيمها, إلى فراغات وتكوينات مكانية يسهل قياسها ومقارنتها مع قراءات أخرى , واستنتاج الفروقات بينها بأرقام دقيقة ومحددة جدا, وتساعد هذه القراءات والأرقام والمقاييس والمؤشرات إلى سهولة تطوير نهج إنساني نحو التصميم المكاني للبيئات المبنية الحضرية الناشئة في البلد.

هناك مؤشرات ومقاييس أخرى طرحتها النظرية تعطي تحاليل أكثر تفصيلا ولمقاييس مختلفة للفراغات تبدأ من فراغ المنزل إلى الساحات والميادين إلى فراغات المدينة ككل . لذلك من الضروري تعزيز الدراسة لمدن أخرى لمقارنة وتحليل الهياكل المكانية للمدن, وفهم البيئة المبنية الحضرية لها. وقد بينت هذه الدراسة أنه أصبح من الممكن قياس وضوح البيئات المبنية للمدن والفراغات لغرض سهولة التعرف عليها خاصة من قبل الزوار ومساعدتهم في إيجاد طرق لوجهاتهم المختلفة داخل الهياكل المكانية الحضرية , كما أن هذه المقدرة على قياس الهياكل المكانية على المستوى الأكاديمي ساعد كثيرا على التخلص من إشكالية الانتقائية (Selective) التي كانت تواجه الباحث عند قياسه للوضوح الحضري من خلال نظرية الصورة الذهنية للمدينة (The Image of The City) والخرائط الذهنية (Mental Map) لكيفن لنش Kevin Lynch لوحدها , والتي كانت تعتمد على الكثير من التعقيدات كمدى جودة البيئة المرئية أو رداءتها ومدى وضوح أو رداءة العناصر المرئية والتي غالبا ما تكون انتقائية لاعتمادها على عمر وجنس ومزاج الأشخاص وحالة البيئة أثناء المقابلات مما يعطي نتائج مختلفة صعبة في تحليلها وغير واضحة أو محددة لاعتمادها على خصائص بيئية وإنسانية مختلفة.وأصبح ممكنا تطبيق النظريتين معا والاعتماد على المقارنة وتكامل نتائجهما كلتاهما للوصول لنتائج أفضل.

شكر وعرفان:

اود أن اشكر مشرفتي الدكتورة أوزلام أوزير لأن هذه الورقة تعبر عن جزء من اجزاء رسالتي لنيل درجة الدكتوراه. أطروحة في العمارة والتخطيط الحضري,جامعة اوكان تركيا .

Acknowledgment:

I wish to thank my supervisor Dr. Ozlem Ozer because this paper is a part of my Ph.D. thesis in Architecture and urban planning , Okan University, Istanbul, Turkey.

References **المراجع:**

[1]. Bandura, Albert. 1989. Social cognitive theory . Greenwich : Stanford University, JAI Press, 1989.

[2]. Batty M, M and Rana , S. 2002. Reformulating space syntax: the automatic definition and generation of axial lines and axial maps. Center for Advanced Spatial Analysis, University College, London. WP58, 2002.

[3]. Das, D. (2008). Urban quality of life: A case study of Guwahati, Springer Science+Business Media B.V., Soc Indic Res. 88, 297–310.

[4]. Egenhofer , M. J and Mark, D. M. 1995. Naive Geography, in: Spatial Information Theory: A Theoretical Basis for GIS, edited by A. U. Frank and W. Kuhn. Berlin : Springer-Verlag, 1995.

[5]. Gifford, R. (2002). Environmental Psychology: Principles and Practice (3rd ed.). Toronto, Canada: Optimal Books.

[6]. Hillier , B, Hanson, J and Peponis, J. 1987. The syntactic analysis of settlements. Architecture et Comportement/Architecture and Behavior. vol. 3, , 1987, Vol. no. 3.

[7]. Hillier, B. 2002. A theory of the cityas object: or, how spatial laws mediate the social construction of urban space . Urban Design International . Vol. 7, 2002.

[8]. Hillier, B and A , Penn. 1992. Dense Civilisations: the Shape of Cities in the 21st Century. Applied Energy. 43, 1992.

[9]. Hillier, B and Hanson, J. 1984. The social logic of space. . Cambridge : Cambridge University Press, 1984.

[10]. Hillier, B. 2011. Is architectural form meaningless? A configurational theory of generic meaning in architecture, and its limits. The Journal of Space Syntax. Vol.2, 2011, Vol. 2.

[11]. Hillier, B. 1996 . Space is the machine: configurational theory of architecture. Cambridge : Cambridge University Press, 1996 .

[12]. Hillier, B. 1999. The common language of space: a way of looking at the social, economic and environmental functioning of cities on a common basis. Journal of Environmental Sciences. Vol. 11 , 1999, Vol. 3.

[13]. Hillier, B. 2012. The genetic code for cities:Is it simpler than we think? London : Springer, 2012.

[14]. Hillier, B, et al. 1993. Natural movement; or, configuration and attraction in urban space use. Environment and Planning B: Planning and Design. Vol. 20, 1993.

[15]. Jiang B, B, Claramunt , C and Klarqvist , B. 2000. An integration of space syntax into GIS for modeling urban spaces. International Journal of Applied Earth Observation and Geo information. 2, 2000.

[16]. Jiang , B. 2007.Ranking spaces for predicitng human movement in an urban environment. s.l. : Preprint, arxiv, 2007.

[17]. Jiang , B. 2006. Ranking spaces for predicting human movement in an urban environment. International Journal of Geographical Information Science. 2006..

[18]. Jiang, B and Liu, C. 2009. Street-based topological representations and analyses for predicting traffic flow in GIS. International Journal of Geographical Information Science. 23, 2009, Vol. 9.

[19]. Johnston R .J. et. al. (2000). The dictionary of human geography. Oxford: Blackwell.

[20]. Karimi, K. 2012. A configurational approach to analytical urban design: Space syntax methodology. Urban Design International. 17, 2012, Vol. 4.

[21]. Lang, J. (1994). Urban Design: the American experience. New York: John Wiley & Sons, Inc.

[22]. Laurens J. M. (2012). Changing behavior and environment in a community-based Program of the Riverside Community. Procedia - Social and Behavioral Sciences, 36, 372 – 382.

[23]. Masoudi K, 2011. Urban public area. the place of social interaction. Municipalities, 26: 34-45.

[24]. Mehta, V. (2013). The street : a quintessential social public space. Abingdon, Oxon ; New York, NY: Routledge .

[25]. Moeini, M. (2012). Attitudes to urban walking in Tehran. Journal of E&PB.

[26]. Montello, D. R. 1993. Scale and Multiple Psychologies of Space, in: Spatial Information Theory. Berlin : Springer-Verlag, 1993.

[27]. Rapoport, Amos. 1990. The Meaning of the Built Environment: A Nonverbal Communication Approach. Tucson, Arizona : Published by University of Arizona Press, 1990. ISBN 10: 0816511764 / ISBN 13: 9780816511761.

[28]. Rapoport, Amos. 2003. Culture, Architecture, and Design. Barcelona : s.n., 2003. ISBN: 84-8301-680-X.

[29]. Whyte, W. H. (1980). The social life of small urban spaces. Washington, D.C.: Conservation Foundation.

Key Performance Indicators in Libyan Oil and Gas Projects

Mahmoud Matoug[1], Abdulbaset Frefer[2], Haleema Omer[3]
[1]mmmatoug54@ymail.com, [2]drfrefer@hotmail.com,[3]haleemaomer884@gmail.com
[1, 2] Mechanical and Industrial Engineering Department, University of Tripoli
[3] Engineering Management Department, University of Tripoli

ABSTRACT

Nowadays, the management system based on key performance indicators (KPIs) is one of the most effective systems from a project management perspective. Unfortunately, common key performance indicators do not exist for the assessment of the performance and success of Libyan oil and gas projects (LOGPs). A project's success or failureno longer depends solely on whether or not it meets traditional key performance indicators (cost, time and quality), instead, the assessment of a project's success is required from the beginning until the end of the project and product lifecycle. The purpose of this study is to advance understanding of KPIs and to develop the most common key performance indicators (KPIs) for the Libyan oil and gas projects. By reviewing the existing research and literature, 11 (eleven) most important KPIs were identified. Questionnaire surveys and semi-structured interviews were administered to gauge the opinions of project practitioners representing clients, consultants and contractors on the KPIs most relevant to the local oil and gas industry. The findings indicate that the traditional KPIs are no longer applicable in measuring performance and success of oil and gas projects in Libya. Other key performance indicators such as Health, Safety and Environment (HSE), Efficiency of use resource, Profitability, Experience gain from the project, Shareholder Satisfaction, Sustainability, Maintainability and Reliability are increasingly becoming more important. Key performance indicators for the assessment of Libyan oil and gas projects are far more complex than simply meeting cost, time and quality.

Keyword— Key Performance Indicators (KPIs), Libyan Oil and Gas Projects (LOGPs), Project Management, Project Success, Management Tools.

1. Introduction

Oil and gas projects with high level of uncertainty and risks have proven to be one of the most complex in business with high level challenges that are faced by the petroleum companies these days. These projects are executed at different stages of the oil and gas industry value chain and almost always involve multiple stakeholders, multiple nationalities and large number of staff [1]. The size and complexity of these projects require special attention in the project management process. Bodicha [2] argue that despite the globalization and much acquired knowledge for organizations to engage in project management, the use of project management tools and techniques does not automatically guarantee project success. A project performance and success can be measured traditionally by three indicators: namely; cost, time and quality. Many

researchers suggest that success can't be accessed only through these three key performance indicators, since project success is more complex. They advocate the expansion of success measurement towards project management success and product success [3]. Libya exports about 80% of its crude oil and earns about 96% of its revenue from oil and gas exports [4]. Unfortunately, common KPIs do not exist for the assessment of the performance and success of Libyan oil and gas projects. The purpose of this research paper is to advance understanding of KPIs and to develop a set of the most common KPIs for Libyan oil and gas projects.

2. Performance Measurement

Performance measurement is the first step in any performance improvement program. It helps to identify gaps in performance, opportunities for improving performance and to develop programs for continuous improvement. According to Fleming, et al. [5], the heart of effective project management is the establishment of performance measurement baseline and performance reporting. Salaheldin [6] stated that performance measurement is a critical factor for effective management since without measuring something; it is difficult to improve it.

Ofori-Kuragu [7] reported that there isn't distinction between measures and indicators. In fact, measurement alone is not enough to improve performance. The indicators are important within projects since they assess what should be measured and the control limits within which the performance should be. Also, the level of performance that project reaches is based on the efficiency and effectiveness of the actions taken. According to Alarcon, et al. [8], the result of a project is the product of various processes and decisions that interact during its execution.

Along the same line, Libyan oil and gas industry represented by the National Oil Corporation (NOC) and its subsidiaries, most of which are focusing on traditional key performance indicators (cost, time and quality). Although KPIs have long been used to evaluate and judge the performance and success of projects; many researchers suggest that success can't be accessed only through those traditional KPIs, since project success is more complex, and these indicators do not provide an adequate vision of the potential for improvement [9]. In a recent study conducted to determine the strength of the relationship between different elements of project management performance indicators and project success, the results showed that the project management performance indicators have positive association with the project success [10].

Many studies that were carried out to determine KPIs to evaluate the performance and success of projects did not distinguish between "indicators and criteria", describing both as measures used to measure the performance and success [1]. In this research paper, "indicators" and "criteria" are both used as means to measure the performance and success, and hence used interchangeably.

In order to cover key performance indicators in greater depth, it is important to consider the various studies conducted on the construction industry. Although the oil and gas projects have unique characteristics, they have similarities with construction projects. Some of the construction projects in the oil and gas industry

include the construction of oil refineries, of petrochemical plants or of gas treatment plants. Table 1 shows summary of key performance indicators in any project from the fifteen literature reviews discussed in this research paper [3,7,11-23].

The broad categories of stakeholders have been identified by many researchers, such as clients, contractors, consultants and material suppliers as the internal project stakeholders; where, the external stakeholders were identified as local communities and the government. Stakeholder participation in project evaluation is essential since it keeps the projects on track and often ensures early detection of problems that can reduce the likelihood of having major cost overruns or time delays and non-conformity to project specification [14].

Many researchers identified clients, contractors and consultants as the major internal stakeholders in projects, and their participation is essential in the evaluation of any project. The clients are considered as the financiers interested in how much had been spent and its corresponding progress. Whereas the contractors and the professional consultants were integral to the project implementation and the success or failure of the project depends on their performance [15]. In this research paper the authors consider stakeholders as clients, contractors and consultants.

Table 1: Summary of KPIs in Project from the Literature Review.

KPI \ Sources	Al Hammadi [11]	Ahmed [12]	Sylvester et al.[13]	Bahia [14]	Olaku et al. [15]	Khosravi [16]	Toor et al. [3]	Al-Tmeemy et al. [17]	Ofori-Kuragu et al. [7]	KPI Working Group [18]	Lim et al [19]	Yeung et al. [20]	Ling et al. [21]	Ali et al. [22]	Cross et al. [23]	Frequency %
Cost	√	√	√	√	√	√	√	√	√	√	√	√	√		√	93.3%
Time	√	√	√	√	√	√	√	√	√	√	√	√	√		√	93.3%
Quality	√		√	√	√	√	√	√	√	√	√	√	√	√	√	93.3%
Customer Satisfaction	√			√	√	√		√	√	√			√	√	√	66.7%
Health, Safety andEnvironment	√			√		√	√		√	√	√			√		53.3%
Scope		√	√	√												20%
Efficiencyof use resources					√		√						√			20%
Effectiveness					√		√						√			20%
Productivity									√						√	13.3%
Business performance									√	√						13.3%
Profitability													√	√		13.3%

3. Data Collection

This research paper was conducted based on intensive literature reviews to identify key performance indicators for oil and gas projects and to develop a survey questionnaire. Based on these literature reviews eleven (11) key performance indicators were identified in Libyan oil and gas sector. Table 1 presents the proposed key performance indicators of oil and gas projects success. The questionnaire consists of two sections. The first elicits information on the respondents' background as shown in Table 2, where the second consists of questions related to key performance indicators. The questionnaire survey was carried out in Libya in the beginning of 2017. Internal consistency of the data reliability analysis was achieved by employing Cronbach's Alpha coefficient. Cronbach's Alpha reliability coefficient ranges from 0 to1. The closer the coefficient value to 1, the greater is the internal consistency of the data [13,24,25]. Cronbach's Alpha coefficient for each field of the questionnaire is 0.843, this is considered high; the result is ensuring the reliability of each field of the questionnaire.

One hundred and twenty (120) questionnaires were administered to project practitioners, including clients, consultants and contractors who have experience in oil and gas projects that were recommended by the NOC, as part of the most important companies whichhave great experience in oil and gas projects in Libya. Out of the 120 distributed by hand, eighty-eight (88) were received back. Therefore, the questionnaires returned have a response rate of 73.33%. The respondents were requested to indicate their views on the importance of each key performance indicator. They were asked to use five-point Likert Scale ranging from 1 to 5, where 1 represents strongly disagree and 5 strongly agree. This scale was introduced by Likert in 1932 [26-27].

Table 2: Summary of Respondents' Profile.

Companies	%
Client	48.86
Consultant	23.86
Contractor	27.27

Qualification	%
HND	4.55
BSC	53.41
MSC	39.77
PHD	2.27
Other	0

Experience (years)	%
1-5	13.95
6-10	29.07
11-15	16.28
16-20	13.95
Above 20	26.74

4. Results and Discussion

4.1. Data Analysis

The data collected were analyzed with the aid of Statistical Package for Social Sciences (SPSS). Descriptive statistics were used to analyze the respondents' profiles using SPSS. The Relative Importance Index (RII) method [22,28-30] was used to rank the key performance indicators. This method provides a score calculated upon the weight given to i^{th} response (Wi), (i=1,2,3,4,5); frequency of the i^{th} response (Xi); maximal weight (A) (5 in this research paper); and total number of respondents (N). RII refers to a value within [0–1] interval. The higher the RII, the more important the KPI. The RII for each KPI is calculated using the formula below [22]:

$$RII = \frac{\sum_{i=1}^{5} Wi\ Xi}{A * N}$$

4.2. RII and KPIs Used to Assess Performance and Success of LOGPs

From the perspective of the clients, consultants and contractors, all the eleven key performance indicators identified in the literature review were significant in the Libyan oil and gas industry, since all had RII score values above 0.7. The different categories of respondents seem to have a few different views about the most important KPIs. Table 3 shows the full details of RII scores of all key performance indicators.

Table 3: Shows the full details of RII scores of all key performance indicators.

Key Performance Indicators	RII (Client)	Rank	RII (Consultant)	Rank	RII (Contractor)	Rank	Overall RII	Overall Rank
Quality	0.9395	2	0.9333	1	0.9333	1	0.9364	1
Time	0.9442	1	0.9238	2	0.9250	2	0.9341	2
Cost	0.9395	2	0.8952	3	0.9167	3	0.9227	3
Health, Safety and Environment	0.9023	3	0.8571	5	0.8500	7	0.8773	4
Scope	0.8791	4	0.8476	6	0.8500	7	0.8636	5
Customer satisfaction	0.8279	5	0.8857	4	0.8833	5	0.8568	6
Efficiency of use of resources	0.8093	6	0.8476	6	0.9000	4	0.8432	7
Effectiveness	0.8047	7	0.8476	6	0.8417	8	0.8250	8
Productivity	0.7953	8	0.8476	6	0.8250	9	0.8159	9
Profitability	0.7814	9	0.8190	7	0.8667	6	0.8136	10
Business performance	0.7395	10	0.7429	8	0.7667	10	0.7477	11

The overall rankings of the most important key performance indicators are; Quality with an overall RII of 0.9364, followed by Time with 0.9341, then Cost with 0.9227, and finally Health, Safety and Environment (HSE) with 0.8773. RII scores equal or less than 0.8 were omitted.

The results from this research paper indicate that quality has been ranked by the clients as the second most important indicator, while consultants and contractors ranked the quality as first indicator, this is an

indication that quality is the most important indicator for consultants and contractors. Time has been ranked by the clients as the first, this is an indication that time is the most important indicator for clients because overrun of time shatters all subsequent planning. However, both consultants and contractors ranked time as the second most important indicator. Cost has been ranked by the clients as the second, while consultants and contractors ranked it as the third; indeed, most project managers must ensure that the implemented projects do not experience cost overruns.

In one hand, Health, Safety and Environment (HSE) indicator has been ranked by the clients as the third indicator. Many industries, especially the oil and gas sector need to give priority consideration to the HSE, this necessitates that companies musttrack the number ofdangerous occurrences, occupational injuries and oil spillsto avoid damaging their reputation and to maintain the competitive advantage. On the other hand, HSE has been ranked by the consultants as the fifth indicator and by the contractors as the seventh indicator. Scope indicator has been ranked by the clients, consultants and contractors the fourth, sixth, and seventh indicator, respectively. Projects in oil and gas are carried out with specific scope aiming to achieve specific deliverables [13].

While clients and contractors ranked the Customer' Satisfaction indicator as the fifth, consultants ranked it as the fourth. Customer satisfaction is considered as an important KPIs when evaluating a project's performance and the success of a project that meets the end-users' expectations [11]. Efficiency of use of resources has been ranked by both the clients and consultants as the sixth indicator; it was ranked as the fourth indicator by the contractors. Effectiveness has been ranked by the clients as the seventh indicator but it was ranked by consultants and contractors as the sixth and eight indicator, respectively.

Productivity has been ranked by the clients as the eight indicator. The consultants and contractors ranked productivity as the sixth and ninth, respectively. Profitability has been ranked by the clients and consultants as the ninth and seventh indicator, respectively. However, it has been ranked by the contractors as the sixth indicator. The fact that survival of companies in the long-term depends on their ability to be profitable, this indicator is used to assess project success in the mid-term and long-term [25]. Business performance has been ranked by the clients and contractors as the tenth indicator and ranked as the eight indicator by the consultants.

4.3. Interviews and New Key Performance Indicators

Following the analysis of the questionnaire survey results, interviews were conducted with experts in the Libyan oil and gas projects from oil and gas industry to validate the results of this research and add any absent key performance indicators in the initial questionnaire survey. Five semi-structured interviews were conducted based on the result of the initial survey.

Interviewees were asked to comment on the outcome of the questionnaire survey and make suggestions for the final list of KPIs for Libyan oil and gas projects. The questions sought to establish whether the interviewees agreed with the outcome of the questionnaire analysis. The interviewees agreed and added more

five indicators; namely, Experience Gain from the Project, Shareholder Satisfaction, Achievement of Project's Objectives, Reliability, Maintainability and Sustainability as the KPIs for Libyan oil and gas projects.

5. Conclusions

One of the most important conclusions that were reached from the literature and confirmed in this research paper is that the key performance indicators in projects in the construction industry seem to have similarities with the key performance indicators in projects in the oil and gas industry. Although many researchers have proposed various key performance indicators to measure both oil and gas project and construction success, there is no general agreement. Other significant conclusions are; the oil and gas industry are slowly departing from the traditional quantitative performance measurement to a rather mix of both quantitative and qualitative performance measurement; the results indicate that the traditional (Iron Triangle) KPIs only, are no longer applicable in measuring the performance and success of oil and gas projects in Libya. This fact should serve as an encouragement in finding a commonly accepted set of KPIs that will be used for performance benchmarking of the oil and gas projects. From the results of this research paper, other key performance indicators, such as Health, Safety and Environment (HSE), Efficiency of use resource, Profitability, Experience Gain from the project, Shareholder Satisfaction, Sustainability, Maintainability and Reliability are increasingly becoming more important. Libyan oil and gas companies need to think in more depth about the key performance indicators that are currently used globally in evaluating their projects and serve towards further setting new indicators to meet short-term, mid-term and long-term objectives in future projects. Sustainability has been identified as one of the most key performance indicators of oil and gas projects in Libya, also through literature review, the sustainability is considered to be one of the future developments in project management. Therefore, the researchers recommend further study to find the relationship between project management and sustainability, and the ability of oil and gas companies to implement sustainability's principles in project management in Libya.

References

[1]. H. Omer, "Assessment of Projects Using Key Performance Indicators in Oil and Gas Companies", *MSc Thesis*, University of Tripoli, 2017.

[2]. H. Bodicha, "How to Measure the Effect of Project Risk Management Process on the Success of Construction Projects: A Critical Literature Review", *The International Journal of Business & Management*, vol 3, no. 12, 2015.

[3]. S. Toor and O. Ogunlana, "Beyond the 'Iron Triangle': Stakeholder Perception of Key Performance Indicators (KPIs) for Large Scale Public Sector Development Projects", *International Journal of Project Management*, pp. 228–236, 2010.

[4]. Independent Statistics & Analysis," Country Analysis Brief: Libya", U.S. *Energy Information Administration*, 2015.

[5]. Q. Fleming and J. Koppleman, "Earned Value Project Management", 2nd ed., *Project Management Institute*, NewtonSquare, PA: PMI, 2000.

[6]. S. Salaheldin, "Critical Success Factors for TQM Implementation and their Impact on Performance of SMEs",*International Journal of Productivity and Performance Management*, vol. 58, no. 3, pp. 215-237, 2009.

[7]. J.Ofori-Kuragu, F. Edum-Fotwe and E.Badu, "Key Performance Indicators for Project Success in Ghanaian Contractors" ,*International Journal of Construction Engineering and Management*, vol. 5, no. 1, pp. 1-10, 2016.

[8]. L. Alarcon, A. Grillo, J. Freire and S. Diethelm, "Learning from Collaborative Benchmarking in the Construction Industry", *9th Annual Conference of the International Group for Lean Construction (IGLC-9)*, Singapore, 2001.

[9]. Inkpenand M. Mofett, "The Global Oil and Gas Industry: Management, Strategy, and Finance", *Penn Well Corporation*, Tulsa, USA, 2011.

[10]. H. Maylor, "Project Management", *Pearson Education Limited*, 4th ed., UK, 2010.

[11]. N. Al-Hammadi, "KPIs for Assessing Project Performance in the Oil and Gas Industry of the United Arab Emirates", 6thEngaged Management Scholarship Conference, September 2016, *University Paris-Dauphine*, Paris, France.

[12]. M. Ahmed, "Critical Factors for the Success of Projects in Oil and Gas Sector of Kuwait", *MSc Thesis*, Department of Management Sciences, Virtual University of Pakistan, Pakistan, 2011.

[13]. D. Sylvester, N. Abdul Rani and J. Shaikh, "Comparison Between Oil and Gas Companies and Contractors Against Cost, Time, Quality and Scope for Project Success in Miri, Sarawak, Malaysia", *African Journal of Business Management*, vol.5, no. 11, pp. 4337- 4354, 2001.

[14]. F. Bahia, "Analysis of Success Criteria in Engineering, Procurement and Construction (EPC) Projects", *RevistaGestao e Projetos - GeP*, Sao Paulo, vol. 1, no. 2, pp. 49-67, 2010.

[15]. Olaku, A. Abdulmumin, S. Ibrahim and T. John, "Evaluation of Perception of Stakeholders on Key Performance Indicators for U.B.E Building Projects, *Journal of Multidisciplinary Engineering Science and Technology (JMEST)*,vol. 2, no. 3, pp. 277- 285, 2015.

[16]. S. Khosravi and H. Afshari, "A Success Measurement Model for Construction Projects", *International Conference on Financial Management and Economics*, vol. 11, pp. 186-190, 2011.

[17]. S. Al-Tmeemy, H. Abdul-Rahman and Z. Harun, "Future Criteria for Success of Building Projects in Malaysia", *International Journal of Project Management*, vol. 29, no. 3, pp. 337-348, 2011.

[18]. KPI Working Group, "The KPI Report for the Minister for Construction", *Department for Transport and Environment*, London, 2000.

[19]. Lim and M. Mohamed, "Criteria of Project Success: An Exploratory Re-Examination", *International Journal of Project Management*, vol. 17, no. 4, pp. 243-248, 1999.

[20]. F. Yeung, A. Chan and D. Chan, "A Computerized Model for Measuring and Benchmarking the Partnering Performance of Construction Projects", *Automation in Construction*, vol. 18, no, 8, pp. 1099-1113, 2009.

[21]. F. Ling, S. Low, S.Wang and H. Lim, "Key Project Management Practices Affecting Singaporean Firms' Project Performance in China*", International Journal of Project Management*, 2009.

[22]. H. Ali, I. Al-Sulaihi and K. Al-Gahtani, "Indicators for Measuring Performance of Building Construction Companies in Kingdom of Saudi Arabia", *Journal of King Saud University – Engineering Sciences*, vol. 5, pp125–134, 2013.

[23]. K. Cross and R. Lynch, "The SMART Way to Define and Sustain Success", *National Productivity Review*, vol. 8, no. 1,pp. 23- 33, 1989.

[24]. L. Cronback, "Coefficient Alpha and the Internal Structure of Tests", *Psychometrika*, vol. 16, no. 3, pp. 297-334, 1951.

[25]. Y. Yang and S. Green, "Coefficient Alpha: A Reliability Coefficient for the 21st Century", *Journal of Psychoeducational Assessment*, vol. 29, pp. 377-392, 2011.

[26]. P. Vonglao, "Application of Fuzzy Logic to Improve the Likert Scale to Measure Latent Variables", *Kasetsart Journal of Social Sciences*, vol. 38, no. 3, pp. 337-344, 2017.

[27]. R. Likert, "A Technique for the Measurement of Attitudes", *Archives of Psychology*, vol 22, no 140, pp. 5-55, 1932.

[28]. K. Al-Gahtani, I. Al-Sulaihi, R. Al Rashed and A. Batarfi, "Key Performance Indicators for Value Management in Saudi Construction Industry", *International Journal of Application or Innovation in Engineering & Management (IJAIEM)*, vol.4, no. 11, pp. 54-62,2015

[29]. M. Nourbakhsh, S. Mydin, R. Zin, S. Zolfagharian, J. Irizarry and M. Zahidi, "Relative Importance of Key Performance Indicators of Construction Projects Towards Build ability at Design Stage", *Advanced Materials Research Online*: vols.446-449, pp. 340-344, 2012.

[30]. V. Tam, C. Tam and W. Ng, "On Prefabrication Implementation for Different Project Types and Procurement Methods in Hong Kong", *Journal of Engineering, Design and Technology*, vol. 5, no. 1, pp. 68-80, 2007.

An Investigation of Corrosion Risks in the Oil and Gas Pipelines Using Analytical Hierarchy Process and Fuzzy Analytical Hierarchy Process

Abdulbaset A. Frefer[1], Mahmoud M. Matoug[2] , Fatma L. Haddada[3]
[1] drfrefer@hotmail.com, [2] mmmatoug54@ymail.com, [3] Fatma_haddada@yahoo.com
[1, 2] Mechanical and Industrial Engineering Department, University of Tripoli
[3] Engineering Management Department, University of Tripoli

ABSTRACT

The products of crude oil and gas can be considered as the main backbone of the global economy. The oil and gas industry has faced many potential risks and problems when the oil and gas is pumped into the pipelines during the production, transportation, and processing. Although experts are solving these problems; some have been difficult to resolve and remained as a complex issue. Among these problems, were the issues of corrosion in the oil and gas pipelines. Risk assessment of the oil and the gas pipelines is considered as the core content of the integrated management of the entire pipelines. This paper aims to assess the risks of corrosion in the oil and gas pipelines in Sabratha platform and Wafaa field. First, the Analytical Hierarchy Process (AHP) is used to identify the risk rate of the different types of corrosion. Second, the technique of Fuzzy Analytic Hierarchy Process (F-AHP) is also used to identify the risk rate of the different types of corrosion. The comparison between the classical (AHP) and the (F-AHP) indicate that the results of both techniques were close.

Keyword— Analytical Hierarchy Process (AHP),Fuzzy Analytical Hierarchy Process (F-AHP), Oil and Gas, Pipelines Corrosion, Pipelines Risk Assessment (PRA),Risk Assessment (RA).

1. Introduction

There are many reasons for the reduced strength capacity and destruction of pipelines. One of these reasons is the appearance of defects during its manufacture, construction, and operation. According to [1], defects may be visible, hidden, as well as critical, significant and insignificant. Out of all defects of pipeline systems the corrosion defects are considered to be the most significant ones.

Corrosion and other defects in oil and gas pipelines have been serious risks facing operators, inspectors, and corrosion management experts concerned with the offshore/onshore fields; the effects of these risks may be fatal. Oil and gas pipelines risk assessment (PRA) is the core content of the integrated management of the entire pipelines. The PRA allows detecting the danger factors on the pipelines, to facilitate control and prevention of corrosion & other risks, and to guarantee safe operation of the pipelines[2].

Research studies have been conducted on various topics to ensure pipeline integrity, reliability, and safety, such as qualitative, semi-quantitative, and quantitative risk assessment techniques [1,3-20]. Examples of these techniques are; the risk assessment matrix, the fuzzy Bayesian Belief network, the Fuzzy Petri net model, Fuzzy logic, AHP, and F-AHP, and the combined Analytical Hierarchy Process - Fault Tree Analysis (AHP-FTA), Monte Carlo, and hazard and operability study (HAZOP). The quantitative and semi-quantitative techniques are considered more accurate and provide more details prioritization of risks than the outcome of qualitative risk assessments techniques that can be evaluated quickly to assess risks.

2. Statement About the Pipelines Understudy

This study carried out on five pipelines, which are used in transporting oil and gas at both offshore and onshore fields :namely;(i) 10″ condensate, (ii) 16″ oil [section A, B, C], (iii) 36″ dry gas.

The historical report of the company regarding the detection of these pipelines after pigging (cleaning and inspection)indicates that there are several types of corrosion and other defects in each part of these pipelines, which can be summarized as: (i) Internal Metal Loss, (ii) External Metal Loss, (iii) Gouge Metal Loss, (iv) Dent Metal Loss, (v) Pipe Mill Metal Loss. All types of pipelines defects have been defined and classified in [22] and many more references were cited in [21].

3. Risk Assessment Techniques Proposed for the Analysis of the Pipelines

Several techniques have been proposed in order to analyze the risks of the pipelines, identify their causes and limiting their impacts, such as the AHP and the FAHP.

3.1. The Classical Analytical Hierarchy Process (AHP)

The theory of AHP is based on the fact that the elements of the problem can be arranged within a separate group, each of which has a specific hierarchical level within the overall hierarchical structure, each level affects directly the above level; therefore, the bottom level is affected too.

3.1.1 Hierarchical Structuring of the Problem

The assessment is decomposed into a hierarchy consisted of the problem (goal), then the criteria, followed by sub-criteria and alternatives in lower levels. At the core of the hierarchy is the goal of the problem being studied and analysed. The leaf nodes are the alternatives to be compared.

3.1.2 Priority Analysis

The AHP calculates the priorities between the elements of the hierarchy and collecting the opinions, to obtain a set of the overall priorities, and to check the stability of these opinions to draw a final decision based on the results of this process.

3.1.3 Identification Priorities

Priority setting is represented by making binary comparisons between elements in the second level of the hierarchy with values ranging from (1 to 9) as shown in Table 1.

Table 1: Saaty' Scale for Quantitative Comparison of Alternatives[5].

P.L	E.S	E.T.M.S	M.S	M.T.S.S	S.S	S.T.V.S.S	V.S.S	V.S.T.E.S	E.S
N.V	1	2	3	4	5	6	7	8	9

Abbreviations in this table mean: P.L=Preference Level, N.V=Numerical Value, E.S=Equally Serious, E.T.M.S= Equally to Moderately Serious, M.S=Moderately Serious, M.T.S.S=Moderately to Strongly Serious, S.S=Strongly Serious, S.T.V.S.S=Strongly to Very Strongly Serious, V.S.S=Very Strongly Serious, V.S.T.E.S=Very Strongly to Extremely Serious, E.S=Extremely Serious.

3.1.4 Estimating Priorities

To estimate the priorities in an approximate way; (i) sum of the values in each column should be calculated; (ii) each value should be divided by the summation of the column that allows meaningful comparisons between elements; (iii) the mean of the rows should be calculated by summation of the values in each row and divided by the number of elements in that row [11-13, 23].

3.1.5 Consistency Verification

When the matrix is steady, the normalized summation for each row shows how much each element is dominated by the other relative elements [24-25]. If the rules are contradictory, this value known as (Consistency Ratio), will be greater than 10% [10,26].

3.1.6 Estimating the Consistency Ratio

The consistency ratio is calculated as shown in equation (1) and is required to be less than 0.1 for acceptable consistency [24].$CR = \frac{CI}{RI}$

$$CR = \frac{CI}{RI} \quad (1)$$

Where: CR= Consistency Ratio; RI= Random Index, CI = Consistency Index

3.2. The Fuzzy Analytical Hierarchy Process

In F-AHP, the factors that affect the decision-making are hierarchically arranged from the overall goal to the criteria, sub-criteria, and alternatives in successive levels.

Triangular Fuzzy Numbers (TFNs)

Da-Yong [27] has used the extent analysis technique and the principle of (TFN) comparison to obtain the priorities of alternatives from pair-wise comparison. TFNs contain three levels of comparison values;

minimum possible value (L), the most possible value (M), and the maximum possible value (U). These values follow the scale shown in Table 2. The technique of F-AHP can be applied by using the equation (2), the fuzzy synthetic extent value (Si) with respect to the (ith) criterion is defined as [14,28]:

$$S_i = \sum_{j=1}^{m} M_{gi}^{j} \times \left[\sum_{i=1}^{n}\sum_{j=1}^{m} M_{gi}^{j}\right]^{-1} \quad (2)$$

$S_i = \sum_{j=1}^{m} M_{gi}^{j} \times \left[\sum_{i=1}^{n}\sum_{j=1}^{m} M_{gi}^{j}\right]^{-1}$ For Si=(Li,Mi,Ui) and Sj=(Lj,Mj,Uj), the degree of possibility that Sj ≥ Si for a convex fuzzy number can be obtained from equation (3):

$$V(S_j \geq S_i) = \begin{cases} 1 & if\ m_j \geq m_i \\ 0 & if\ l_i \geq u_j \\ \frac{l_i - u_j}{(m_j - u_j) - (m_i - l_i)} & otherwise \end{cases} \quad (3)$$

To obtain estimates for sets of weight values under each criterion, one must consider a principle of comparison for fuzzy numbers, the degree of possibility of Si ≥ Sj=(1, 2, 3...n) should be estimated by using equation (4).

$$V\ (S_j \geq S_1, S_{2,\ S3} \ldots S_n) = \min V\ (S_i \geq S_{i=1,\ 2,\ 3\ldots n}) \quad (4)$$

Then, the normalized weight W (Si) will be formed in terms of a weight vector as follows:

$$W = \left(w(S_1), w(S_2), \ldots, w(S_n)\right)^T \quad (5)$$

Table 2: Linguistic Terms and the Corresponding Triangular Fuzzy Numbers [28].

	FAHP								
L.S.F.I	E.I	I.1	M.I	I.2	I	I.3	V.I	I.4	A.I
T.F.N	1,1,1	1,2,3	2,3,4	3,4,5	4,5,6	5,6,7	6,7,8	7,8,9	9,9,9
T.F.R.N	1,1,1	1/3,1/2,1/1	1/4,1/3,1/2	1/5,1/4,1/3	1/6,1/5,1/4	1/7,1/6,1/5	1/8,1/7,1/6	1/9,1/8,1/7	1/9,1/9,1/9

Abbreviations in this table mean: L.S.F.I=Linguistic Scales for Importance, T.F.N=Triangular Fuzzy Numbers, T.F.R.N= Triangular Fuzzy Reciprocal Numbers, E.I=Equally Important, I.1=Intermediate 1, M.I=ModeratelyImportant, I.2=Intermediate 2, I=Important, I.3=Intermediate 3, V.I=Very Important, I.4=Intermediate 4, A.I=Absolutely Important.

4. Results and Discussion

The pair-wise comparison for the basic consequences in AHP and F-AHP techniques are done between the three types of consequences listed in Table 3.

Table 3: The Basic Consequences Definitions.

Consequence Types	**Symbol**
Environmental Impact	EV-I
Economic Impacts	EC-I
Health-Safety Impacts	HS-I

Table 4 clearly shows that the results of both the classical AHP and F-AHP techniques were close enough to agree that health and safety impacts are more important thaneconomic and environmental impacts. The quantitative values explain that the criterion "Health and Safety", would have a higher importance of being attentive than the other two.

Table 4: The Normalized Pair- Wise Comparison Matrix.

Criteria	EV-I	EC-I	HS-I
AHP	0.1637	0.2972	0.5389
F-AHP	0.0769	0.3563	0.5667

Table 5 shows that the main type of corrosion, which should receive all the attention is the internal metal loss. The obtained result of the F-AHP for (EC-N) has value of zero, which means that the corresponding criterion has no importance as was stated by Liyuan[28].

Table 5: Corrosion Risk Rates of AHP VS. F-AHP for 10" Condensate Pipelines.

	AHP	**FAHP**
IC-N	0.7851	1.0000
EC-N	0.2148	0.0000

Table 6 shows the risk rates of corrosion types for each section in 16" oil pipeline by using both techniques, risk rates in section (A) were very close. The other two types of risks in section (B) are both cancelled in F-AHP, whereas the (IC-B) in AHP is the most important (0.7591). In section C, the classical AHP indicates the (IC-C) is the most important (0.5971), and that the (EC-C) is the next most important (0.2507); whereas the result of F-AHP cancelled both (MD-C) and (DC-C) and left the (IC-C) as the most important, this can be an advantage for F-AHP, where the decision maker can focus on the more important risks as was also reported by Ozdagoglu, et al. [26].

Table 6: Corrosion Risk Rates of AHP VS. F-AHP for 16" Oil Pipelines for Each Section.

Section A			**Section B**			**Section C**		
	AHP	**F-AHP**		**AHP**	**F-AHP**		**AHP**	**F-AHP**
GC-A	0.4879	0.4809	**GC-B**	0.1132	0.0000	**MD-C**	0.0725	0.0000
MD-A	0.5120	0.5190	**IC-B**	0.7591	1.0000	**IC-C**	0.5971	0.8300
			DC-B	0.1276	0.00000	**EC-C**	0.2507	0.1700
						DC-C	0.0796	0.0000

In 36", dry gas pipeline, pair-wise comparison proofed that (MD-D) was less important than the (IC-D) in AHP. Relatively, this type of risk has no importance in F-AHP,but (IC-D) was rated with value of one as the most risky type of corrosion in this study as shown in Table 7.

Table 7: Corrosion Risk Rates of AHP VS. F-AHP for 36" Dry Gas Pipelines.

	AHP	**FAHP**
IC-D	0.8648	1.0000
MD-D	0.1351	0.0000

5. Conclusions

The analysis of the risk assessment results as was discussed elsewhere [3,29] indicates that there is a range from convergent to divergent. Results showed that these pipelines are subject to damage due to high-risk rates of some types of corrosion and other defects. In the 10" condensate pipeline and by using the classical AHP, the type of corrosion that should receive all the attention is the (IC-N) (0.7851). However; in the 16" oil pipeline section A, the defect of (MD-A) when using the classical AHP was the most important (0.5120) than the other (GC-A). These results were close enough to the results of the F-AHP. In section B, the (IC-B) in the classical AHP was the most important (0.7591) and the other two types of risks were both cancelled in F-AHP. In section C, the classical AHP indicates the (IC-C) is the most important (0.5971), and the (EC-C) was the next most important (0.2507); whereas the result of F-AHP cancelled both (MD-C) and (DC-C) and left the (IC-C) as the most important. Decision maker may be able to focus on the most significant types of risks. In oil and gas pipelines, assessment techniques allow corrosion risks to be assessed after the inspection processes (in this study, Pigging was the process used to inspect the five (5) pipelines). This can help the inspectors focus on the types that have high influence on pipelines.

References

[1]. GOST 15467, "Quality Management. Basic Concepts. Terms and Definitions*, IPK Izd-vostandartov*, Moscow, 2009.

[2]. D. Hang, W. Lixin, and W. Qiannan, "A Study on Oil Pipeline Risk Assessment Technique Based on Fuzzy Analytic Hierarchy Process", *The Open Petroleum Engineering Journal*, pp. 125-129, 2014.

[3]. F. Afaf, "Corrosion Risk Assessment Study Onshore Field", *M.Sc. Thesis*, College of Engineering, University of Tripoli, 2008.

[4]. K. Golam, S. Rehan, and T. Solomon, "A Fuzzy Bayesian Belief Network for Safety Assessment of Oil and Gas Pipelines", *Structure and Infrastructure Engineering Journal*, vol. 12, no. 8, pp. 874-889, 2016.

[5]. Z. Tan, J. Li, Z. Wu, J. Zheng, and W. He, "An Evaluation of Maintenance Strategy Using Risk Based Inspection", *Safety Science*, vol. 49, pp. 852-860, 2011.

[6]. G. Yanbao, M. Xiaoli, W. Deguo, M. Tao, L. Shuhai, and H. Renyang, "Comprehensive Risk Evaluation of Long-Distance Oil and Gas Transportation Pipelines Using a Fuzzy Petri Net Model", *Journal of Natural Gas Science and Engineering*, vol. 33, pp. 18-29, 2016.

[7]. H. Abid, "Security of Cross-Country Oil and Gas Pipelines: A Risk-Based Model", *Journal of Pipeline Systems Engineering and Practice*, vol.7, no.3, pp. 1-8, 2016.

[8]. S. Oleg and T. Solomon, "Internal Corrosion Hazard Assessment of Oil & Gas Pipelines Using Bayesian Belief Network Model", *Journal of Loss Prevention in the Process Industries*, vol. 40, pp. 479-495, 2016.

[9]. Z. Qi, W. Wei, L. Dongpeng, L. Kaikai, and Q. Qiao, "Estimation of Corrosion Failure Likelihood of Oil and Gas Pipeline Based on Fuzzy Logic Approach", *Engineering Failure Analysis*, vol. 70, pp. 48-55, 2016.

[10]. C. Briggs, "Risk Assessment in the Upstream Crude Oil Supply Chain: Leveraging Analytic Hierarchy Process", *Ph.D. Dissertation*, Transportation and Logistics, College of Graduate and Interdisciplinary Studies, North Dakota State University, April 2010.

[11]. R. Izak, "Applying the Analytic Hierarchy Process to Oil Sands Environmental Compliance Risk Management". *Ph.D. Dissertation*, College of Management and Technology, Walden University, 2014.

[12]. B. Abdul-Lateef, M. Abdul-Nasir, and M. Adekunle, "A Fuzzy Multi-Criteria Decision Support System for Evaluating Subsea Oil Pipeline Routing Criteria In East Malaysia", *Environmental Earth Sciences*, vol. 74, pp. 4875-4884, 2015.

[13]. T. Solomon and S. Rehan, "Risk-Based Environmental Decision-Making Using Fuzzy Analytic Hierarchy Process (F-AHP)",*Stochastic Environmental Research and Risk Assessment*, vol. 21, pp. 35-50, 2006.

[14]. K. Dey, "Analytic Hierarchy Process Analyzes Risk of Operating Cross-Country Petroleum Pipelines in India", *Natural Hazards Review*, vol. 4, no.4, pp.213-221, 2003.

[15]. B. Yongqiang, L. Lv, and W. Tong, "The Application of the Semi-Quantitative Risk Assessment Method to Urban Natural Gas Pipelines", *Journal of Engineering Science and Technology*, pp. 74-77,2013.

[16]. Bertuccio and M. Moraleda, "Risk Assessment of Corrosion in Oil and Gas Pipelines Using Fuzzy Logic", *Corrosion Engineering, Science and Technology*, vol.47, no.7, pp. 553-558, 2012.

[17]. D. Prasanta, "Analytic Hierarchy Process Helps Evaluate Project in Indian Oil Pipelines Industry", *International Journal of Operations & Production Management,* vol. 24, no. 6, pp.588-604, 2004.

[18]. Dawotola, P. van Gelder, and J. Vrijling, "Risk Assessment of Petroleum Pipelines Using A Combined Analytical Hierarchy Process - Fault Tree Analysis (AHP-FTA)", *Proceedings of the Seventh International Probabilistic Workshop*, pp.491-501, 2009.

[19]. S. Mubin and G. Mubin, "Risk Analysis for Construction and Operation of Gas Pipeline Projects in Pakistan", *Pakistan Journal of Engineering & Applied Sciences*, vol.2, pp.22-37, 2008.

[20]. J. Yadhushree, P. Shiva, and S. Keerthi, "Qualitative Risk Assessment and HAZOP Study of a Glass Manufacturing Industry". *International Journal of Advance Research, Ideas and Innovations in Technology*, vol. 3, pp. 776-787, 2017.

[21]. M. Xieand Z. Tian, "Risk-Based Pipeline Re-Assessment Optimization Considering Corrosion Defects", *Sustainable Cities and Society*, vol. 38, 746-757, 2018.

[22]. J. Roland, T. Susannah, and H. Phil, "Proposal for the Development of an International Recommended Practice in Pipeline Defect Assessment and Repair Selection", *International Conference on the Evaluation and Rehabilitation of Pipelines Prague*, pp. 1-27, 2008.

[23]. R. Dejan, "A Tool for Risk Assessment", *Safety Engineering*, pp.121-122, 2013.

[24]. J. Alonso and M. Lamata, "Consistency in the Analytic Hierarchy Process: A New Approach", *International Journal of Uncertainty*, pp. 445-459, 2006.

[25]. M. Ayhan, "A Fuzzy AHP Approach for Supplier Selection Problem.", *International Journal of Managing Value and Supply Chains*, pp.11-23, 2013.

[26]. Ozdagoglu and G. Ozdagoglu, "Comparison of AHP and Fuzzy AHP for the Multicriteria Decision Making Processes with Linguistic Evaluations", *Istanbul Ticaret University Fen Bilimleri Dergisi*, pp. 65-85, 2007.

[27]. Da-Yong, "Applications of the Extent Analysis Method on Fuzzy AHP", *European Journal of Operational Research*, pp. 649-655, 1996.

[28]. Z. Liyuan, "Comparison of Classical Analytic Hierarchy Process (AHP) Approach and Fuzzy AHP Approach in Multiple-Criteria Decision Making", *M.Sc. Thesis*, University of Nebraska-Lincoln, Nebraska, 2010.

[29]. F. Haddada, "Assessment of Corrosion Risks in the Oil and Gas Pipelines in Libya's Onshore/offshore Field", *M.Sc. Thesis*, College of Engineering, University of Tripoli, 2017.